1154

Eng. Library

key words:
1- Tee Type Connections
2- offshore Structures
3- Tubular Connections

PMFSEL REPORT NO. 86-2
MARCH 1986

Strength and Behavior of Double-Tee Tubular Joints in Tension

by

DAVID H. SANDERS

and

JOSEPH A. YURA — primary author

PHASE 3—FINAL REPORT

Volume 2 of 3

Sponsored by

American Bureau of Shipping
Amoco Production Company
Brown and Root, Inc.
Chevron Oilfield Research Company
Conoco, Inc.
Exxon Production Research Company
Gulf Oil Exploration and Production Company
Marathon Oil Company
McDermott, Inc.
Phillips Petroleum Company
Shell Oil Company
Texaco USA, Inc.
Union Oil Company of California

PHIL M. FERGUSON STRUCTURAL ENGINEERING LABORATORY
Department of Civil Engineering / Bureau of Engineering Research
The University of Texas at Austin

01391

David H. Sanders
12400B Coronet St.
Austin, TX 78727
July 5, 1986

Mr. Nestor R. Iwankiw
Assistant Director of Engineering
Research & Education
AISC Education Foundation
400 N. Michigan Ave.
Chicago, IL 60611

Dear Mr. Iwankiw:

Here is the final draft of the report written from the research conducted for my thesis and during my AISC fellowship. I eventually plan to condense the report for publication purposes in various journals.

Sincerely,

David H. Sanders

David H. Sanders

Strength and Behavior
of
Double-Tee Tubular Joints in Tension

by

David H. Sanders
and
Joseph A. Yura

Phase III Final Report
Vol. 2 of 3

Submitted to:

American Bureau of Shipping
Amoco Production Company
Brown and Root, Inc.
Chevron Oilfield Research Co.
Conoco, Inc.
Gulf Oil Exploration and Production Company
Exxon Production Research Company
McDermott, Inc.
Marathon Oil Company
Phillips Petroleum Company
Shell Oil Company
Texaco USA, Inc.
Union Oil Company of California

Phil M. Ferguson Structural Engineering Laboratory

The University of Texas at Austin

May, 1986

ABSTRACT

A majority of the current data base of tubular joint tests consists of specimens loaded in compression; therefore the purpose of this study was to increase the understanding of double-tee (DT) joints loaded in tension. Five tests were conducted on DT joints with $\beta = 1.0$ and seven tests on $\beta = 0.34$ joints. The program concentrated on the following topics: the failure limits of first crack and ultimate load, the effect of chord stress on the ultimate strength, the contribution of the chord length to joint strength and the effect of reserve yield capacity in the branch on post-crack strength. The results of this program are compared with a screened data base.

The results showed that compression chord stress has no effect on ultimate strength of $\beta = 1.0$ DT joints. The significance of the chord length contribution to joint strength is very related to the β value. The $\beta = 1.0$ joints with a short chord showed no reduction in strength while the $\beta = 0.34$ joints with a short chord showed a significant reduction in strength of 75%. Therefore the API recommendation for chord strengthening is adequate for $\beta = 1.0$ joints, but for $\beta = 0.34$ joints further research needs to be done to determine if the standard is adequate. Tests conducted on $\beta = 0.34$ joints also showed that

the amount of reserve yield capacity in the branch does not affect post-crack strength. Hence, API should consider the elimination of the first crack concept for tension strength capacity.

Using the data from the research program and the existing data base, the following equations for mean ultimate strength and first surface crack were developed:

Ultimate Equation

Mean: $P = 35.4\ \beta\ F_y T^2 Q_{\beta\gamma} \ldots\ldots\ldots\ldots (5.1)$

$$Q_{\beta\gamma} = 1 \qquad \text{for } \beta < 0.9$$

$$Q_{\beta\gamma} = \frac{0.035\gamma^{.75}}{1-0.86\beta} \qquad \text{for } \beta > 0.9$$

Lower Bound: $P = 0.818 \times$ Eq. 5.1

First Crack Equation

Mean: $P = 0.94(6 + 20\beta)\ F_y T^2 Q_{\beta\gamma} \ldots (5.3)$

$$Q_{\beta\gamma} = 1 \qquad \text{for } \beta < 0.7$$

$$Q_{\beta\gamma} = \frac{0.035\gamma^{.75}}{1-0.86\beta} \qquad \text{for } \beta > 0.7$$

Lower Bound: $P = 0.866 \times$ Eq. 5.3

The equations incorporate the beta-thinness factor at high β values to improve the accuracy. The current API uses a first crack limit for design, but the equation is very conservative at high beta values. In order to improve the accuracy of predicted strength in tension, as a minimum the API equation should incorporate the compression DT equation Q_β factor in the formula for tension.

API Modified First Crack Equation

$$P = (3.4 + 19\beta)F_yT^2 \, Q_\beta$$

$$Q_\beta = 1 \qquad \beta < 0.6$$

$$Q_\beta = \frac{0.3}{\beta(1-0.833\beta)} \qquad \beta > 0.6$$

ACKNOWLEDGEMENTS

A special thanks to the technical advisory committee consisting of K. Chang, C. Caracostis, M. Dwyer, D. Grimm, J. Hansford, T.M. Hsu, D.K.Y. Kan, J. Saunders, J. Teymourian, C. Wang, W.J. Wang, W.C. Yu, and N. Zettlemoyer who represented the project sponsors and were active and helpful in guiding this research.

The tests were conducted at the Phil M. Ferguson Structural Engineering Laboratory, Department of Civil Engineering, The University of Texas at Austin. The help of the laboratory staff was essential in the success of this project; especially Pat Ball for fabricating the $\beta = 0.34$ specimens, Jean Gehrke for the figure drafting and Sharon Cunningham for assembling the report. Also appreciated was the help of Blake Stassney and Laurie Golding.

PREFACE

The following report gives the results of a study on double-tee tubular joints in tension. The report is part of Phase III in a series of studies on double-tee joints. Other studies conducted during Phase III of the project are given in Ref. 16, "The Effect of Chord Stresses on the Static Strength of DT Tubular Connections" and Ref. 22, "Stress Concentration Factors in Double-Tee Tubular Joints." The study on double-tee joints in tension consisted of tests on $\beta = 1.0$ and $\beta = 0.34$ joints. The study investigated what affects the behavior and strength of the joints. The funds for this research were provided by American Bureau of Shipping, Amoco Production Company, Brown and Root, Inc., Chevron Oilfield Research Co., Conoco, Inc., Gulf Oil Exploration and Production Company, Exxon Production Research Company, McDermott, Inc., Marathon Oil Company, Phillips Petroleum Company, Shell Oil Company, Texaco USA, Inc. and Union Oil Company of California. Their support is greatly appreciated.

TABLE OF CONTENTS

TABLE OF CONTENTS (continued)

LIST OF TABLES

LIST OF FIGURES

LIST OF FIGURES (continued)

LIST OF FIGURES (continued)

LIST OF FIGURES (continued)

Figure Page

CHAPTER 1

INTRODUCTION

Strength equations used in 1985 to design circular tubular connections have been developed by using experimental data. Where data were not available for a particular joint type or load condition, extrapolations were made from the existing data base. Most of the current data base is comprised of connections loaded in compression. In a paper published in 1984 by Ochi et al(13), an extensive listing of the current data base was given. Out of 715 tests listed, only 96 of the test joints were loaded in tension.

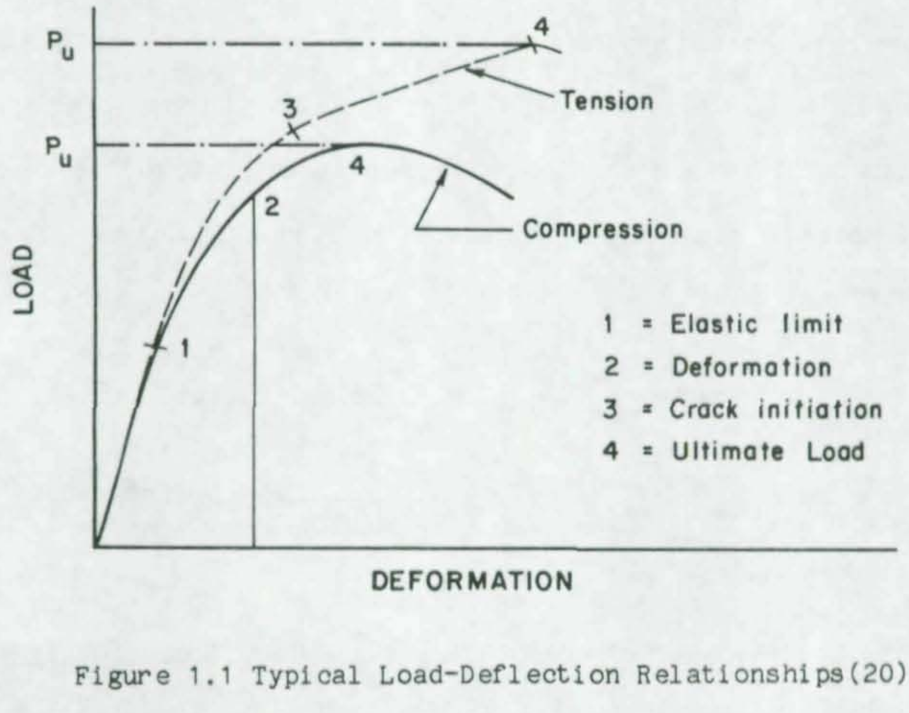

Figure 1.1 Typical Load-Deflection Relationships(20)

Figure 1.1 shows typical load-deflection curves for both joints in tension and compression. The compressive strength of a joint is a lower bound to its tensile strength. A compression failure consists of bending and buckling, therefore the load-deflection relationship rises to a maximum value and then gradually drops off. In a tension joint, the failure consists of material cracking and fracture, usually after extensive yielding.

In API RP 2A 15th Ed., Recommended Practice for Planning, Designing, and Constructing Fixed Offshore Platforms(2), a compression joint design is based on the ultimate load, while a tension joint design is based on the first crack load. First crack was selected because it is a lower bound, there is uncertainty on the amount of post-crack strength and according to Marshall and Toprac (12), first crack would functionally impair the joint for subsequent fatigue service. For DT joints in compression and tension, the API ultimate strength equations are:

Compression: $P = (3.4 + 13\beta)F_yT^2Q_\beta$..........(1.1)

$$Q_\beta = \frac{0.3}{\beta(1-0.833\beta)} \qquad \text{for } \beta>0.6$$

$$Q_\beta = 1.0 \qquad \text{for } \beta<0.6$$

Tension: $P = (3.4 + 19\beta)F_yT^2$............(1.2)

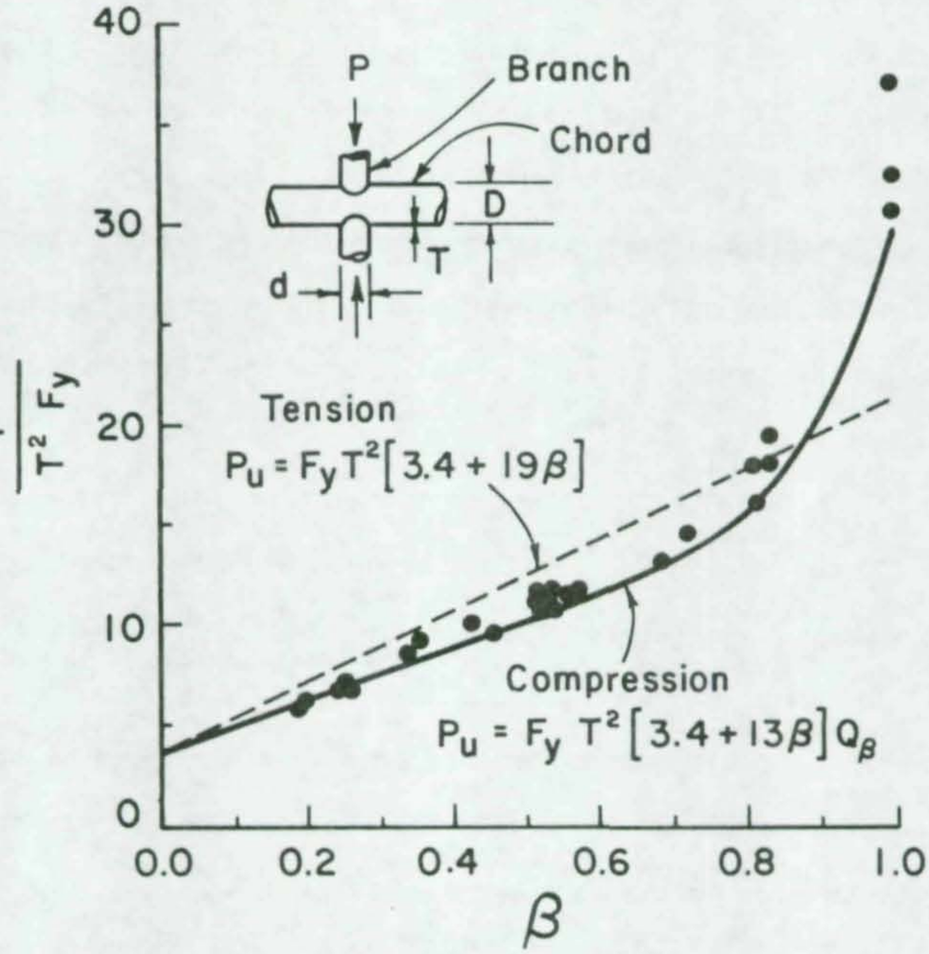

Figure 1.2 Compression Loading of DT Joints

where β(beta) is the ratio of the outer diameter of the branch(d) divided by the outer diameter of the chord(D), T is the thickness of the chord and F_y is the yield strength of the chord. Figure 1.2 shows the API equations and the data base that was used to develop the compression formula(25). At large β ratios, the tension formula becomes a lower bound to the compression formula. This seems inherently incorrect, since the compression failure load is experimentally a lower value than the tension failure load.

Figure 1.3 shows the first crack load data base used by Yura(24) to develop the tension formula. When the first crack load was used to define the tension capacity, the number of available data points was reduced significantly because many references did not report the first crack value. Because there are no data points at $\beta = 1.0$, a conservative approach was taken and the tension formula was not increased by Q_β for $\beta > 0.6$. If the Q_β factor was applied to the tension formula when $\beta = 1.0$, the first crack load would increase by 80%. The figure also shows that scatter is a problem with tension data. For four tests that were very similar, the highest first crack load was 60% greater than the lowest. Perhaps the scatter is caused by the definition of first crack. Two possible definitions of first crack are: first surface crack, a slight crack penetration of the base material, or first through-thickness crack, a crack

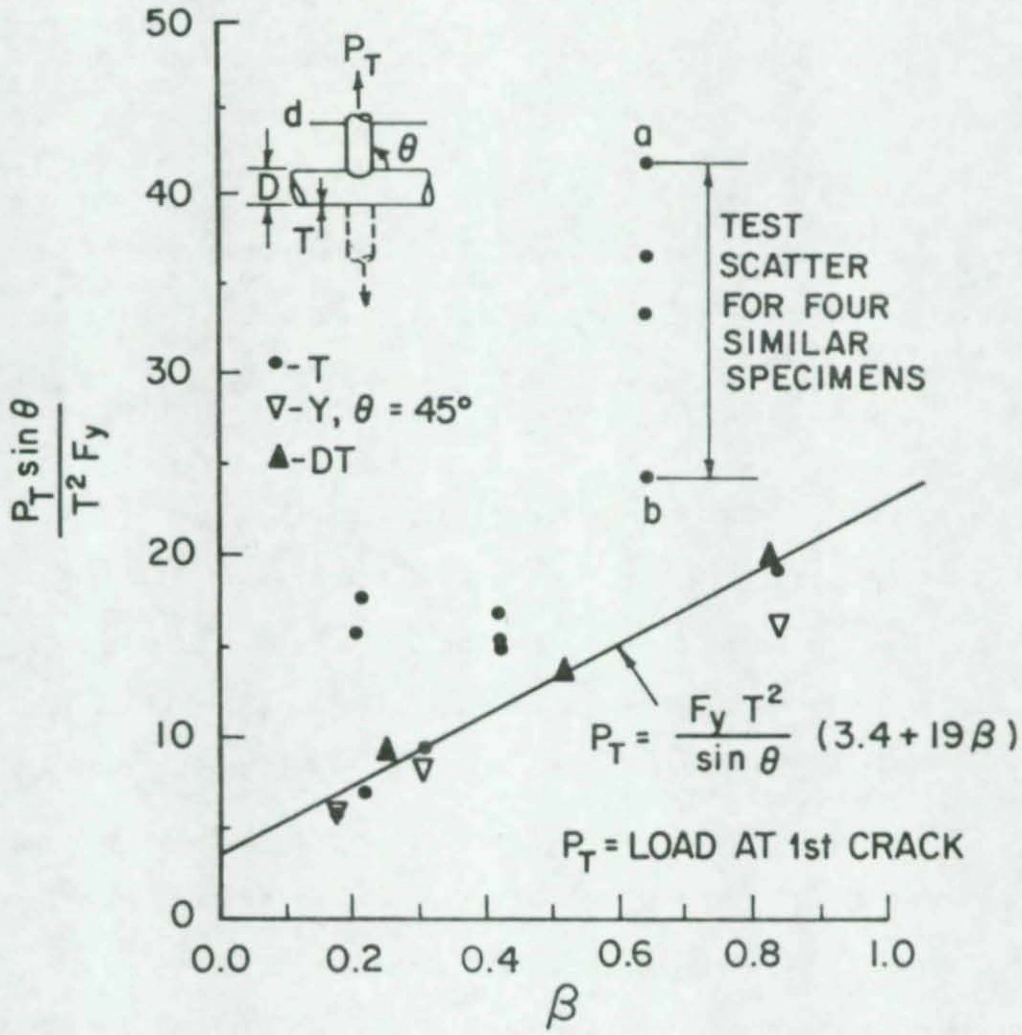

Figure 1.3 Tension Loading of T, Y and DT Joints

penetrating through the entire wall thickness. Also, the methods used to detect the first crack may vary. In most published research, the definition of first crack and the method used to detect it are not reported.

In addition to the β correction factor(Q_β), a correction for chord stresses(Q_f) is also applied to the API ultimate strength formulas and for axial chord load is given by:

$$Q_f = 1 - 0.03\ \gamma\ (P_c/P_y)^2 \ldots\ldots\ldots\ldots (1.3)$$

where P_c is the chord axial compressive load, P_y is the chord yield load, and γ is the thinness ratio(radius of the chord divided by the chord thickness). The Q_f correction factor was developed from a series of compression tests(4) but it is also applied to tension joints. If a joint has a P_c/P_y ratio of 0.9 and a thinness ratio of 25.5, Q_f would be 0.38 or the design load would drop by 62%. The effect of the factor can be very large; therefore the validity of the chord stress correction factor on tension joints needs to be investigated.

If a connection is weak and needs to be strengthened, the API code gives guidelines for joint reinforcement. The 15th Ed. of API RP2A states that chord reinforcement must extend D/4 or 12 in., whichever is the largest, away from the branch. All of the current DT tension data have at least D/2 of chord length extended away from the branch, which is twice the current chord length requirement. Additional tests need to be done that determine at what chord length the joint strength begins to be affected.

One of the reasons first crack was selected to define tension joint strength was the uncertainty of the amount of post-crack strength in actual structures. In laboratory tests the branch is usually overdesigned so that the failure is forced into the weld region of the connection. Figure 1.5 shows that the connection is divided into two portions, the weld region and the effective chord region. The effective chord region is defined as the amount of chord outside the weld region necessary to transfer the branch forces. When a crack forms, the stresses in the branch must be redistributed (See stress distribution in Fig. 1.5). If the branch stresses are low when the crack forms, redistribution of stresses can occur over the remaining net area. If the branch stresses are near the yield limit, redistribution may not be possible and post crack strength may be small. This explanation may account for the variation in post crack strength shown in Gibstein's tests(6) given in Fig. 1.4. The difference between the ultimate load and the first crack load decreased as P/P_y of the branch increased. Of course, the differences in load could also be caused by the variation in β alone. It would be useful to clarify this situation so that a reliable definition of failure could be established.

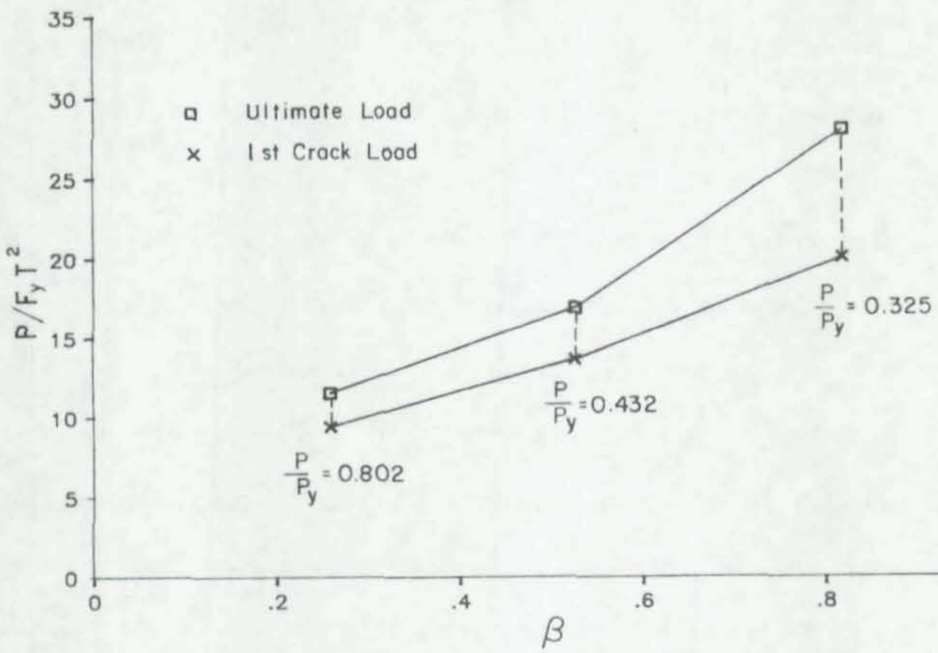

Figure 1.4 Gibstein Tension Tests

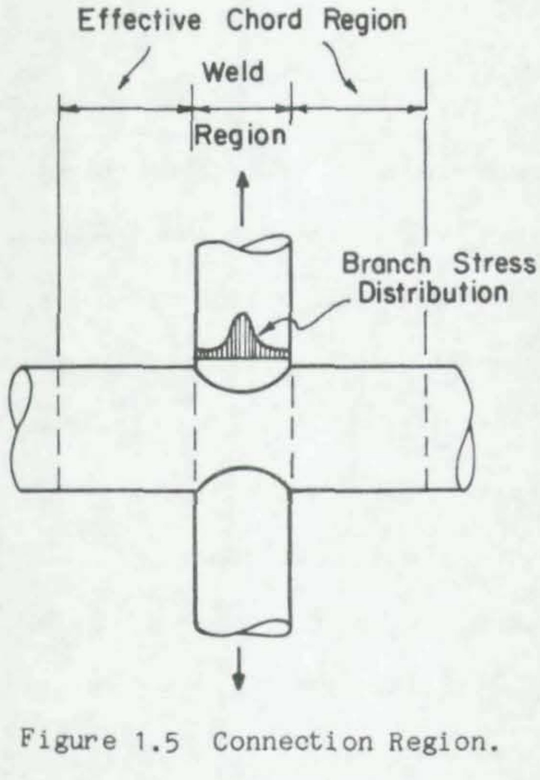

Figure 1.5 Connection Region.

From these observations the following objectives were developed for a research program on tension loaded joint:

1) to increase the data base of DT joints with β = 1.0,
2) to determine what is meant by first crack,
3) to determine if the Q_β factor should also be used on tension joints,
4) to determine if chord stress has an effect on the behavior and/or the capacity,
5) to determine if the correct zone of reinforcement is being used for tension joints, and
6) to determine if the ratio of the branch P/P_y has an effect on the behavior and/or the capacity.

In order to achieve the objectives, two test phases were devised for DT joints, one with β = 1.0 and one with β = 0.34. The β = 1.0 phase of the program consisted of 5 tests:

1) 3 control tests, where all variables would remain constant including fabrication techniques in order to strengthen confidence in the scatter band of results, and
2) 2 tests to study the effect the chord has on joint performance one to study the effect of chord

load, the second to determine how much of the joint strength comes Arom the chord adjacent to the connection.

DT joints with a $\beta = 0.34$ were selected for the second portion of the program so that the joints could be fabricated at Phil M. Ferguson Structural Engineering Laboratory(PMFSEL). The objective of this portion of the program was to determine if the branch P/P_y ratio affects the capacity of DT joints in tension. Seven tests were conducted, four with low strength steel branches to achieve a high P/P_y ratio and three with high strength steel branches to obtain a low P/P_y ratio. The specimens were basically the same except for the branch strength. Replicate tests were done in order to be confident in the ultimate and first crack values.

In the chapters that follow, the 12 tests that were conducted in the research program will be discussed. Test specimens, setup and procedures that were used are presented in Chapter 3. The results from the tests are reported in Chapter 4 and are analyzed in Chapter 5, followed by conclusions and recommendations. Before discussing the experimental program in detail, the next chapter will review previous research on tension loaded DT tubular connections.

CHAPTER 2

PREVIOUS WORK

The current data on DT joints consists of 149 tests of which 57 are DT joints loaded in tension. Many sources were checked to find tension tests that were done on DT joint. The most comprehensive source of data was a paper published by Ochi et al(13). Once the data base was accumulated, the objectives of the following data base investigation were as follows:

1) determine which data points are valid,
2) determine what theoretical equations are available for strength prediction and how well they agree with the experimental data, and
3) determine if there are any trends in the data.

The first step in studying the data base was to decide what tests constituted valid data points. The criteria used to evaluate data points was developed by Yura et al. (25) and is very similar to the criteria used by the UEG(20). Data points were evaluated with four criteria: size, material properties, deformation limits, and failure type.

Many DT tension tests have been conducted on very small joints with chord diameters as small as 102 mm(4 in.) and with branch diameter as small as 34 mm(1.34 in.). With small joints it is very difficult to model the local behavior of the connection around the weld toe; this is especially important in tension joints since many of the joints fail by ductile fracture near the weld toe. Because of this problem with small joints, no joints that had chord diameters less than 140 mm or 5.5 in. were included in the data base

The second criterion involved material properties. In order for a test to be included, the actual yield strength in the tubular member had to be measured. It is not sufficient to use the minimum specified yield strength. The actual yield strength of a tubular member can be twenty percent or more above the minimum specified yield strength.

The last two criteria dealt with the type of failure. The deflection at failure of each test was checked to verify that each test did not exceed the deformation limit. The deformation limit, Δ_L, was set at:

$$\Delta_L = \frac{2F_yL}{E}$$

where E = Young's Modulus, F_y = the chord yield stress and L = the branch length. A member length can be modeled as 30 times its diameter, a typical member length for an offshore structure. Each test was also checked to verify that failure occurred at the connection and not by gross section yielding. A table of the screened DT tension data is given in the Appendix.

The 15th Ed. of API RP2A uses first crack to define failure of DT joint in tension, but the most common definition of failure is ultimate strength. Strength prediction equations can be established as lower bound, characteristic or mean. Characteristic strength is used in ultimate limit state design and is most commonly defined as a one-sided tolerance limit that has 95 percent of the data exceeding it with a 50 percent confidence. The mean value strength is developed by determining the best fit curve through the experimental data. Table 2.1 shows the different prediction equations that are available for DT joints in tension. Figure 2.1 shows the characteristic and lower bound equations plotted with the current data base, while Fig. 2.2 shows the mean equations with the data base. The newest equation on both plots is the UEG. the UEG is based on 17 samples while the data base contains 31. The Kurobane equation is not plotted because of the different parameters that are used in that equation.

From β = 0.1 to 0.8 the data stay in a fairly tight band, but there is scatter. The largest scatter occurs at a β = 0.36, where the scatter percentage difference between the high and low value is 60%. All of lower bound and characteristic equations stay below 90% of the screened data base, while the mean equations bisect the data. At β = 1.0, the scatter becomes very large, and the equations are very conservative for some of the data points. In the worst case, the equation predicts an ultimate load that is four times lower than the experimental value. In Table 2.2 the mean value, the standard deviation and

Table 2.1 Ultimate Strength Prediction Equations for DT Joints in Tension

Equation Type	$\dfrac{P_u}{F_y T^2}$	Bounds
Lower Bound		
API,Yura'80	$3.4 + 19\beta$	
Pan'77	$22.57\beta^{0.64}$	$0.19 < \beta < 0.8$
	$41.50\beta^{3.42}$	$0.80 < \beta < 1.0$
Characteristic		
IIW,SCXV-E'81	$\dfrac{5.8}{1-0.81\beta}$	$0.25 < \beta < 1.0$
UEG'85	$1.2(3 + 15\beta)Q_\beta$	
	$Q_\beta = 1$	$\beta < 0.6$
	$Q_\beta = \dfrac{0.3}{\beta(1-0.833\beta)}$	$\beta > 0.6$
Mean		
DnV'77	$\dfrac{11}{1.2-\beta}$	$0.25 < \beta < 0.85$
UEG,Billington'85	$1.61(4.1 + 20.3\beta)Q_\beta$	
	Q_β = same as in characteristic equation	
Ochi'84	$\dfrac{2.42}{1-0.813\beta}\,(D/T)^{.322}\,(L/D)^{.24}$	

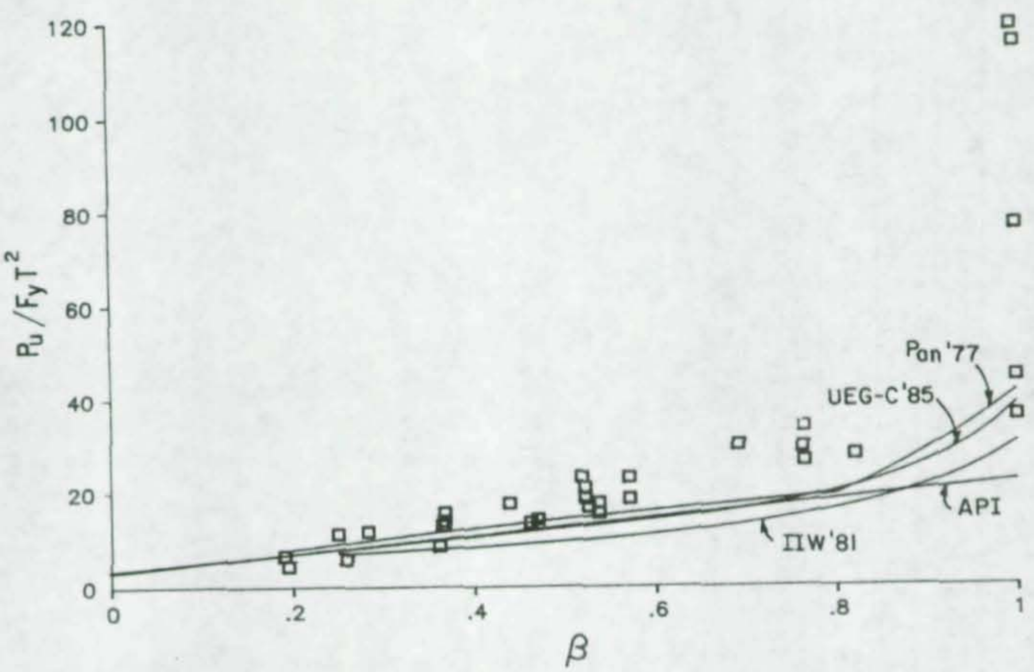

Figure 2.1 Comparison of Ultimate Strength Data with Lower Bound and Characteristic Equations.

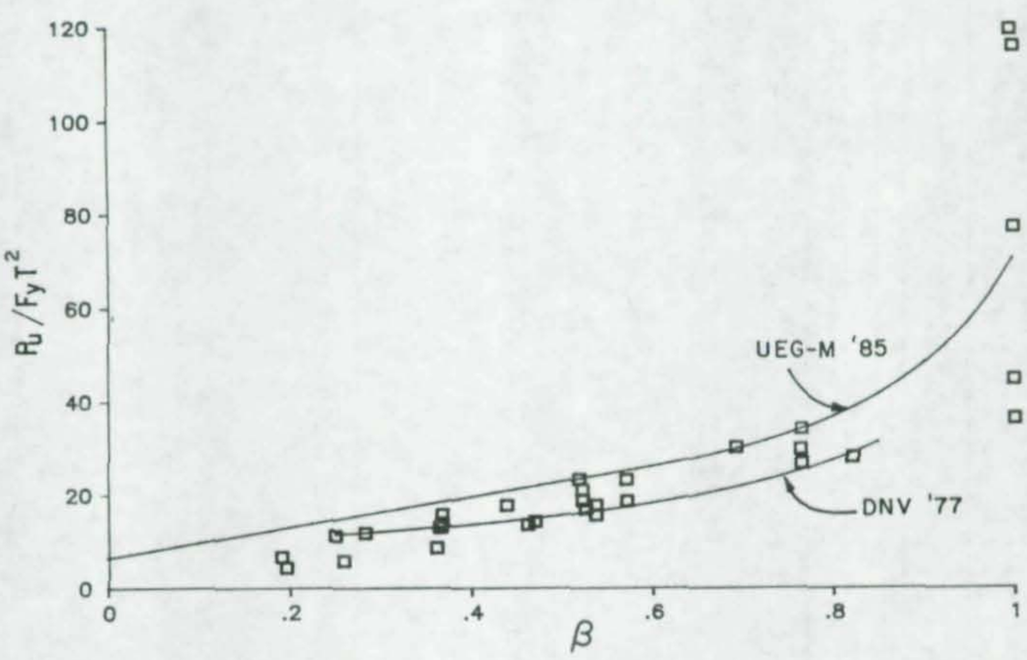

Figure 2.2 Comparison of Ultimate Strength Data with Mean Equations.

TABLE 2.2 Statistical Comparison of Data Base and Strength Prediction Equations.

	ALL BETA VALUES			BETA < 0.9			
EQUATION	TEST PREDICTED	STANDARD DEVIATION*	COEF. OF VARIANCE	TEST PREDICTED	STANDARD DEVIATION*	COEF. OF VARIANCE	PERCENT IMPROVEMENT
API	1.681	1.052 (31)	0.626	1.330	0.312 (26)	0.235	70
Pan	1.307	0.504 (31)	0.386	1.194	0.297 (26)	0.249	41
IIW	1.804	0.690 (31)	0.383	1.655	0.422 (26)	0.255	39
UEG-C	1.447	0.524 (31)	0.362	1.335	0.305 (26)	0.229	42
UEG-M	0.795	0.289 (31)	0.363	0.733	0.168 (26)	0.229	42
Ochi	0.870	0.334 (26)	0.384	0.785	0.260 (21)	0.331	22
DnV	1.089	0.378 (31)	0.371	1.023	0.255 (26)	0.249	33

* Number in ( ) is the number of data points.

the coefficient of variance of the experimental value divided by the predicted value for each of the equations listed in Table 2.1 is given. Two statistical analyses were done. One includes all the experiments listed in the Appendix, while the second one includes only experiments with β values up to 0.9. The average of the actual test result divided by the equation prediction gives a good indication of the location of the prediction equation with respect to the data. The lower bound and characteristic equations have averages between 1.3 and 1.8, while the mean equations were between 0.8 and 1.1. When the large β values are neglected, the equations become much more accurate. The standard deviation for each of the equations improved by at least 22% and in the case of the API first crack formula, 70%, when the joints with β greater than 0.9 were not included. As shown in the graph and now with the statistic, all of the equations do a good job for β values below 0.9. Chapter 5 will discuss ways of modeling tension load behavior in order to increase the reliability of the predictions at $\beta = 1.0$.

The current first crack data along with the percentage of post-crack strength is shown in Table 2.3. The trend of increasing post-crack strength with increasing reserve yield strength in the branch observed in the Gibstein data is not verified by the Makino data. But the Makino tests, shown in Fig. 2.3, help to explain the variations in DT joint tension results.

Table 2.3 First Crack Strength Data

	Reference Beta/Thinness	Ulimate Branch (P/P_y)	First Crack Load (P/F_yT^2)	Ultimate Load (P/F_yT^2)	Post-Crack Strength (%)
	Gibstein(6)				
1)	0.249/14.57	0.802	9.25	11.18	17.3
2)	0.525/14.70	0.432	13.55	16.82	19.4
3)	0.821/14.57	0.325	19.95	27.92	28.7
	Makino(10)				
1)	0.764/49.12	0.302	37.21	33.96	-
2)	0.763/35.97	0.203	30.77	29.76	-
3)	0.765/28.25	0.145	21.57	26.42	18.4
4)	0.282/28.56	0.380	14.08	17.03	17.3
5)	0.470/28.21	0.355	15.69	19.60	20.0

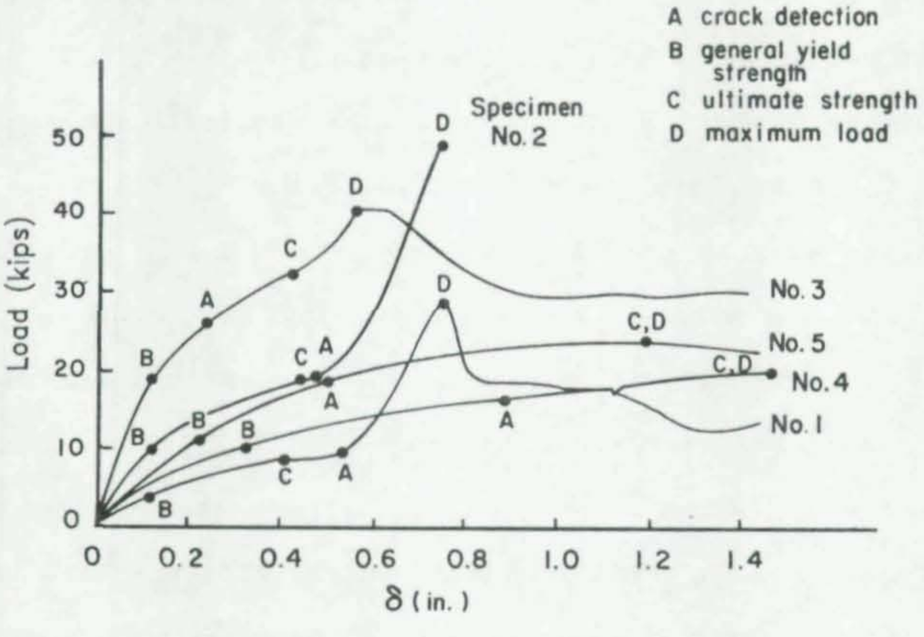

Figure 2.3 Makino Test Data

The definitions shown in Fig. 2.3 were those developed by Makino, and they are not stated in his paper. Tests 1 and 2 were with very thin specimens that had thinness ratios of 49.12 and 35.97 respectively. Specimens 1 and 2 had large increases in stiffness after first crack. Therefore, the ultimate load was taken as the maximum load before the stiffness increase. Tests specimens 3 through 5, had approximately the same thinness, 28, but different β values. Test 3, $\beta = 0.765$, had behavior which was very close to tests 1 and 2, and the ultimate load was determined in the same way. Test 4, $\beta = 0.282$, has a load-displacement curve that reaches a maximum value on the graph, but it was not possible to determine whether the failure was a deformation limit or a sudden failure. Test 5, $\beta = 0.47$, looks much like a compression curve with a gradual reduction in stiffness as load is increased. The varying definition of ultimate load is not inconsistency by the author, but due to the differences in DT tension joint behavior. Details on the Makino test series is given in the Appendix.

Besides the ultimate limit state, Fig. 2.3 shows the other behavioral limit states: first crack, yield strength, and maximum load. The following chapters will focus on the first crack and ultimate limit states.

CHAPTER 3

TEST SPECIMENS, SETUP AND PROCEDURE

Test Specimens

Even though the test program had two distinct parts, DT joints with $\beta = 1.0$ and DT joints with $\beta = 0.34$, there were many similarities between the two. The following section will discuss the test specimens, setup, and procedure used during both parts of the program.

$\underline{\beta = 1.0}$. The specimen, which was identical to ones used in compression studies conducted during other phases of the tubular joint research program at the University of Texas, is shown in Fig. 3.1. The dimensions shown were specified for all but one of the tension specimens. In specimen T4, the chord length on each side of the branch was reduced to D/4 or 4 in. by cutting the basic specimen at the dashed locations in Fig. 3.1. The ends of the chord where left open with no flanges in order to get a conservative indication of chord length effects. The branch length was 4 ft 4 in. to fit the specimen into the testing apparatus while keeping the end fixture as far from the connection area as possible. The chord length was 11 ft 8 in., and the thinness ratio was 25.5 so that chord loading equipment used in previous phases could be used again. The chord length of eight times the chord diameter was selected to reduce any

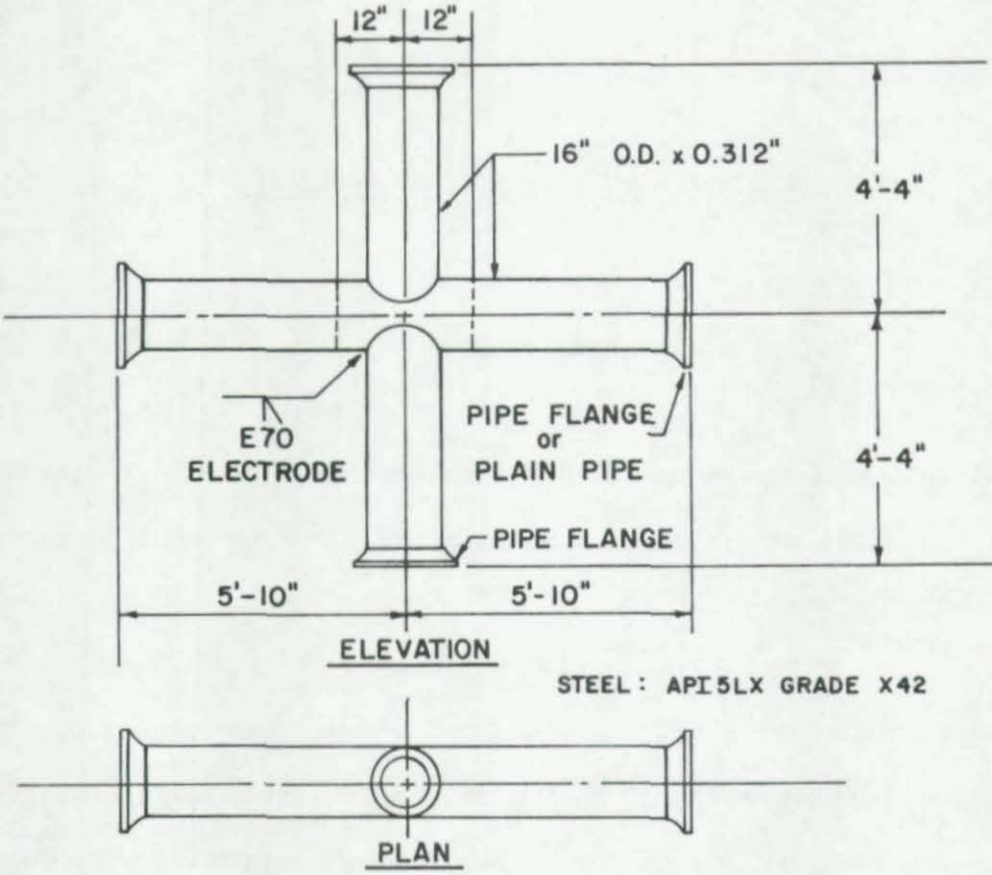

Figure 3.1 Specimen Detail $\beta = 1.0$

effects from the end flanges, and the thinness ratio was selected so that high chord stresses could be applied without high loads.

The specimens were fabricated by J. Ray McDermott, Incorporated, Morgan City, Louisiana. The specimens were made from API-5LX Grade X-42 welded line pipe. Both the branch and the chord are nomimally 16 in. O.D. with a 0.312 in. wall thickness. The section properties for all the test specimens are given in Table 3.1. All of the chord material came from the same heat, as did the branch material.

Table 3.1 Measured Specimen Section Properties

Size	O.D. (in)	Thick-ness (in)	Area (in^2)	I (in^4)	S (in^3)	Z (in^3)	P_y (kips)
16" Ø x 0.312"	16.04	0.314	15.513	479.75	59.82	77.66	758.6
5-9/16" Ø x 0.258"	5.608	0.262	4.400	15.758	5.62	7.49	174.2
5-5/16" Ø x 0.312"	5.320	0.322	5.056	15.853	5.96	8.05	345.3

In order to verify the material properties of the specimens, test coupons from several of the specimens were machined and tested in accordance with ASTM A370-77 Specifications for Standard Methods and Definitions for Mechanical Testing of Steel Products(3). Coupons were cut from the chord of a tested specimen away from the connection zone at 90 degrees from the weld seam. The results from the coupon tests are given in Table 3.2. Coupons A-1, A-2, B-1 and B-2 were fabricated from specimens used in the compression phase of the project while B-3 came from a tension test specimen. The compression and tension specimens were fabricated at the same time. The result for the coupon taken from the tension specimen is within 1% of the compression specimen coupon results. Therefore, an average of

Table 3.2 Tension Coupon Results

Location	Static Yield (ksi)	Dynamic Yield (ksi)	Ultimate Strength (ksi)	Percent Elongation (2-in. gage)
16" Ø X 0.312"				
A-1	48.9	50.6	64.2	48
A-2	48.7	50.3	64.7	46
B-1	49.0	50.8	64.8	46
B-2	48.7	50.2	64.3	46
B-3	49.4	51.7	64.1	37
Average	48.9	50.7	64.4	44
Mill Report	-	47.0	75.5	36
API 5LX(min)	-	42.0	60.0	24
5-9/16" Ø X 0.258" (Low Strength Branch)				
A-1	39.2	43.6	70.9	43
A-2	37.9	40.6	73.5	45
B-1	41.8	44.3	72.1	--
Average	39.6	42.8	72.2	44
Mill Report	-	42.0	67.3	35
ASTM A53-GrB	-	35.0	60.0	23
5-5/16" Ø X 0.312" (High Strength Branch)				
A-1	70.0	74.8	87.2	47
A-2	66.4	69.5	87.2	49
B-1	64.9	67.4	84.2	42
B-2	71.2	74.0	85.5	46
Average	68.1	71.4	86.1	46
Mill Report	-	60.3	80.2	33
ASTM A572-50	-	50.0	65.0	21

all the coupon specimens was used. The average static yield strength was 48.9 ksi.

The static yield point of the tensile coupons was determined by using the 0.2% offset method. The technique consisted of taking 3 to 4 static points, holding deformations for 5 minutes before recording the load, along the yield plateau and then using these point to extrapolate back to a 0.2% offset line. The interaction of the 0.2% offset line and the static yield strength line defines the static yield point. The percent elongation was calculated using a 2 in. gage length. Strain was measured using a 2 in. S1000-2 Tinius Olsen extensometer capable of measuring strains within 0.0001 in/in. The coupons were tested with a Tinius Olsen 120 kips Electromatic IV universal testing machine, which measured the load within 0.25%. A typical load-strain curve for one of the coupons is shown in Fig. 3.2.

$\underline{\beta = 0.34}$. The seven $\beta = 0.34$ joints were approximately the same except for the material used in the branches, as shown in Table 3.2 and Fig. 3.3. Four of the specimens had low strength branches to achieve a high P/P_y ratio, while three had high strength branches to obtain a low P/P_y ratio. All of these joint specimens were fabricated at the PMFSEL and were made from material removed from undamaged branch tubes of previously tested specimens, except for the high strength branch material which was

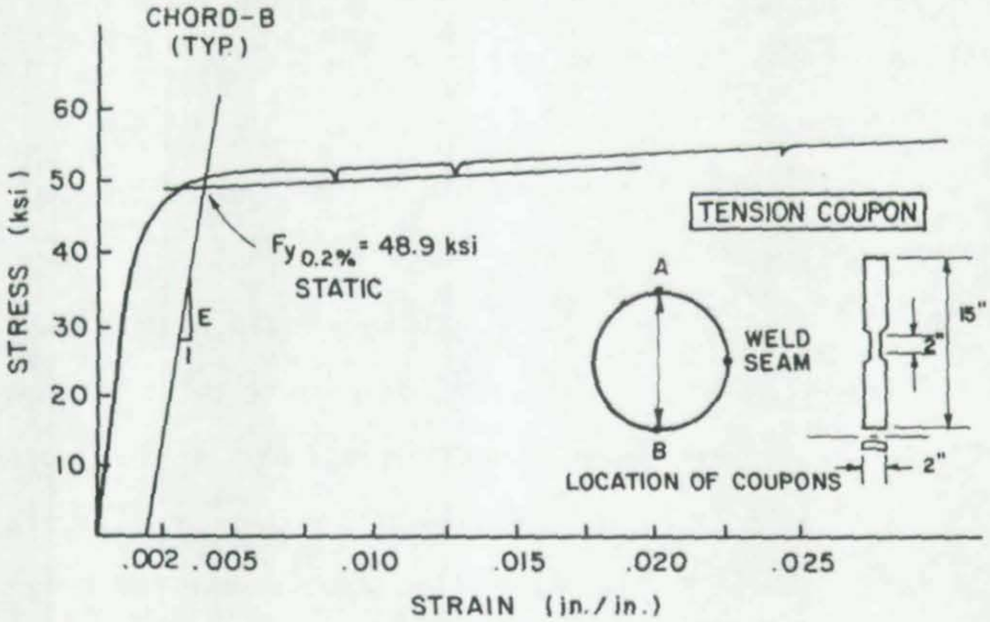

Figure 3.2 Coupon Load-Strain Curve

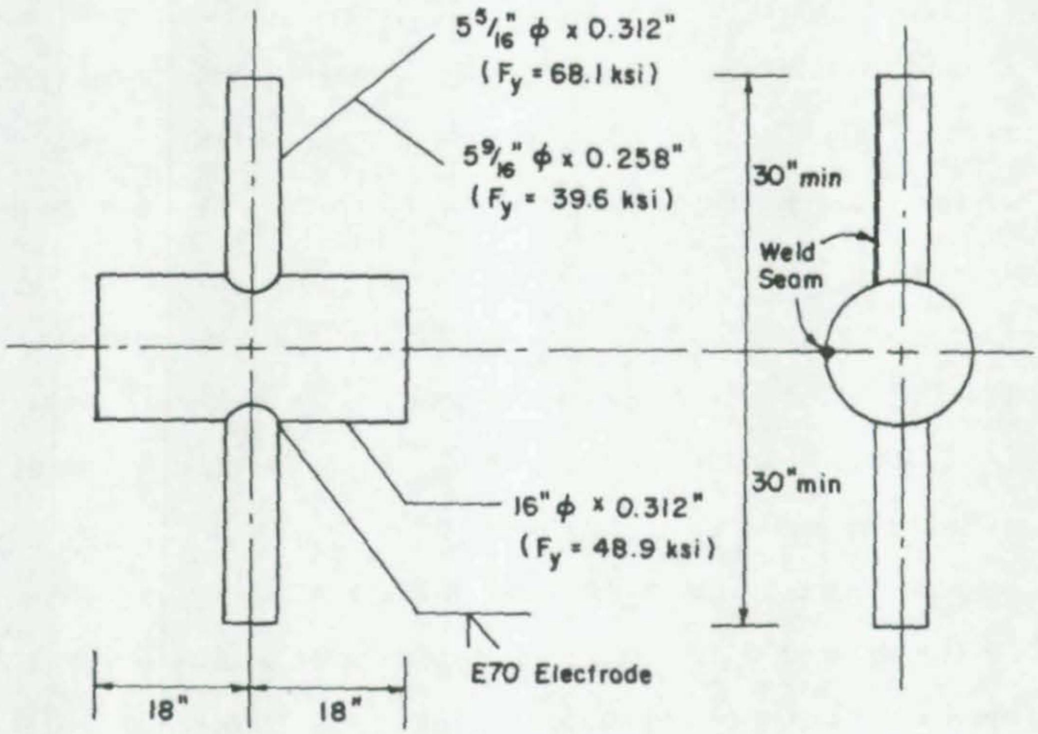

Figure 3.3 Specimen Detail β = 0.34

purchased. The chord material had nominal dimensions of 16 in. O.D. and a wall thickness of 0.312 in.. The low strength branch material had nominal dimension of 5-9/16 in. O.D. and a wall thickness of 0.256 in. The high strength branch material had nominal dimensions of 5-5/16 in. O.D. and a wall thickness of 0.312 in.. A summary of the sections properties is shown in Table 3.1.

Coupons were also tested for the materials used in the β = 0.34 joints. The same procedure and equipment were used for these tests as were used in the β = 1.0 coupon tests. The results from the tests are given in Table 3.2. The low strength branch had an average yield point of 39.6 ksi, while the high strength branch had an average yield point of 68.1 ksi.

In addition to the coupon tests, stub-column compression tests were also performed on each of the branch cross sections. The results from these two tests can be seen in Fig. 3.4 and Fig. 3.5. Since the low strength stub-column stress-deflection plot has a yield plateau, the static yield point, 44.7 ksi, was determined by taking the average of the points along the plateau. The stub-column yield was 12.9% higher than the coupon test results. The static yield point for the high strength column, 74.9 ksi or 10.0% higher than the coupon tests, was determined using the 0.2% offset method since there was no distinct yield plateau. The higher yield points than from the coupon tests is

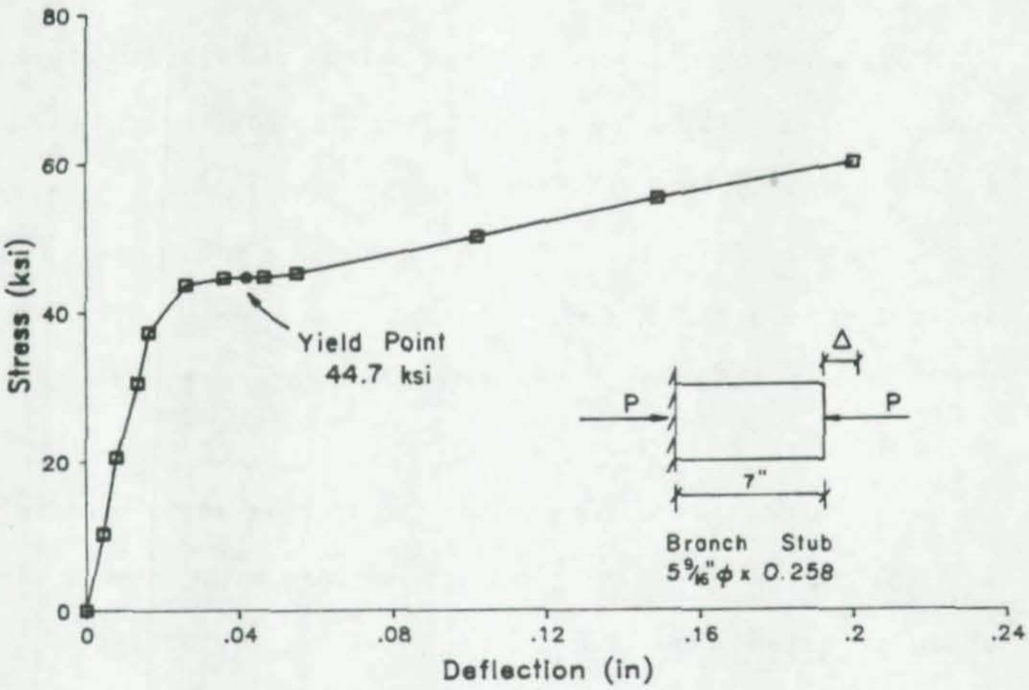

Figure 3.4 Low Strength Stub Column Test

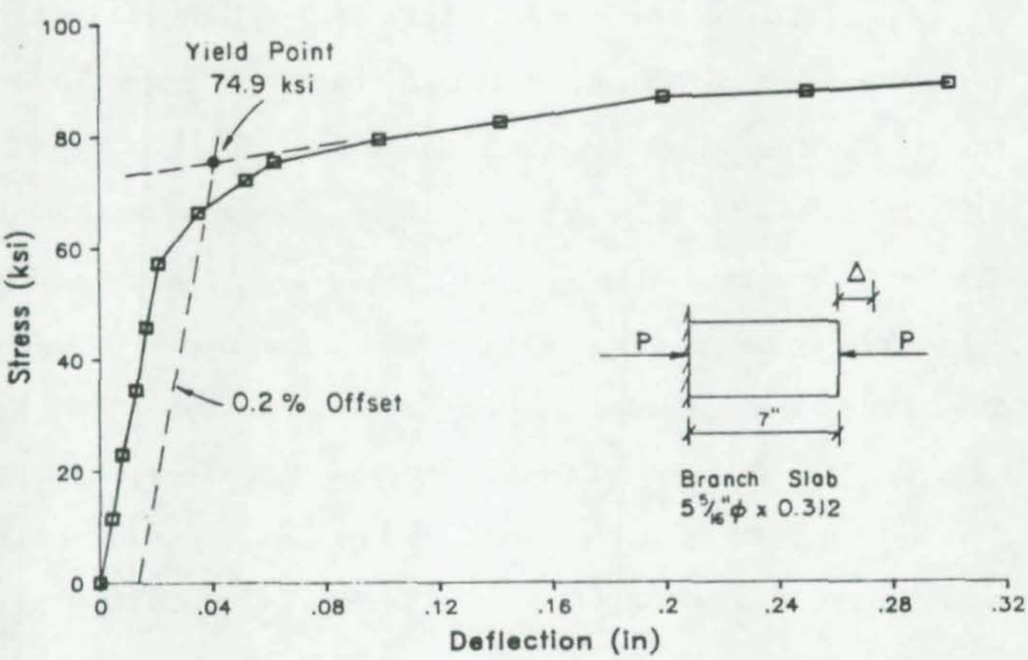

Figure 3.5 High Strength Stub Column Test

partially caused by the inclusion of the high strength weld material. Plus, the stub-column is not as sensitive to local effects. The coupon test results will be used in all calculations to be consistent with other reports.

Test Setup

Both the $\beta = 1.0$ and the $\beta = 0.34$ tests were conducted in a universal testing machine that has a capacity of 600 kips. A photo of the test setup is shown in Fig. 3.6. How the load was transferred and the types of loading cases varied depending on the β value. The unique aspects of each specimen group are described in detail in the following sections.

β = 1.0. Figure 3.7 shows a schematic diagram of the end fixture that was used to transfer the load from the test machine to the test specimen. Figure 3.8 is a photo of the fixture on a specimen.

One specimen with $\beta = 1.0$ was tested with a compressive chord load. The load was applied to the chord by four 200 kips centerhole hydraulic rams at one end of the chord acting with 4 rods, that were located inside the chord. The rods were connected to a flange plate at the other end of the chord. A schematic of the system is shown in Fig. 3.9, while Fig. 3.10 show the chord loading rams on the specimen.

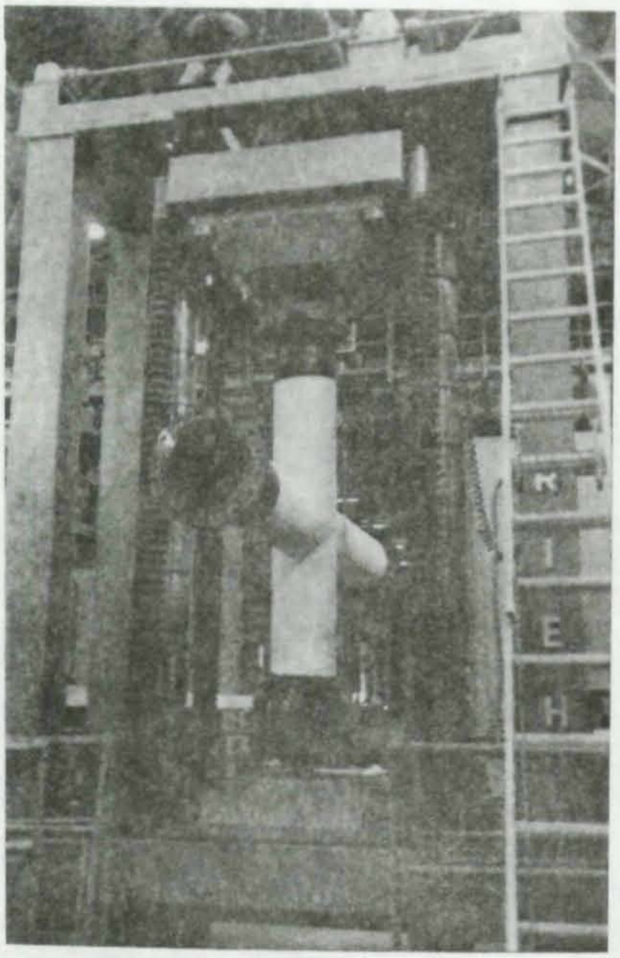

Figure 3.6 Test Setup

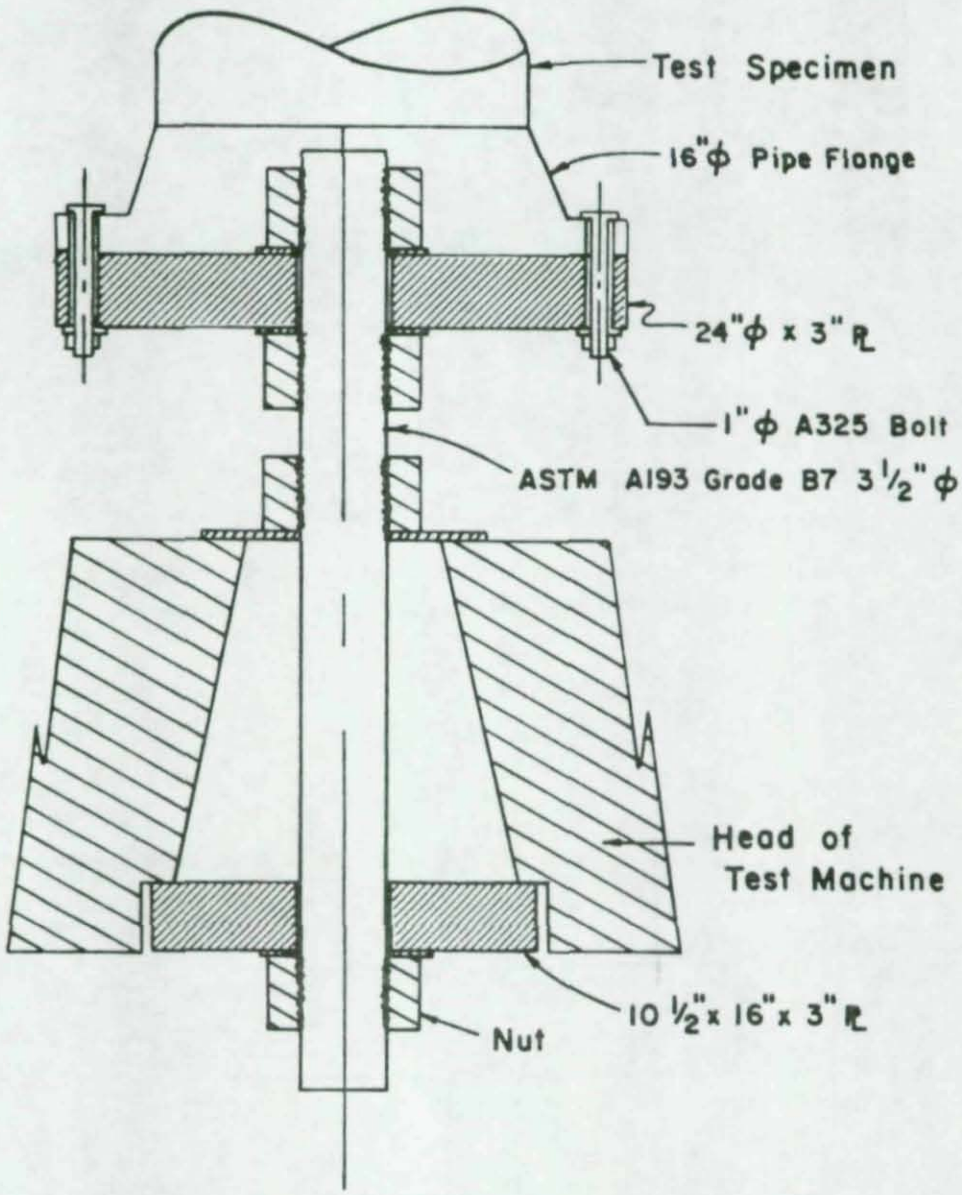

Figure 3.7 Detail of Load Transfer Mechanism

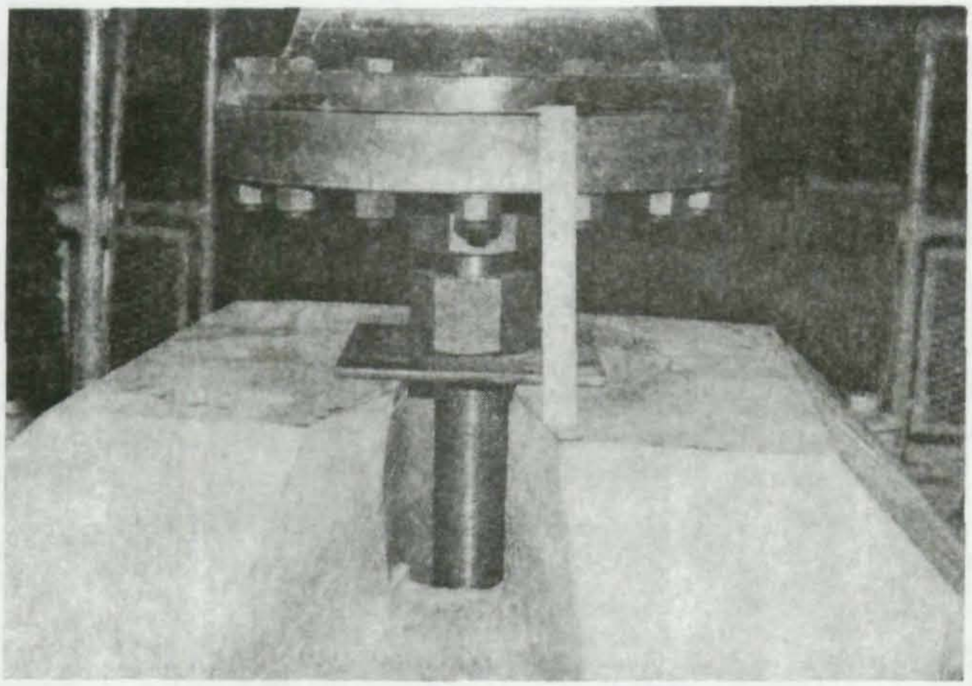

Figure 3.8 Load Transfer Mechanism from the Top of the Loading Head

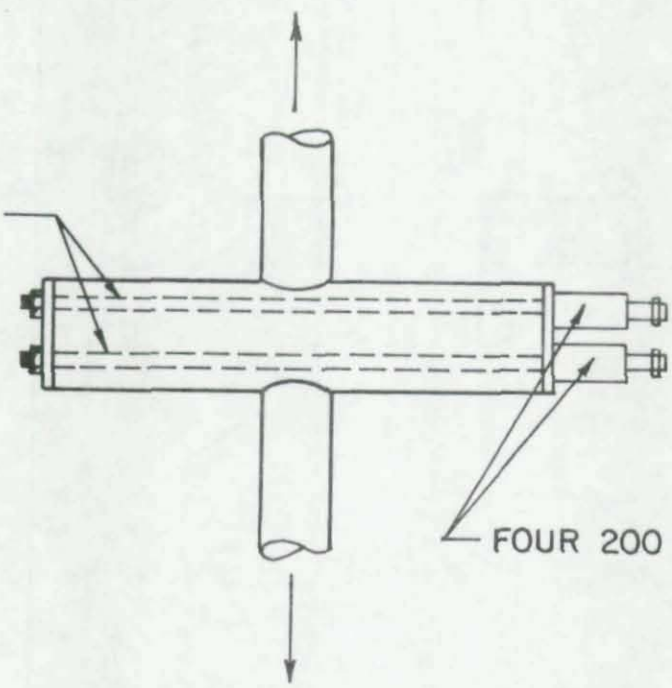

Figure 3.9 Chord Loading Schematic

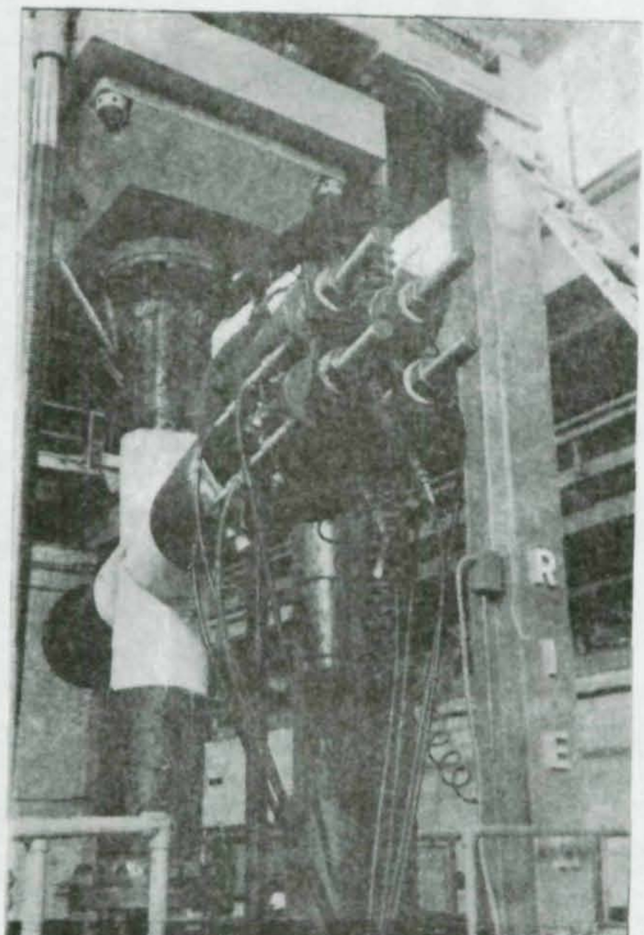

Figure 3.10 Chord Loading Rams

$\underline{\beta = 0.34}$. The $\beta = 0.34$ specimens had no flanges on the ends of the branches, so a different technique was used to apply the tension load to the branches. Standard tension grips supplied with the test machine were used to grip the specimen. Figure 3.11 shows the jaws in the clamped condition. In order to keep the jaws from crushing the hollow branch tube, stiffeners were welded in the ends of the branches, see Fig. 3.11 at the bottom of the branch tube. Both the jaws and the stiffeners only extended 6 inches down the branch, leaving a distance of three times the branch diameter between the top of the chord and the end of the jaws for the forces to become uniform.

Instrumentation

Load, displacement, chord load and chord strain were the types of measurements taken during the test program. The load was measured by the test machine load cells. The testing machine was calibrated and the load accuracy was within 0.2%. Joint displacement was measured by the relative displacement between two points along the branch, the points were approximately 52 in. apart for $\beta = 1.0$ specimens and 36 in. for $\beta = 0.34$ specimens(see Fig. 3.12). Two points on the specimen were used so that end slip would not be included in deflection measurements. The difference in the length between points was dictated by the specimen's dimensions. The devices used to measure the displacement were a mechanical dial gage accurate to

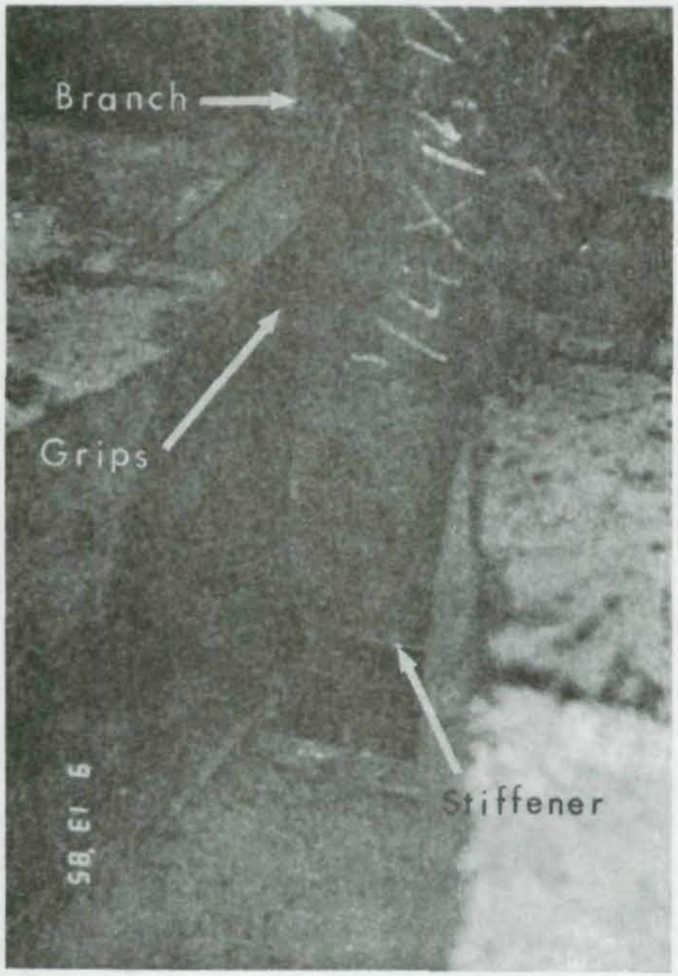

Figure 3.11 Clamping Jaws in Closed Position

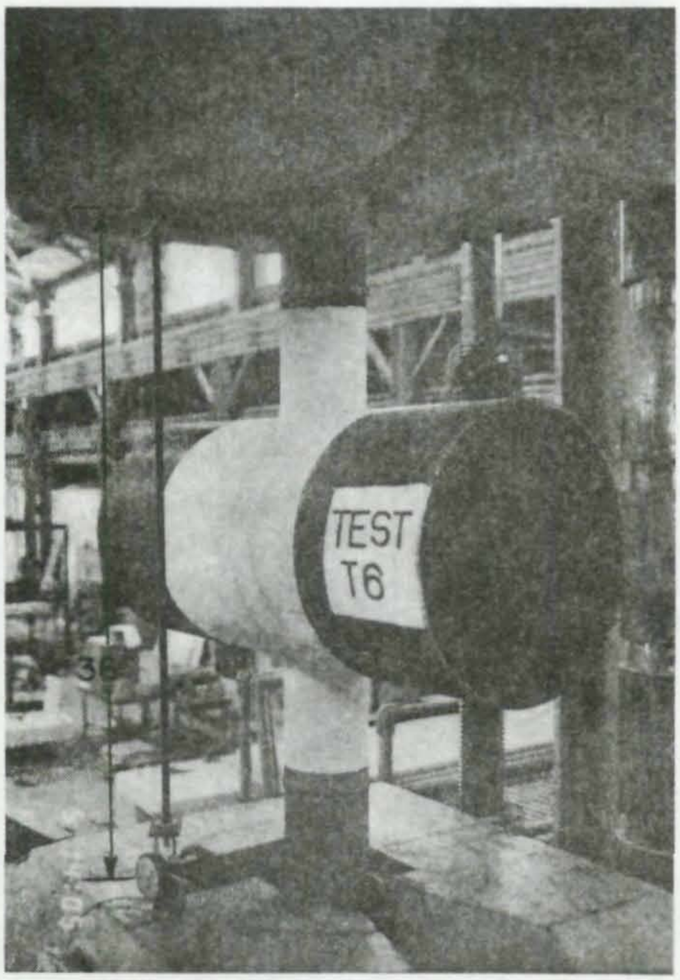

Figure 3.12 Joint Displacement Measurement

0.001 in. and a 2 in. linear voltage displacement transducers (LVDT's) accurate to 0.01 in.. The LVDT's were used to obtain a plot of the load-displacement relationship while the test was in

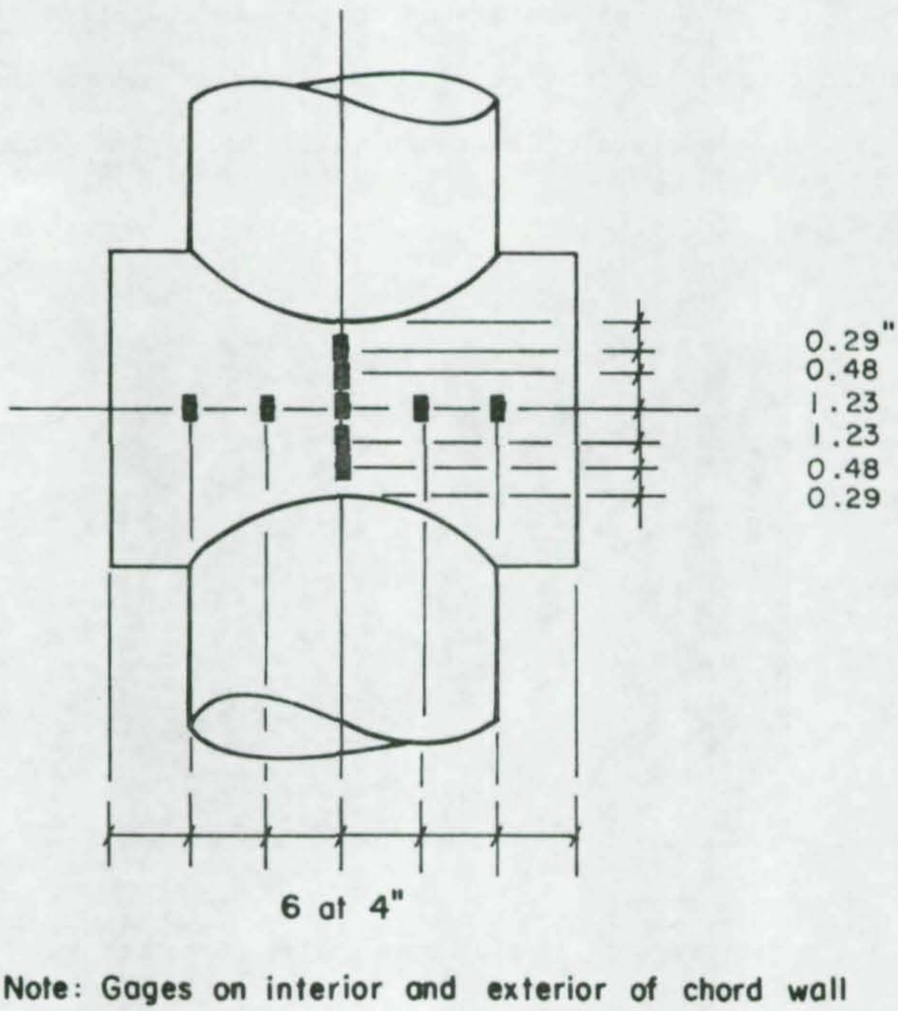

Figure 3.13 Strain Gage Locations

progress. The change in chord diameter was measured at the ends of the chord and at the branch centerline of some of the specimens. The measurement was taken by using large calipers and a scale. For the chord load test, the pressure in the chord rams was monitored by using a 10,000 psi electronic pressure transducer accurate to within 50 psi.

Eighteen single strain gages were applied to the specimen with the short chord, 9 on the interior surface and 9 on the exterior surface of the chord wall. All of the gages were

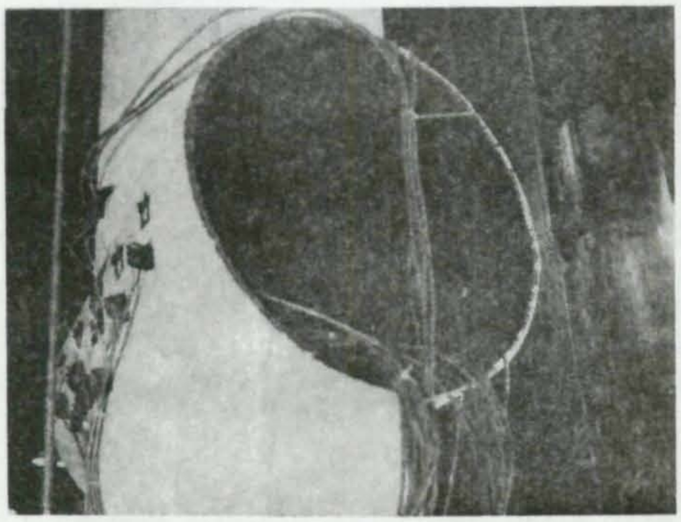

Figure 3.14 Strain Gages on Test Specimen

oriented parallel to the branch. Figure 3.13 shows the location of the strain gages along one of the chord walls. Gages were applied at the same locations on all chord faces, which permitted the strain gradients in the chord wall to be measured along with membrane stresses. The gage length of the gages was 0.125 in.. Figure 3.14 shows the specimen with the gages applied; gages can be seen both on the interior and exterior chord surface. The strains, loads and displacements for this test were recorded using a Hewlett-Packard 86 Data Acquisition System.

All of the specimens were whitewashed with a combination of lime and water prior to testing. The whitewash was used to detect yielding on the specimen. As the material yields, the brittle mill scale flakes away from the steel surface, causing the whitewash to also flake away from the surface.

Test Procedure

The same basic test procedure was used for all of the tests. At each load stage deflection readings were taken and the specimen was examined for yielding, crack initiation and/or crack propagation. As the loads moved into the inelastic range, a dynamic load was recorded and then after five minutes a static load was recorded. As cracks formed on the chord wall, very close attention was paid to whether the crack was a surface crack or a full penetration crack. First crack was defined as a surface crack that just penetrates the chord wall surface. This was very difficult to detect, because it was hard to tell the difference between a break in the mill scale and a base material crack. Crack growth was monitored by using a 60 power microscope that could be placed directly on the crack surface. A through-thickness crack was defined as one which penetrated through the entire wall thickness. The chords' of two $\beta = 1.0$ specimens, T2 and T3, were sealed at the ends and pressurized to 10 psi to determine when the first through-thickness crack occurred. When the crack penetrated the chord wall, the air would be detected leaking through the crack.

As the specimen approached failure, the interval between load stages was reduced in an effort to obtain a load stage close to failure. If failure was a sudden fracture, the maximum load was taken as the peak load minus the difference between the dynamic load and the static load of the previous load stage, and the failure deflection was recorded as the deflection just prior to failure. The ultimate load was then checked against the deflection limit of $\Delta_L = 60F_yd/E$. If the deflection limit was exceeded, the ultimate load was taken at the deflection limit.

CHAPTER 4

TEST RESULTS

The research program consisted of 12 DT tension tests, five with $\beta = 1.0$ and seven with $\beta = 0.34$. The particular characteristics of each test are given in Table 4.1 and are described in detail in the following sections. The numerical results for each test are reported in the Appendix.

Table 4.1 Test Characteristics

Test Designation	β	Test Characteristics
T1, T2 & T3	1.0	Reference
T4	1.0	Short Chord Length
TP4	1.0	Axial Chord Stress of $0.60F_y$
T6	0.35	Reference, Low Strength Branch
T7, T8 & T9	0.35	Low Strength Branch, F_y=39.6 ksi
T10, T11 & T12	0.33	High Strength Branch, F_y=68.1 ksi

β = 1.0 Tests

Figure 3.1, Table 3.1 and Table 3.2 give the dimensions and material properties of the DT joints. The investigation was divided into two parts:

1) three reference tests to establish the mean values and corresponding scatter bands, and
2) two tests to study the effects of chord length and chord load.

<u>Reference Tests(T1, T2, & T3).</u> The load-displacements curves of the three identical test specimens, T1, T2 and T3, are given in Fig. 4.1. The tests had very similar load-displacement curves and behavior. Therefore a detailed description of only Test T3 is given. None of the tests were controlled by the deformation limit of 1.61 inches.

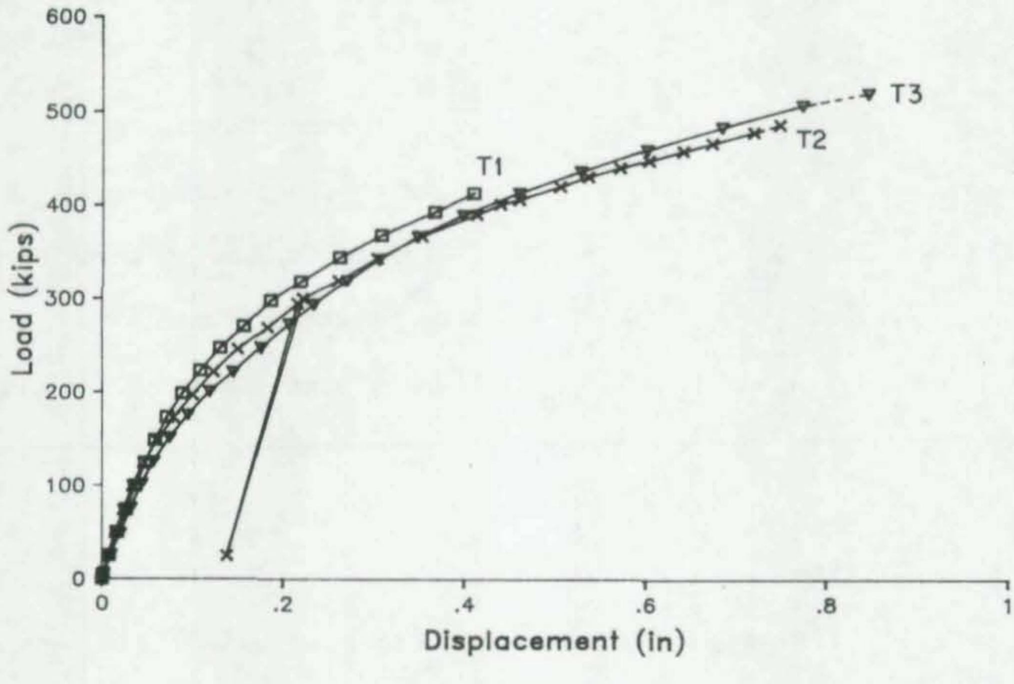

Figure 4.1 Load-Displacement Curves: Test T1, T2 & T3

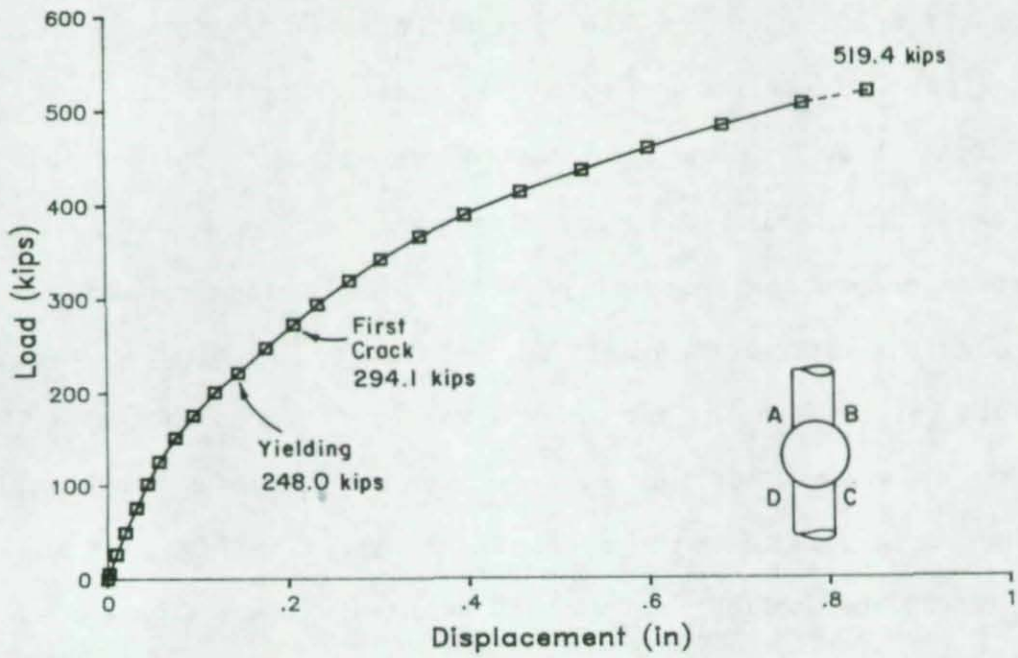

Figure 4.2 Load-Displacement Curve: Test T3

Figure 4.2 shows that test T3 behaved elastically until a load of 100 kips. The first yielding occurred at a load of 248 kips at the base of the weld toe in each of the four saddle regions, points A, B, C and D, the hot spot locations for axially loaded DT joints. At 273 kips, yielding started between the saddle points A and D at the centerline of the chord. By 275 kips, the portion of chord wall between both sets of saddle points had become straight as represented by the dashed lines in Fig. 4.3. The first surface crack, when the crack had penetrated the chord wall surface, occurred at 294.1 kips and was located two inches away from the branch centerline at location C. At a load of 437 kips, an additional surface crack was located one inch off of the branch centerline at location B. At a load of 460 kips, a surface crack formed at location B, approximately 2.0 inches away from the branch centerline, opposite the previous crack at B. During the remaining portion of the test, the surface cracks continued to grow but none of them penetrated through the entire chord wall until failure. Yielding between saddle points A and D, and B and C was confined to an area 4.5 inches in width. The yield surfaces and surface crack locations (black tick marks) on the specimen are shown in Figs. 4.4 and 4.5, where the applied load was 460 kips. The black tick marks, designate the location of surface cracks and the darkened regions are the yielded areas. At the failure load of 519.4 kips, a crack 11.50 inches in length formed at location A(see Fig. 4.6). An examination of the crack surface showed that the crack had penetrated through approximately half of the chord thickness, then at failure propagated quickly through the remaining material and grew to its final state. On the side of the specimen opposite the fracture, the chord wall was still intact but there were large yield surfaces at the centerline of the chord and at each weld toe in the saddle region(see Fig. 4.7). The length between the saddle points was 31% longer than at the start of the test.

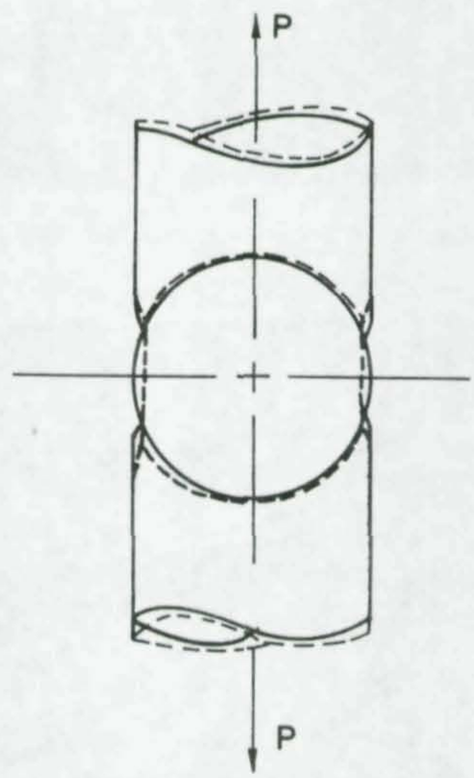

Figure 4.3 Chord Deformation Between Saddle Points

Figure 4.4 Surface Cracks in T3: Side AD

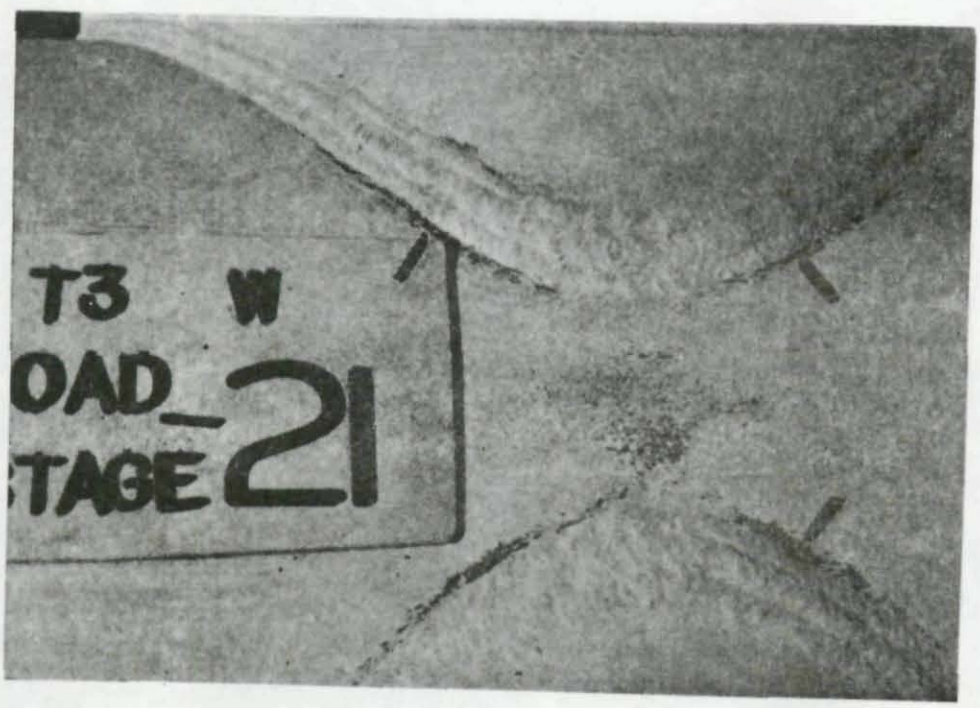

Figure 4.5 Surface Cracks in T3: Side BC

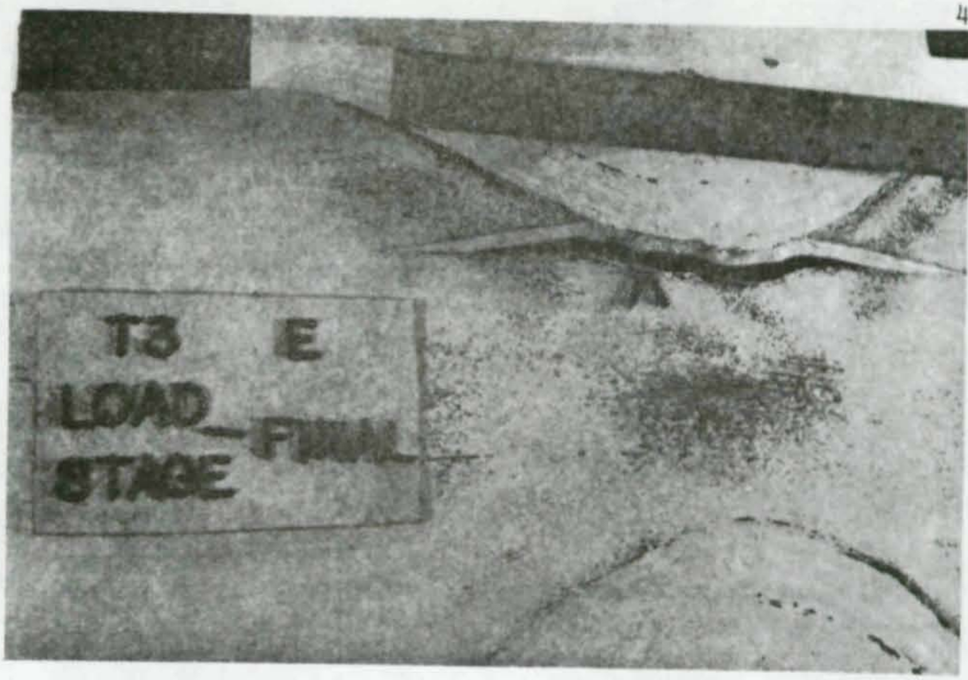

Figure 4.6 Fracture of T3

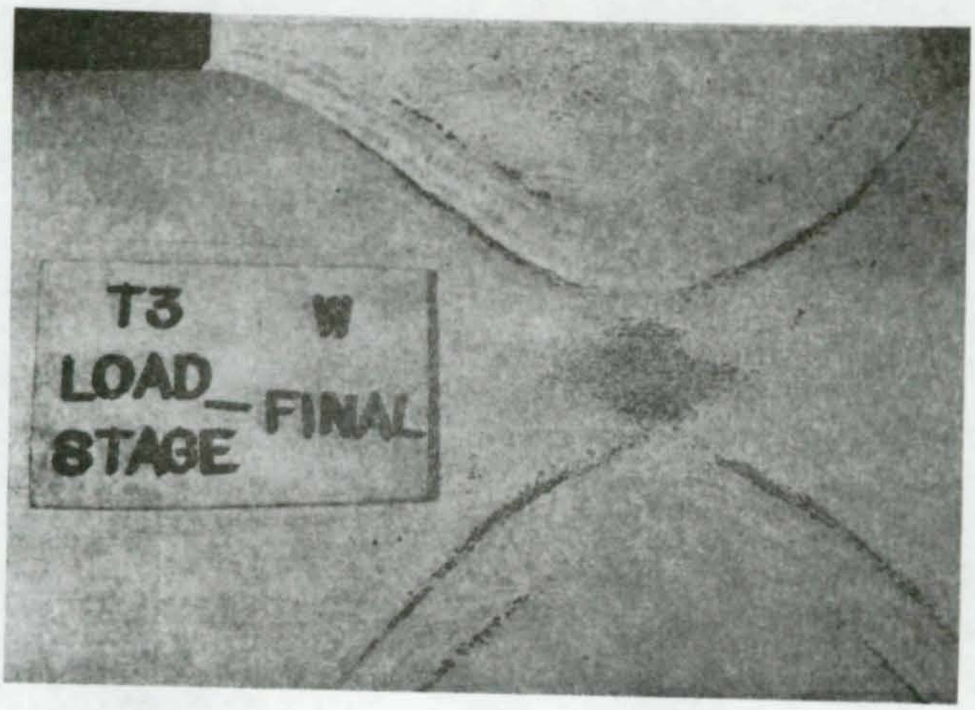

Figure 4.7 Non-Fracture Side of T3 at Failure

Table 4.2 gives summary of the results from all the reference tests. Table 4.2 shows the first crack load, the ultimate load and the location of the fracture that caused failure. Also shown is the final deflection reading before failure minus the elastic branch deformation, and the initial gap between saddle points on each side of the specimen. The load history was slightly different for all the tests. In test T1, the specimen was unloaded and then reloaded when the specimen had become inelastic to determine if the joint would behave elastically during unloading. The slope of this portion of the load-displacement curve matched with the elastic slope(see Fig. 4.1).

Table 4.2 $\beta = 1.0$ Test Results

Test No.	First Crack (kips)	Ultimate Strength (kips)**	(Deflection - PL/AE*) (in)	Initial Gap AD (in)	BC
T1	296.2	413.2 (B)	0.322	3-3/4	3-5/8
T2	295.2	491.5 (A)	0.694	3-15/16	3-9/16
T3	294.1	519.4 (A)	0.714	4-1/4	2-5/8
T4	342.1	475.2 (B)	0.658	2-7/8	3-5/16
TP4	408.1	461.3 (D)	0.775	3-3/4	4

* Deflection and load at load stage before failure
L = 52 in., which was the distance between the points used to measure deflection

** The letter in parenthesis is the location where fracture occured.

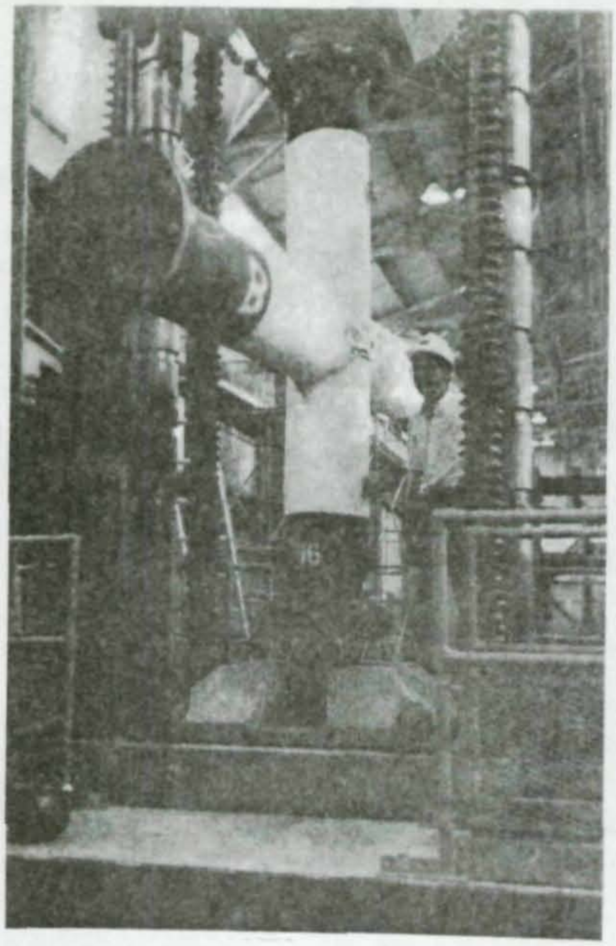

Figure 4.8 Test T2 at Failure

In test T2 and T3, the ends of the chord were sealed and the chord was pressurized and maintained at 10 psi in an effort to verify that the first through-thickness crack occurred at failure. Figure 4.8 shows specimen T2 at failure note that the ends of the specimen are sealed. The ends were sealed with two three-quarter inch pieces of plywood nailed together, bolted on to the end flanges and then sealed with silicon seal. It was felt the amount of air pressure would not effect the performance of the specimen. No leaking air was detected around the weld toe area until failure for both Test T2 and T3, therefore no full penetration cracks took place until the specimen had failed.

Chord Length Test(T4). In test T4, a short chord length was used to determine the amount of strength the DT tension joint obtains from the chord outside the connection region. The load-displacement curve is shown in Fig. 4.9. The maximum displacement is below the displacement limit of 1.61 in.

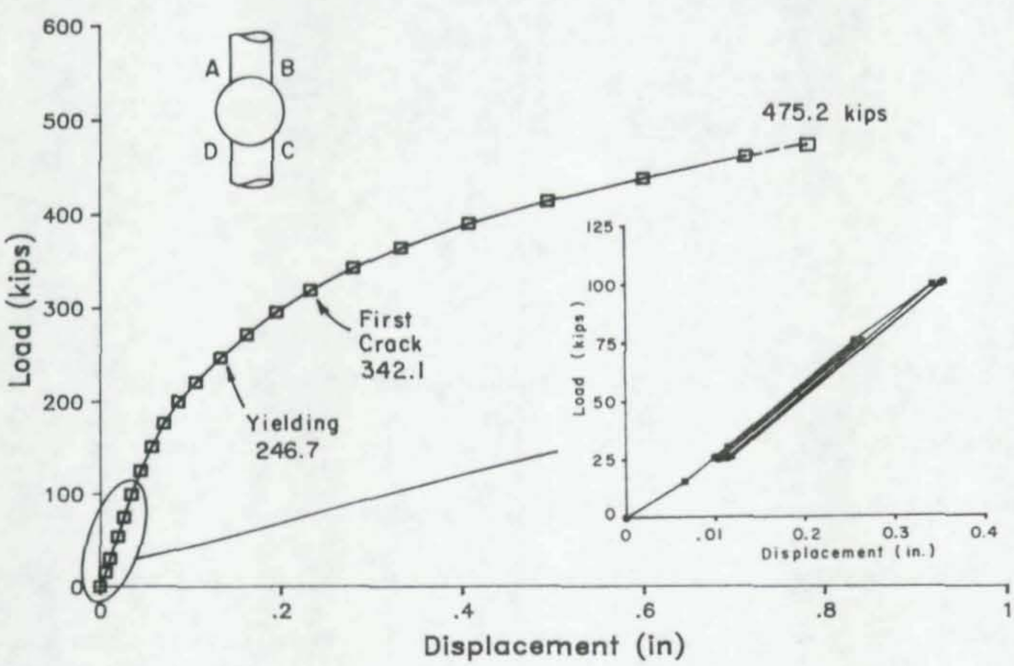

Figure 4.9 Load-Displacement Curve: Test T4

The specimen's behavior was very similar to that described for test T3. The specimen remained elastic through 125 kips. Yielding was first seen at 246.7 kips. The first surface crack occurred at 342.1 kips at location B. When the load reached 460 kips the area of chord wall between the saddle points had become greatly distorted. Figure 4.10 shows the change in the chord diameter at the branch centerline(I) and the end of the chord(II). Failure occurred at 475.2 kips when the surface crack, first noticed at 342 kips at location B, propagated through the chord wall. The final joint condition can be seen in Fig. 4.11. The final crack length was 15.5 inches.

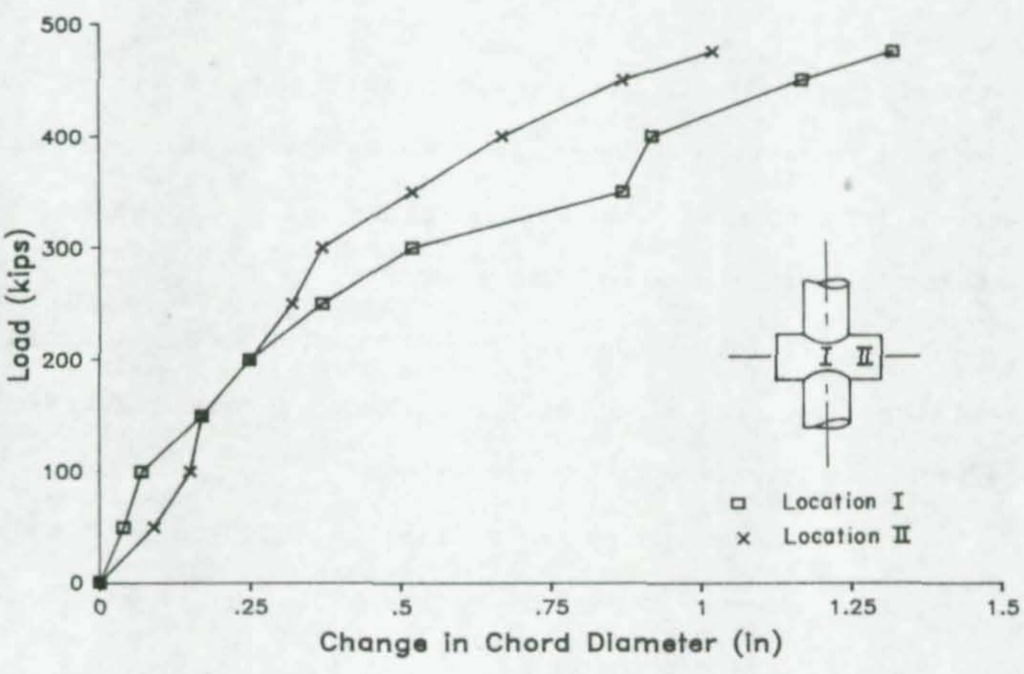

Figure 4.10 Chord Deflection Test T4

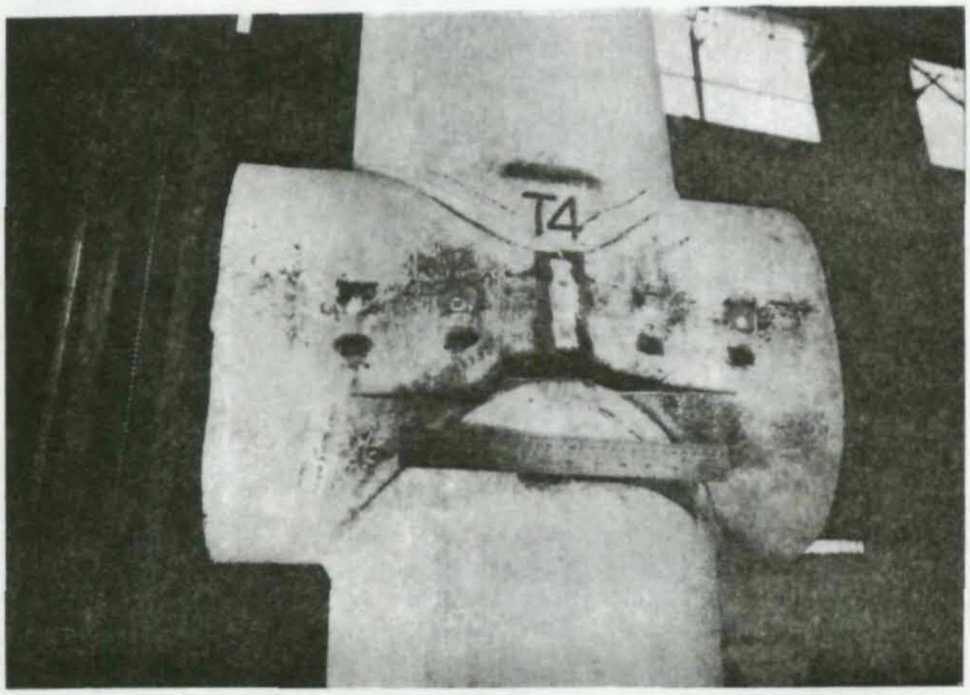

Figure 4.11 Test T4 at Failure.

On the side opposite of the fracture, yielding had occurred but there were no through-thickness cracks. At the conclusion of the test the length between the saddle points had elongated by 18%. Test statistics are shown in Table 4.2.

During Test T4 many more load stages were taken because strain reading were also being recorded. Strain gages were applied to the specimen for three reasons:

1) to determine the stress distribution across the chord length both on the inside and the outside of the chord wall,

2) to determine the stress distribution between the upper and lower saddle points, and

3) to determine the strain concentration factor at the saddle points.

This report presents data related to the first two objectives, while the data for the third objective is contained in Ref. 16. Relationships between the strain gages will be discussed in Chapter 5.

Chord Load Test(TP4). In test TP4, chord load was applied to the specimen to determine if chord stress affected the first crack or ultimate strength of the joint. The load-displacement curve can be seen in Fig. 4.12.

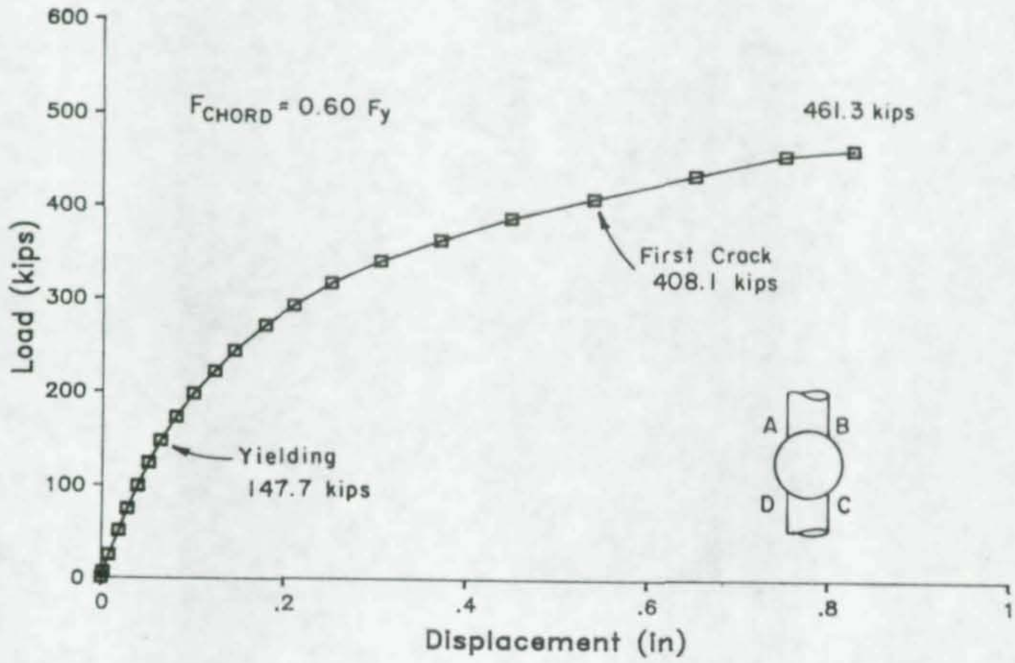

Figure 4.12 Load-Displacement Curve: Test TP4

As in test T4, the behavior was very similar to test T3. The test remained in the elastic range until a load of 125 kips. First sign of yielding occurred at 147.7 kips at locations B, C and D. Figure 4.13 shows the development of the yield surface at a load of 251 kips. By 377 kips yielding had occurred

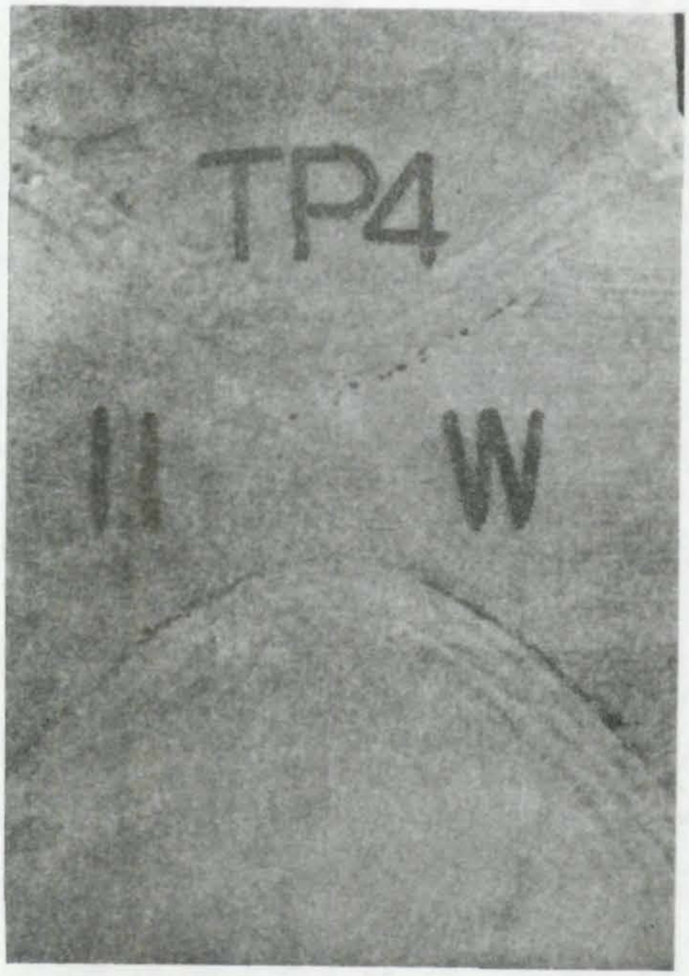

Figure 4.13 Yield Surfaces of TP4 at 251 kips

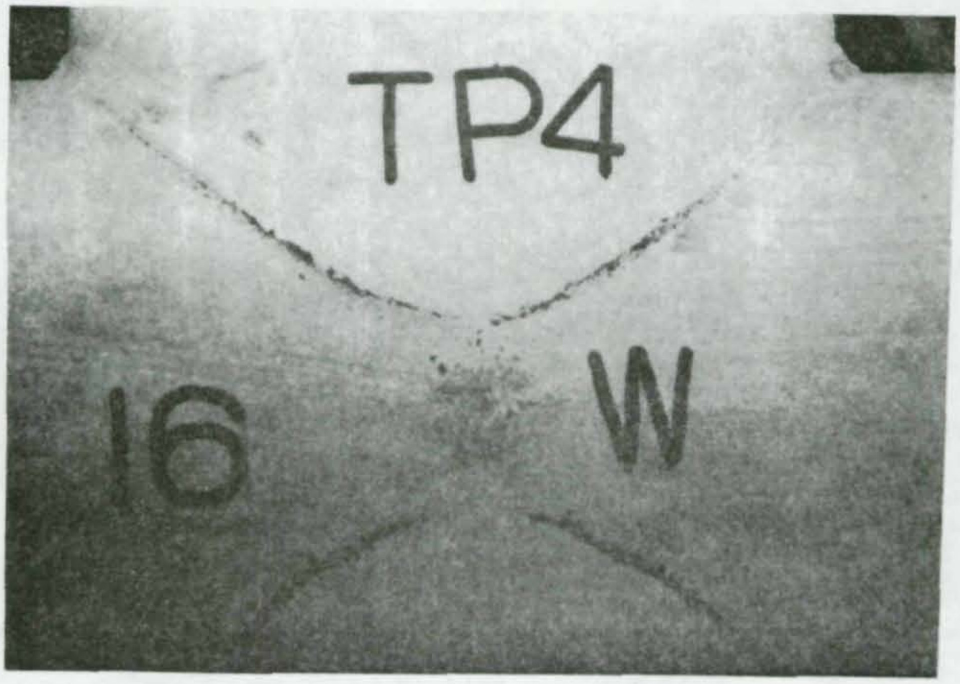

Figure 4.14 TP4 at 377 kips

between saddle points, as shown in Fig. 4.14. The first surface crack occurred at a load of 408.1 kips at location B. Failure occurred at location D at a load of 461.3 kips. The initial through-thickness crack size was 2 inches long and with further straining grew to 15 inches. The specimen at failure can be seen in Fig. 4.15. Yielding between the saddle points was restricted to a band approximately 5 in. wide until failure. When the specimen fractured, yield surfaces formed away from the branch centerline on the fractured side. Figure 4.16 shows the non-fractured side of the specimen where there were large yield surfaces at the chord centerline and along the weld toes in the

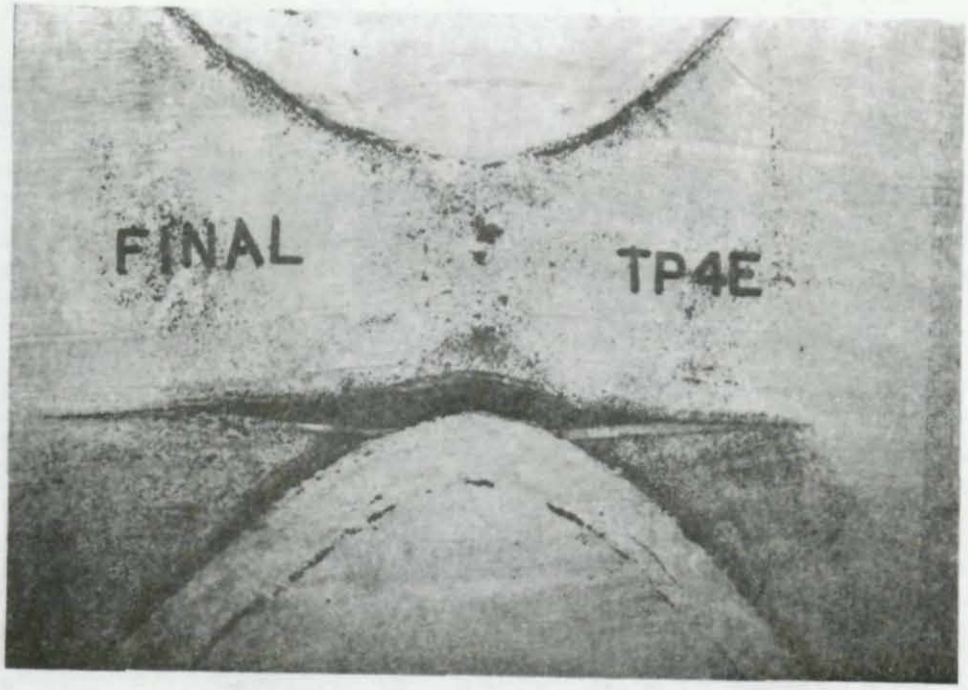

Figure 4.15 Fracture of TP4

Figure 4.16 Non-Fracture Side of TP4 at Failure

saddle region. The non-fractured side of the specimen had elongated by 28% at the end of the test. Test statistics are shown in Table 4.2.

$\underline{\beta = 0.34}$ Tests

The purpose of the $\beta = 0.34$ tests was to study the effect of the branch load to branch yield strength ratio on the ultimate strength of the joint. Figure 3.3, Table 3.1 and Table 3.2 give the dimension and material properties of the specimens. The program can be divided into three parts:

1) one test on general joint behavior(T6),
2) three tests on joints with low strength branches(T7, T8 & T9), and
3) three tests on joints with high strength branches(T10, T11 & T12).

General Joint Behavior(T6). The branches for T6 were made from the low strength(F_y=39.6 ksi) steel. The load-displacement curve of test T6 is shown in Fig. 4.17. The load was still increasing when the test was stopped due to large chord deformations. Figure 4.18 shows the diameter deformation history of the chord ends during test. By the end of the test the 16 in. diameter chord had been stretched to 19.4 inches in the direction of the load. Figure 4.19 shows the final condition of the chord, which was at a load of 53.1 kips. The first surface cracks were detected at 33 kips at all saddle points, whereas the first through-thickness crack occurred at 49 kips. Once the crack had penetrated the chord wall, the fracture started to unzip around the weld toe surface. Figure 4.20 shows the fracture at the conclusion of the tests; the crack had unzipped one-third around the weld. When the deformation limit of 0.56 in. is applied, the ultimate load drops to 23.3 kips. This test can not be used to study the effects of P/P_y because the chord failed and not the connection. The effective chord *region was not large enough to carry the branch force (See Fig.* 1.5). But the test does indicate that a $\beta = 0.34$ joint receives much of its strength from the chord outside the weld region. The

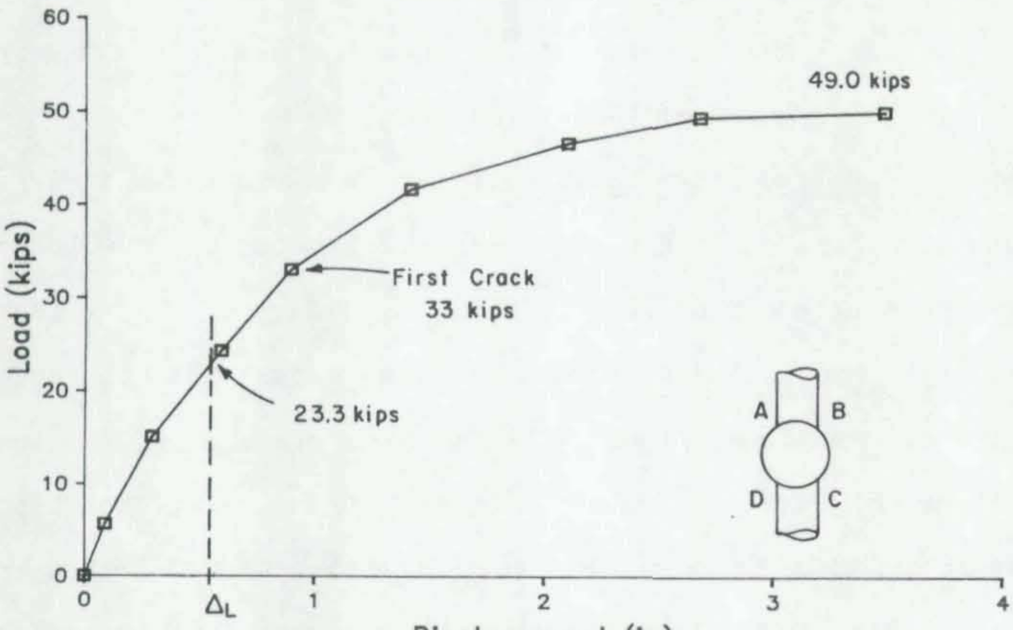

Figure 4.17 Load-Displacement Curve: Test T6

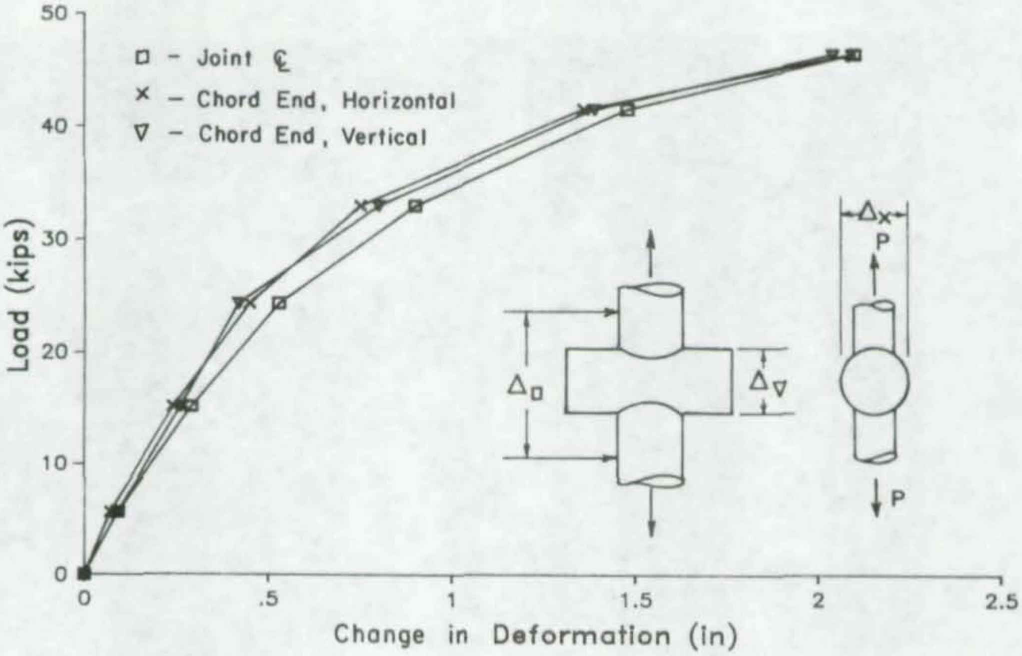

Figure 4.18 Diameter Deformation History: Test T6

Figure 4.19 T6 Chord at Failure

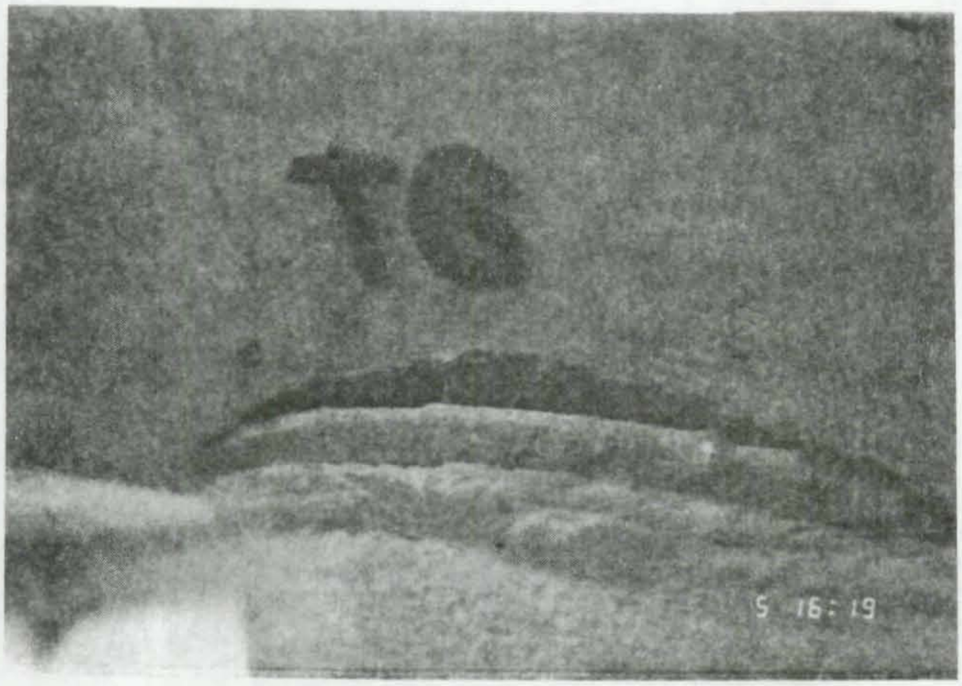

Figure 4.20 T6 Weld Toe at Failure

joint configuration used for T6 was originally designed for all of the $\beta = 0.34$ joints. Due to the results of this test, the ends of the chord were stiffened in all other $\beta = 0.34$ tests to force a connection failure.

Low Strength Branch Tests(T7, T8 & T9). The three low strength branch tests had an average branch yield strength of 39.6 ksi. The specimens were identical to specimen T6, except that stiffeners were added to the ends of the chord to prevent the chord from deforming.

The load-displacement curve for test T7 is given in Fig. 4.21 and Fig. 4.22 shows the detail of the chord end stiffeners. Surface cracking was first observed at 48.1 kips at all of the saddle hot spot location. At a load of 57 kips, the weld on one of the end braces fractured(see Fig. 4.23), and the load dropped to 43.5 kips. The end of the chord was then clamped(see Fig. 4.24) which prevented further chord deformation. Failure took place at 74.8 kips when the crack at location D penetrated through the specimen wall. As soon as the load was reapplied to the specimen, crack surfaces opened up at other hot spots and no additional load could be carried. Figure 4.25 shows the final weld toe condition. The deformation limit,

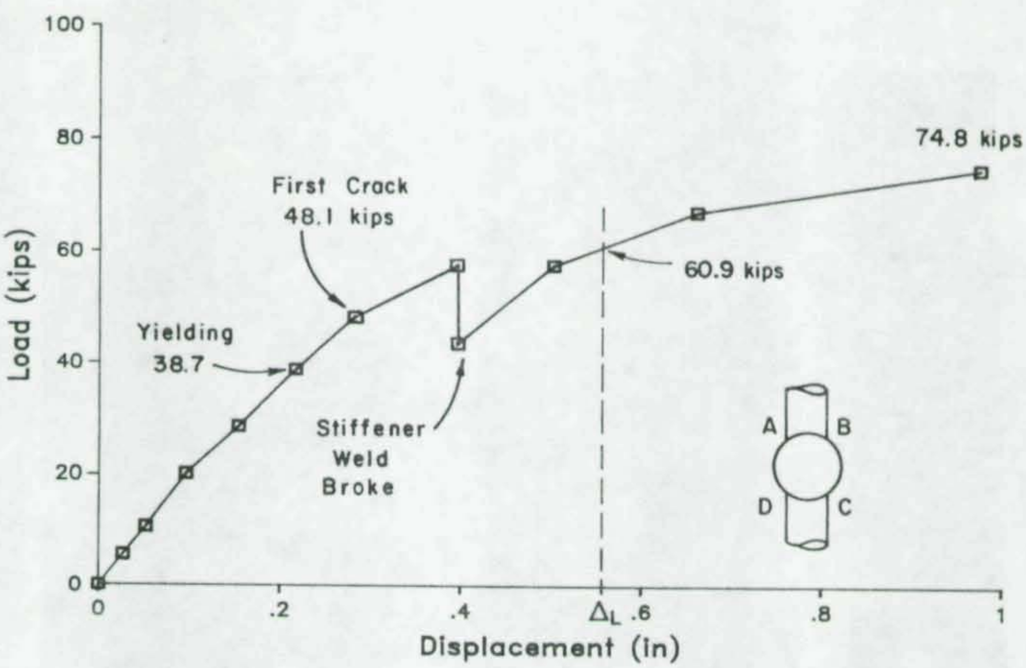

Figure 4.21 Load-Displacement Curve: Test T7

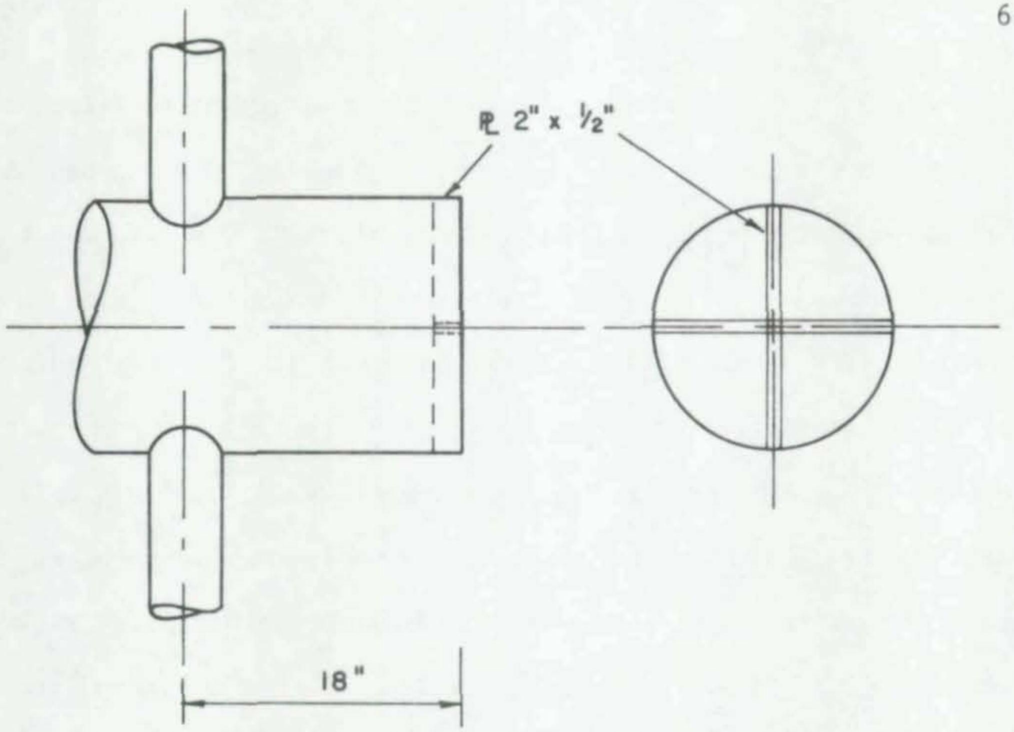

Figure 4.22 Detail of End Stiffeners Specimen T7

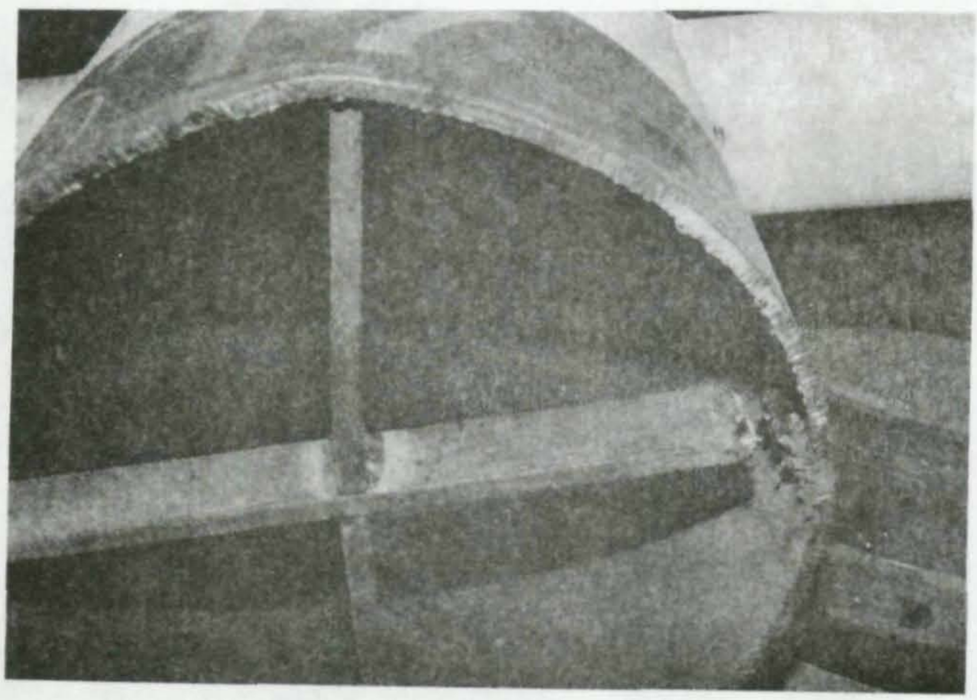

Figure 4.23 Snapped Weld on T7 Stiffener

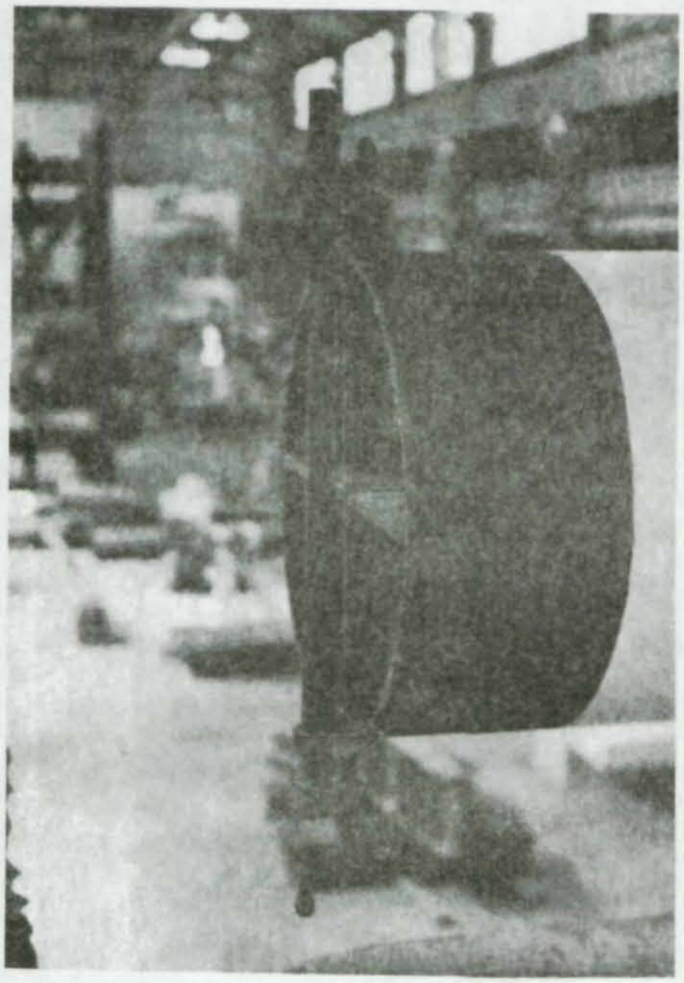

Figure 4.24 Temporary Brace on T7

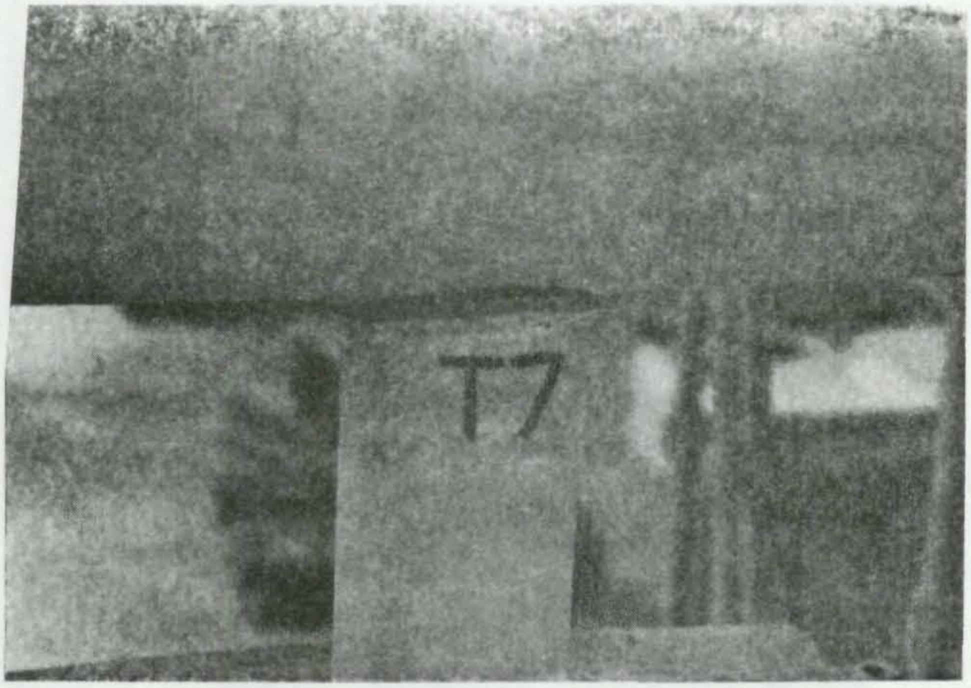

Figure 4.25 Final Fracture Surface T7

0.56 in., controls the ultimate load but the displacement readings were inaccurate because of the weld break. Therefore, the test can not be used in the post-crack strength results, but it does show that the entire chord length is being utilized by the joint.

After the failure of the stiffener weld in test T7, the width of the stiffeners for tests T8 and T9 was increased from 2 in. to 4 in. plate to increase the weld length. Figure 4.26 shows specimen T8 before testing. The load-displacement curves for tests T8 and T9 are given in Fig. 4.27. The tests

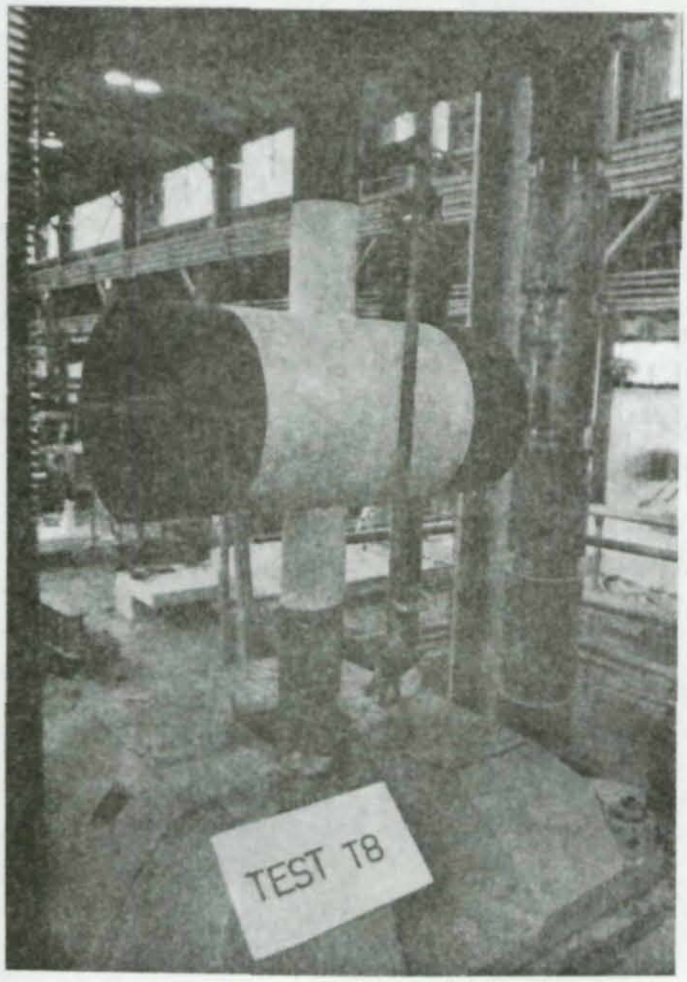

Figure 4.26 Specimen T8

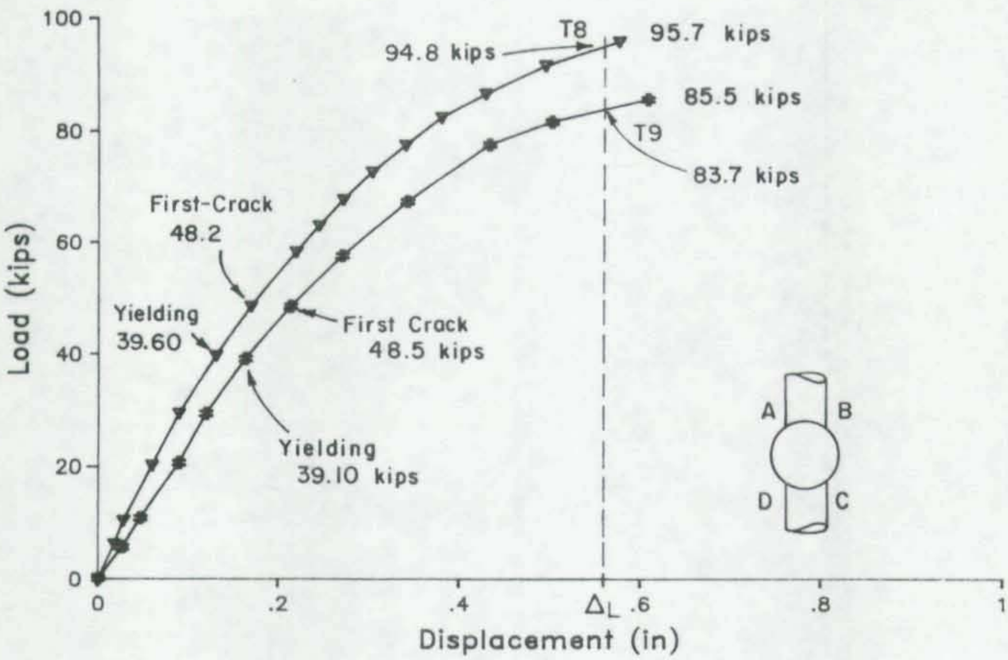

Figure 4.27 Load-Displacement Curves: Test T8 & T9

behaved very similarly, so a detailed description of only test T9 is given below.

First yielding occurred at 39.1 kips at all four weld toes. The first surface cracks were observed at 48.5 kips at all four hot spot locations. By 82 kips, the surface cracks had begun to open up but no through-thickness crack could be seen on the inside of the chord wall. The crack surface at location D was the largest and is shown in Fig. 4.28. At the same load, the inside chord wall at the branch connection, shown in Fig. 4.29, indicates a large yield surface ring but no surface cracks, At 85.5 kips, the crack at location D propagated through the chord wall to form a full penetration crack. Upon reapplication of the load, no load higher than 85.5 kips could be applied and the crack expanded around the weld toe surface at location D and an additional through-thickness crack opened at location C. Figure 4.30 from test T8 shows the failure mode for the low strength branch tests and the extent of chord deformation along its length. The deformation limit controlled the ultimate load for both T8 and T9, but the deformation limit is so very close to the

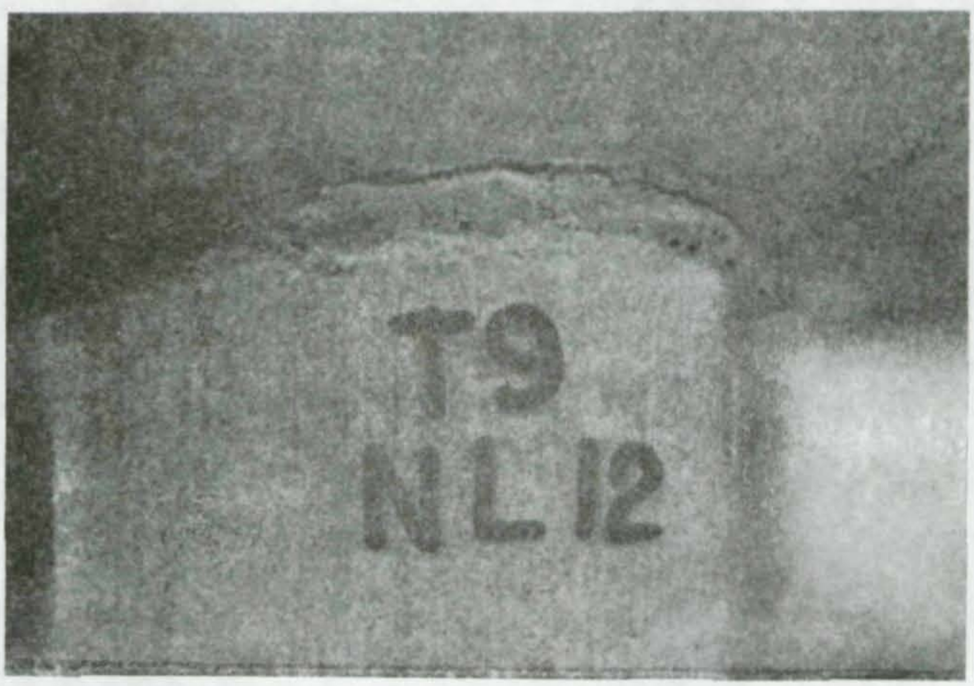

Figure 4.28 Surface Cracking: Test T9

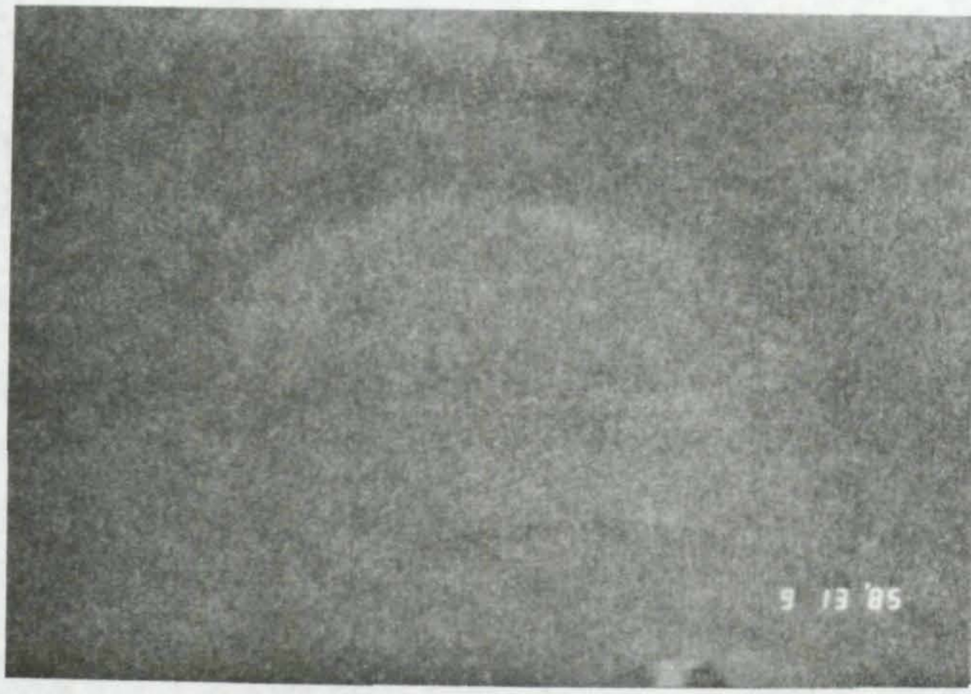

Figure 4.29 Interior Chord Surface Before Full Penetration Crack

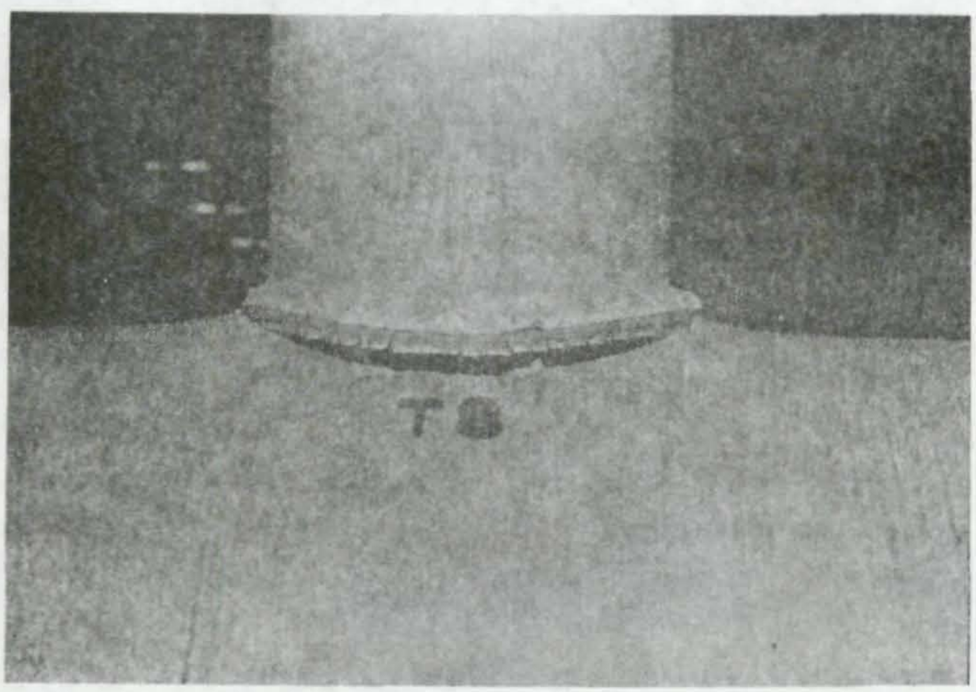

Figure 4.30 Chord Deformation at Failure

Table 4.3 $\beta = 0.34$ Test Results

Test Designation	First Surface Crack (kips)	Deformation Limit Load (kips)	Ultimate Load (kips)
T7	48.1	*	74.8
T8	48.2	94.8	95.7
T9	48.5	83.7	85.5
T10	47.8	na	84.9
T11	47.1	na	83.8
T12	53.3	75.4	82.7

* -Deformation should have controlled
na-not applicable

actual failure. The ultimate load for T8 and T9 will be reported as 95.7 and 85.5, respectively. A summary of low branch strength test data are given in Table 4.3.

High Strength Branch Tests(T10, T11, T12). The three high strength branch tests had a branch yield strength of 68.1 ksi. The specimen specifications were identical for all three tests. The specimens had the dimensions shown in Fig. 3.3 and, as in tests T8 and T9, 4 in. stiffeners were welded at the ends of the chord. Figure 4.22 shows the 2-inch brace detail. The load-displacement curves for T10, T11 and T12 are shown in Fig. 4.31. The deformation limit for the three tests was 0.54 in.. The three test have very close ultimate strength values, but the load-displacement curve for test T11 is different. Unlike the other joints, the joint in test T11 gained stiffness in the middle of the test which is questionable. The gain in stiffness could be caused by slippage of the deflection gage or by the straighting of the branch members. Since the deformation limit is not greatly affecting the ultimate strength values for the other high strength tests, the test can be used in the post-crack study. For future reference, the problem could have been resolved, if deflection gages had been placed on both sides of the specimen. The other two tests, T10 and T12 are very similar, therefore only a description of test T12 is given.

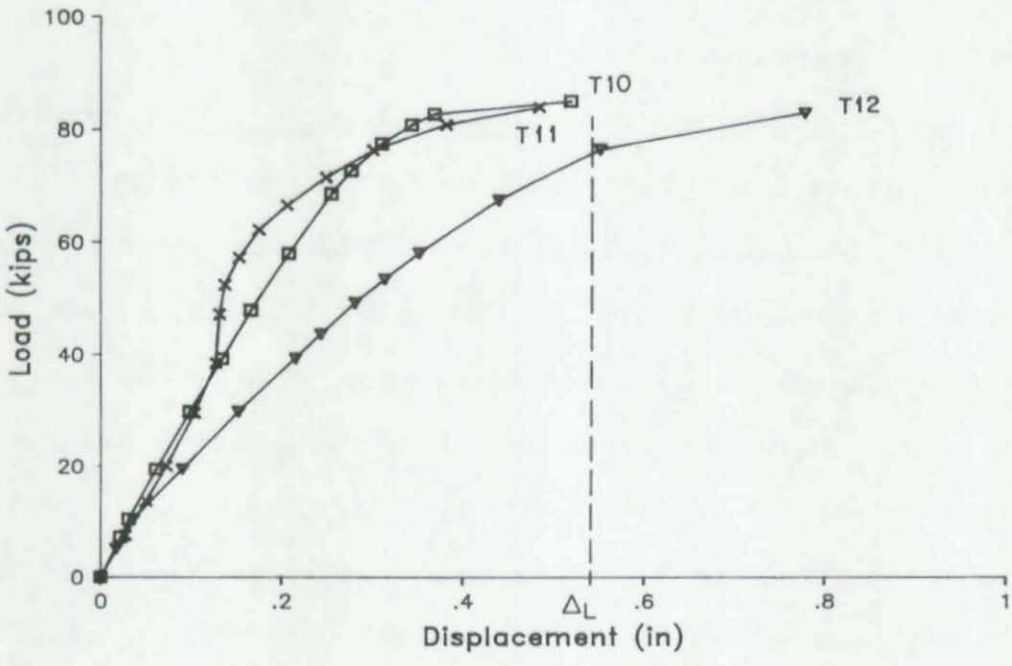

Figure 4.31 Load-Displacement Curves: Test T10, T11 & T12

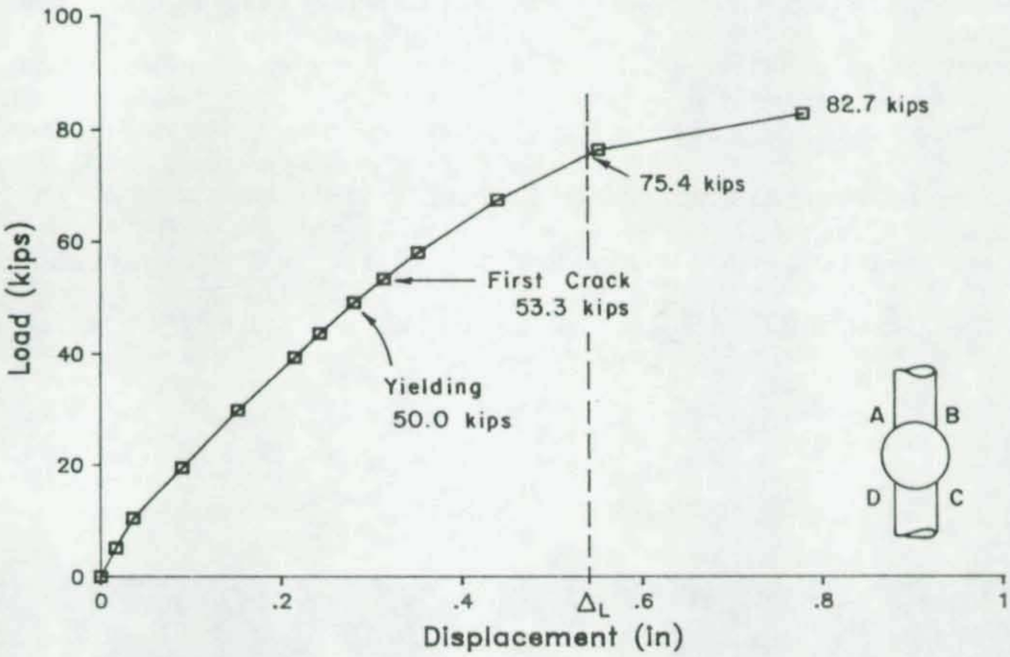

Figure 4.32 Load-Displacement Curve: Test T12

Figure 4.32 is the load-displacement curve for test T12. The first yielding occurred at 50 kips and the first surface crack was found at location D at a load of 53.3 kips. By 58 kips surface cracks were located at all hot spot locations. At 82.7 kips, the crack at location D had opened up to 1/8 in. in width but had not penetrated the surface. After taking the static point at 82.7 kips, the crack at location D penetrated through the chord wall, as soon as the loading continue. The deformation limit controlled and reduced the maximum load to 75.4 kips. The crack surface looked the same as those with the low strength branches. The fracture surface of the bottom branch showed two stages of crack propagation(see Fig. 4.33). The fracture occurred after straightening of the chord between the weld toes. Approximately half way through the chord wall, the fracture surface texture changes, showing that the speed of the crack propagation had increased dramatically. A summary of all the high strength branch test data is given in Table 4.3.

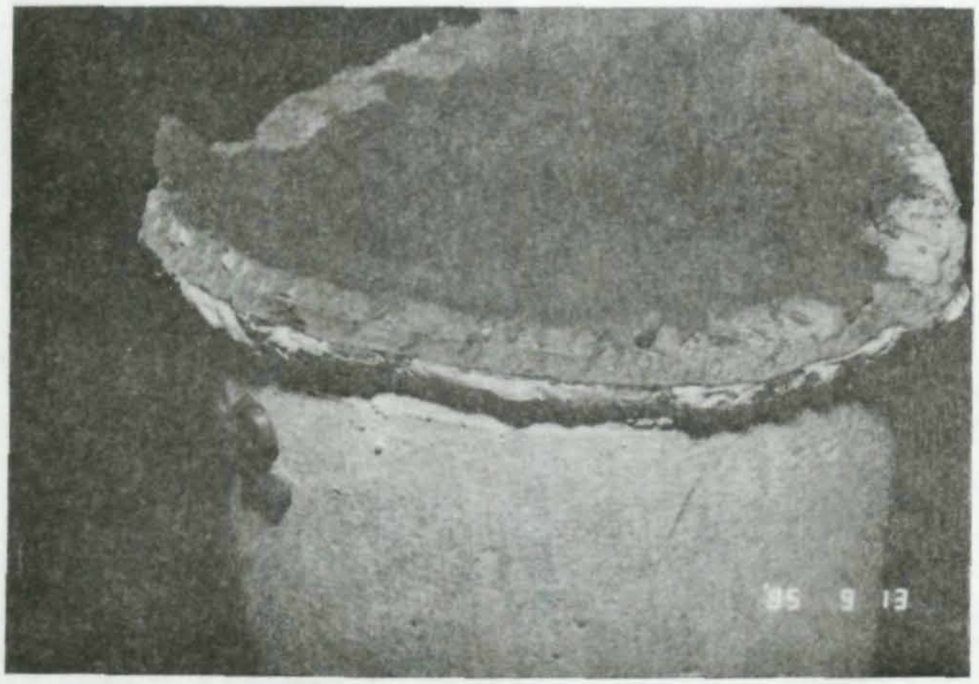

Figure 4.33 Fracture Surface

C H A P T E R 5

DISCUSSION OF RESULTS

In this chapter the results from the research program will be analyzed and compared with the existing data base and empirical equations. The chapter will be divided into four sections: effect of branch stress on post-crack strength, factors affecting ultimate strength, ultimate strength limit, and first crack limit.

Effect of Branch Stress on Post-Crack Strength

One of the objectives of the program was to study how post-crack strength was affected by the magnitude of the stresses in the branch. The amount of reserve yield capacity in the branch was described by the P/P_y ratio at ultimate load. The specimens with low strength branches(P_y = 174 kips) had an average P/P_y ratio of 50%, while the specimens with high strength branches(P_y = 345 kips) had an average P/P_y ratio of 25%. The average first crack and ultimate strength value for the two low strength branch specimens were 49 kips and 83 kips respectively; this gave a post-crack strength of 41%. The three high strength branch specimens had an average first crack and ultimate strength value of 48 kips and 85 kips respectively which gave a post-crack strength of 44%. Despite the large difference in reserve yield capacity of the branch, the post-crack strength and load-displacement behavior(see Fig. 5.1) were very similar for the two P/P_y levels. If a concern of using ultimate strength in design was the uncertainty of the effect of reserve yield strength in the branch on the post-crack strength, this study has found that the reserve strength has no effect. The β = 0.34 tests will not be used in ultimate strength or first crack limit studies because of the closeness of the stiffeners. The stiffeners do not change the relative value between first crack and ultimate but may affect the absolute values.

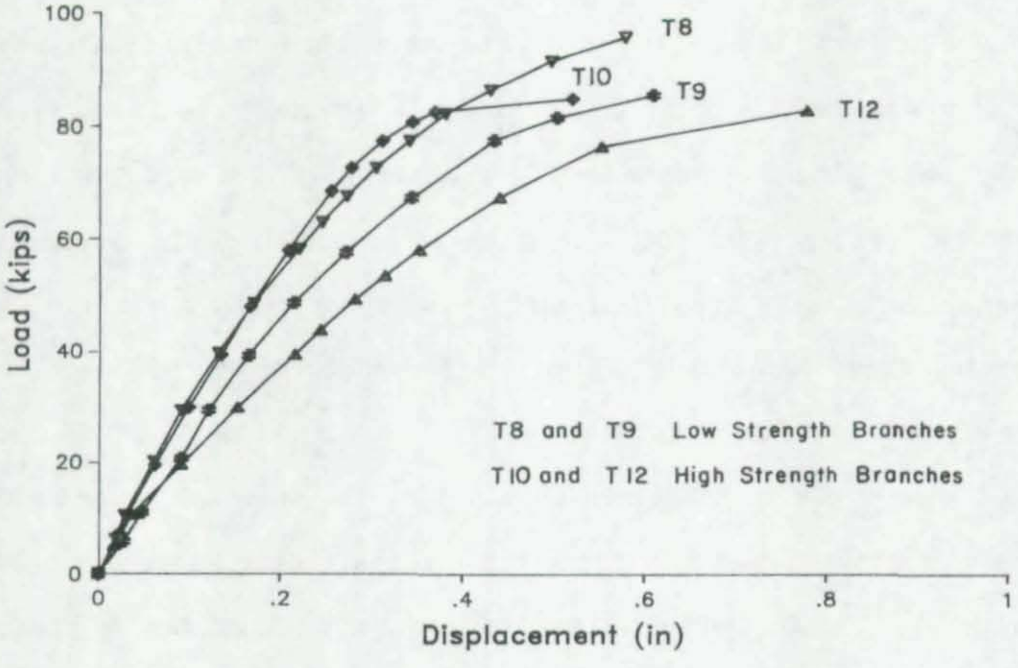

Figure 5.1 Load-Displacement Curves: Post-Crack Strength Tests (β = 0.34)

Factor Affecting Ultimate Strength

In the β = 1.0 portion of the program, the major objectives were to add to the data base and to determine what factors affected the ultimate strength of the joints. The ultimate strength values for the 5 tests are given in Table 4.2, and the load-deflection curves for all of the β = 1.0 tests are shown in Fig 5.2. The three reference tests, T1, T2 and T3, had an average ultimate strength value of 473 kips with a scatter of 106 kips or 22%. The scatter can be attributed to the fracture

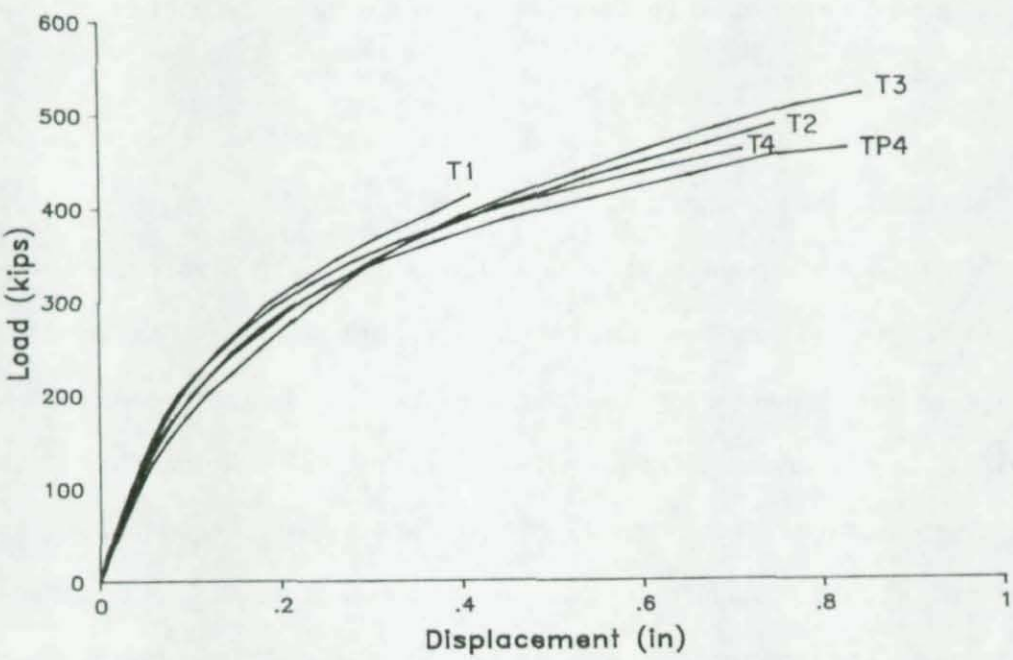

Figure 5.2 Load-Displacement Curves: β = 1.0 Tests

failure that occurred with all of the joints. A fracture failure is sensitive to the condition of the area close to the weld toe in the saddle region. Since the failure is affected by a local effect, the scatter of ultimate load is increased. The following sections will discuss the results from the short chord test, T4, and the chord load test, TP4.

Short Chord Test. The short chord(total length 24 in.) test had an ultimate load of 459 kips which is close to the average of the reference tests(473 kips) and well within the test scatter. The strain gages applied to the specimen explain why there is no reduction in strength even though a majority of the chord was removed.

The chord wall strains in the gap between the branches consists of membrane and bending strains(see Fig. 5.3). By combining exterior wall strains and interior wall strains, it was possible to calculate a uniaxial membrane and bending strain. The gage locations along the chord centerline and between saddle points are shown in Fig. 3.13. Figure 5.4 shows that the membrane strains along the chord wall are mainly concentrated in an area within 4 inches of the branch centerline. The membrane strain at the branch centerline is above yield when the branch load has reached only 21.5% of ultimate. Four inches away from the branch centerline, the membrane strain has dropped off dramatically; at 33% of ultimate load, the membrane strain is only 30% of yield. Eight inches away from the centerline the strain barely gets above zero. Figure 5.5 is the bending strains along the chord wall and looks very much like the bending moment diagram of a simple supported beam. The bending strains in the chord approach zero near the end of the chord, -12 in. and 12 in. from the branch centerline.

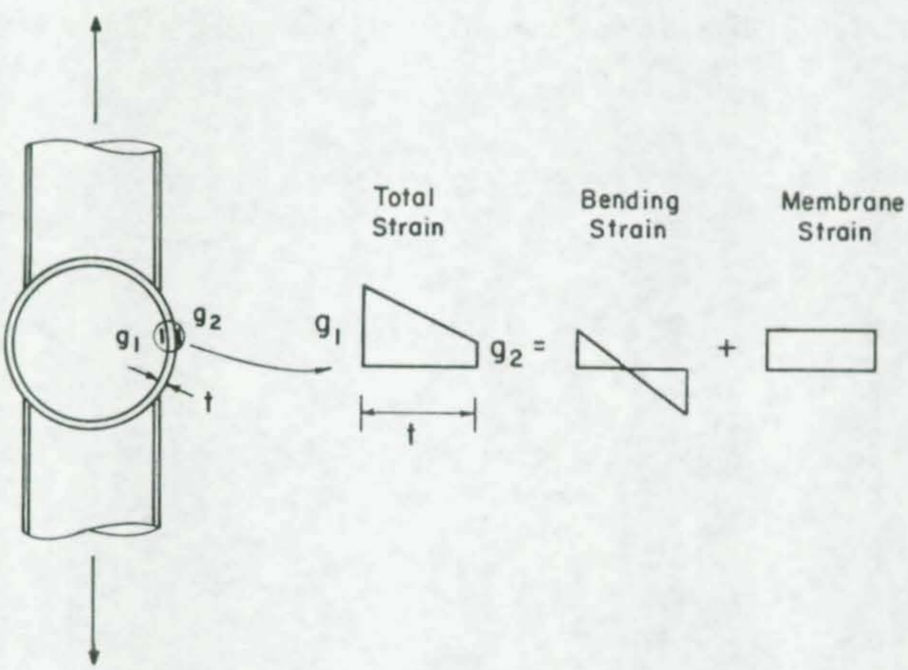

Figure 5.3 Chord Strains.

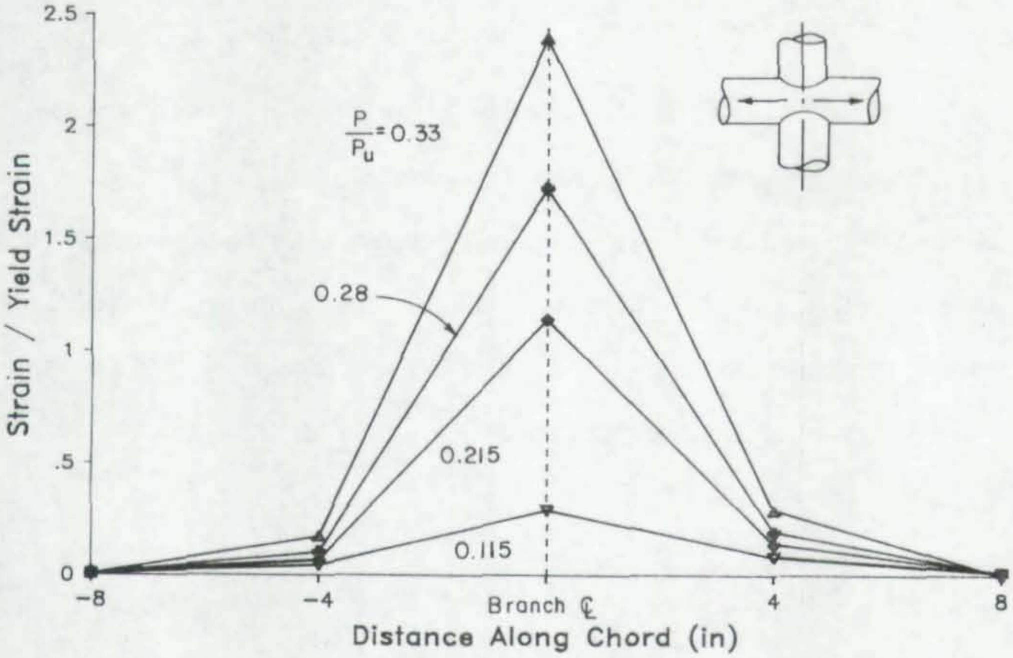

Figure 5.4 Membrane Strains Along the Chord Wall

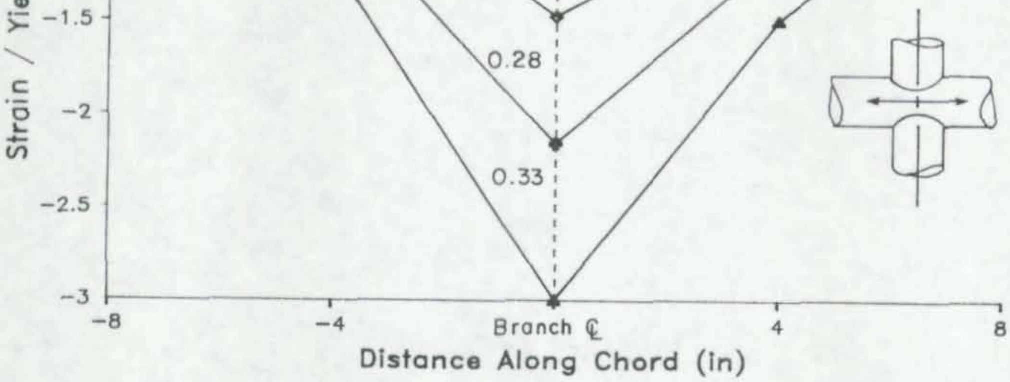

Figure 5.5 Bending Strains Along the Chord Wall

The behavior of the chord between saddle points can be further explained by studying strain gages that were placed between the weld toes to determine strain concentrations factors(16). As with the strain gages along the chord, strain gages were placed on the interior and the exterior of the chord wall. The series of gages on the exterior surface is missing one gage near the weld toe. The behavior of the missing gage can be assumed to be very similar to the other weld toe gage because of the symmetry about the chord centerline. Figure 5.6 shows that the membrane strain is very consistent between the saddle point, as expected. The membrane strains are much higher than the branch strains. At a branch load of $0.215P_u$, the membrane strain is already at yield. Figure 5.7 shows the bending strains between the saddle points. The figure looks very much like a fixed ended beam. The plate of steel between weld toes has high tension bending strains at the ends and high compression bending strains in the middle.

For the β = 1.0 DT connections in tension, the chord between the saddle points plays a very important role in the joint strength while the chord outside this zone contributes very little; this is not true for all tension specimens. In the β = 0.34 specimen, test T6, where there were no chord stiffeners, the capacity was greatly reduced and there were large chord deformations because of the short chord length. When 2 in.

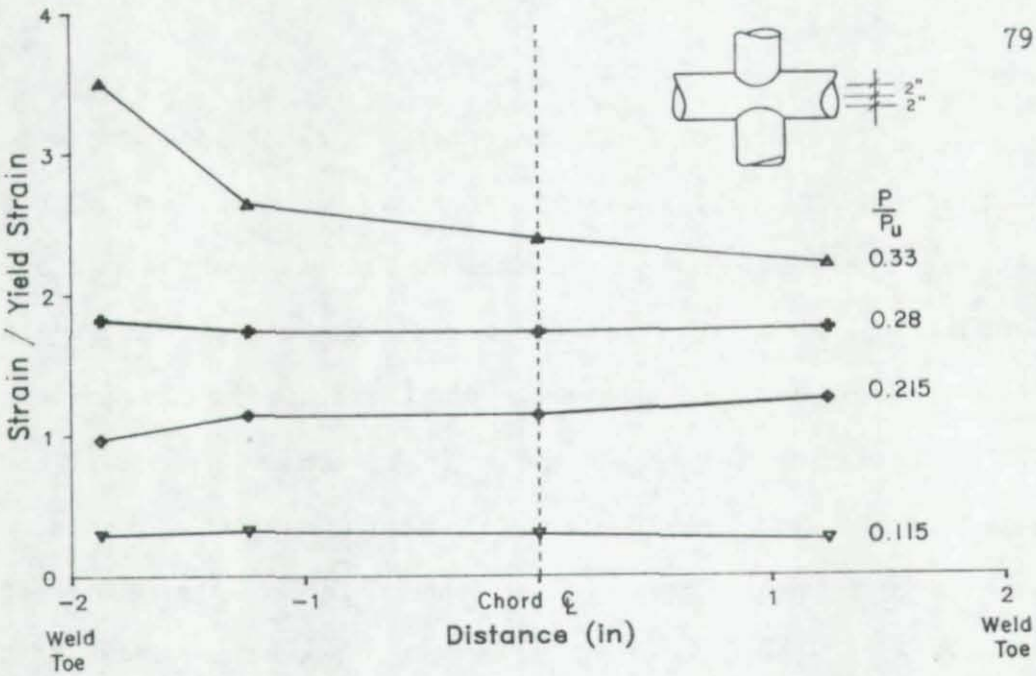

Figure 5.6 Membrane Strains Between Saddle Points

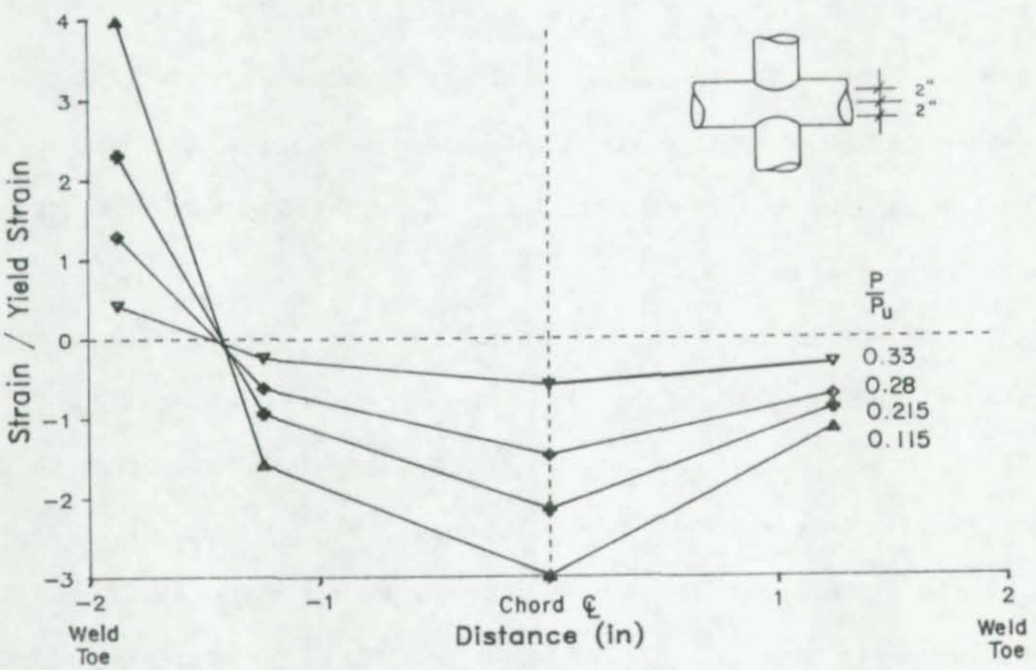

Figure 5.7 Bending Strains Between Saddle Points

plate stiffeners were placed in the ends of the chord for test T7, the capacity increased, but the amount of load being transferred through the stiffeners, caused one of the stiffener welds to break. The distance from the branch to the end of the chord on the $\beta = 0.34$ specimens was 15.5 in. or a little less than the diameter of the chord. For $\beta = 1.0$ connections, the requirement of API for joint strengthening, D/4 or 12 in., is enough, but for $\beta = 0.34$ connections the API chord requirement may not be adequate. The strength of $\beta = 0.34$ is affected by chord strength beyond D/4 or 12 in.. Further research needs to be done on small β DT tension joints to determine a chord length where the ultimate strength is not reduced because of the chord length.

Chord Load Test. The chord load test is the first DT connection tested with the branch in tension and the chord in compression. There have been tests done on DT connections with compression in the branch and the chord; they showed a reduction in capacity due to the chord load. Table 5.1 lists three different correction factors that have been used to modify prediction equations for connections with chord load. The correction equations shown in Table 5.1 are only for axial compression load in the chord, and are applied to joints with a branch compression or tension load. For the API and UEG equations, the factor of safety has been removed from the definition of U. Therefore, the equation can be applied using P/P_y.

Table 5.1 Chord Load Correction Factors

Type	Correction Factor		
UEG'85 (19)	$Q_f = 1 - 0.05\ \gamma\ U^2$		$U = P/Py$
API'82 (2,4)	$Q_f = 1 - 0.03\ \gamma\ U^2$		
Togo'66	$Q_f = 1.0$	for $U \leq 0.44$	
(18,21)	$Q_f = 1.22 - 0.5U$	for $U \geq 0.44$	

Figure 5.8 is a plot of the chord load correction factors(Q_f). Since two of the correction factors use the thinness ratio(γ), a range for the thinness ratio was used in order to plot the curves on the same graph. A maximum thinness of 25 was used because it is an upper bound for most offshore platforms. A lower bound of 16 was used because Togo's equation was developed from specimens with a thinness of 16. Togo did not include a thinness because all of his tests had the same thinness and were the only DT connections with chord load that had been tested at that time. The UEG equation predicts greater reduction in

strength than API or Togo. The UEG has only one formula applicable to all three types of branch load, axial, in-plane or out-of-plane, while API has three separate equations. The UEG

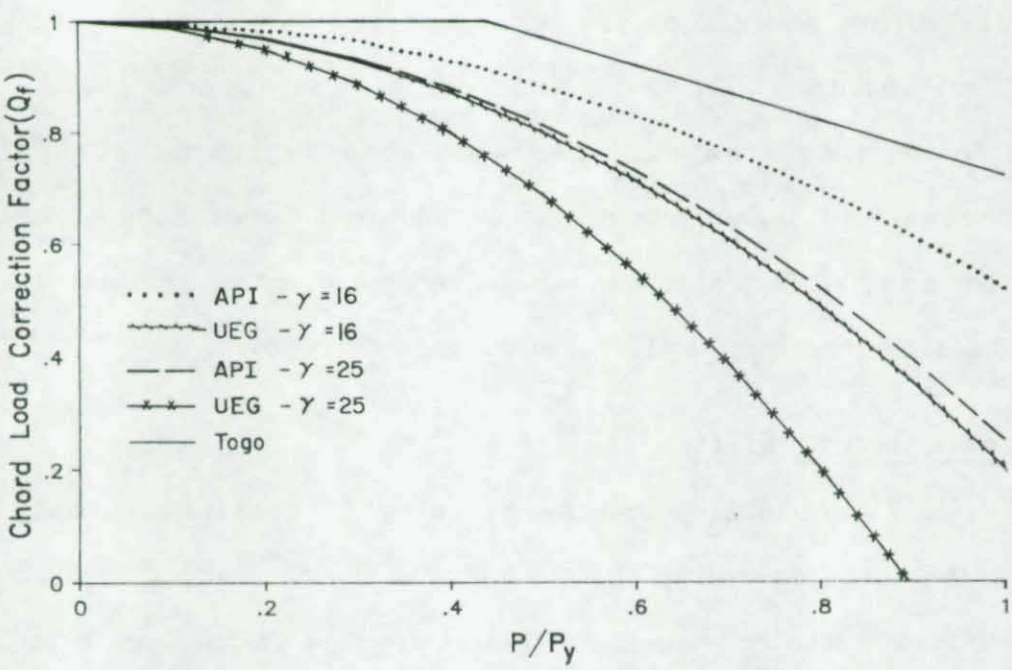

Figure 5.8 Comparison of Chord Load Factors

used a more conservative equation because of scatter in the axial branch load test data and to accomodate in-plane bending; the equation closely resembles the API in-plane equation.

The ultimate load of the chord load test was 461 kips, which is very close to the average of the reference tests(473 kips) and well within the scatter. There is no reduction in ultimate strength due to the chord load when the branch is in tension on β = 1.0 DT joints, therefore the correction factors to reduce the predicted strength are not necessary. The chord load had no effect for β = 1.0, because the joint gets most of its strength from membrane action in the chord material between the saddle points and not by the chord bending as in joints with smaller β values. When the chord cross section distorts locally due to bending strains, the chord load begins to affect performance. The correction factor should be continued to be applied to smaller β specimen, where chord bending contributes to the tension strength, until further research is done.

Ultimate Strength Limit

Figure 5.9 shows the existing DT tension ultimate strength data base with the X's marking the data added by this research project. The new β = 0.34 data is show in the figure but will not be included in the ultimate strength limit study because of the closeness of the stiffeners. The new β = 1.0 data is near the upper limit of the other DT joints. When the ultimate load is non-dimensionalized by F_yT^2 and plotted versus β, the test data shows little scatter except at β = 1.0. The F_yT^2 factor is related to the bending strength of the chord wall which apparently dominates the joint resistance for β less than 0.9. Conversely, the strain gage data on the short chord length

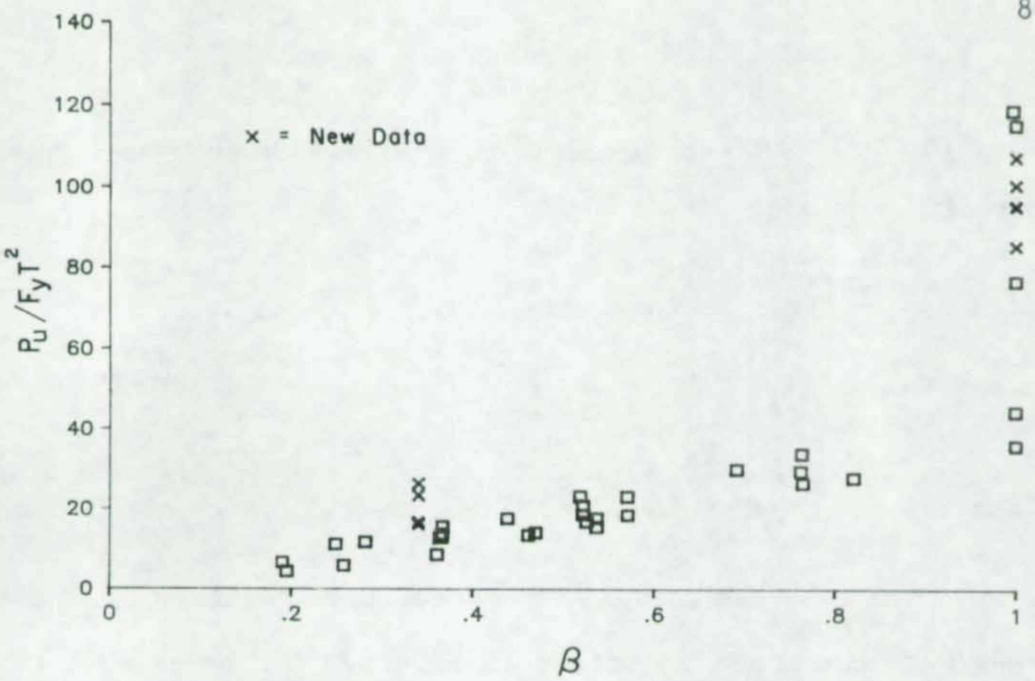

Figure 5.9 Expanded DT Tension Ultimate Strength Data Base

specimen reported herein, indicates very significant membrane chord strains which is related to T rather than T^2.

Since the β = 1.0 connection is transferring the load through membrane forces, the axial strength of the chord wall between saddle points(F_yTD), where the D is used as an effective plate width, is a more accurate way to model the joint strength for high β values. Figure 5.10 shows the DT β = 1.0 tension data base plotted using F_yTD, which organizes the β = 1.0 data fairly well. Therefore what is needed is an equation that utilizes F_yT^2 when β is less than 0.9 and F_yTD when β is greater than 0.9. A β value of 0.9 was selected because at this value, the plate action begins to dominate. A beta-thinness factor, $Q_{\beta\gamma}$, which uses the thinness ratio(D/2T) to make this conversion was developed and is used in the following equation to predict mean value ultimate strength.

$$P = 35.4\ \beta\ F_y T^2 Q_{\beta\gamma} \ldots\ldots\ldots\ldots\ldots\ldots\ldots (5.1)$$

$$Q_{\beta\gamma} = 1 \qquad\qquad \text{for } \beta < 0.9$$

$$Q_{\beta\gamma} = \frac{0.035\gamma^{.75}}{1-0.86\beta} \qquad\qquad \text{for } \beta > 0.9$$

For β less than 0.9, the prediction equation is of the form $F_y T^2$ but after 0.9, the beta-thinness factor changes the form to $F_y T^{1.25} D^{.75}$, which is very close to the original concept of $F_y TD$ shown in Fig. 5.10. No length factor was included because

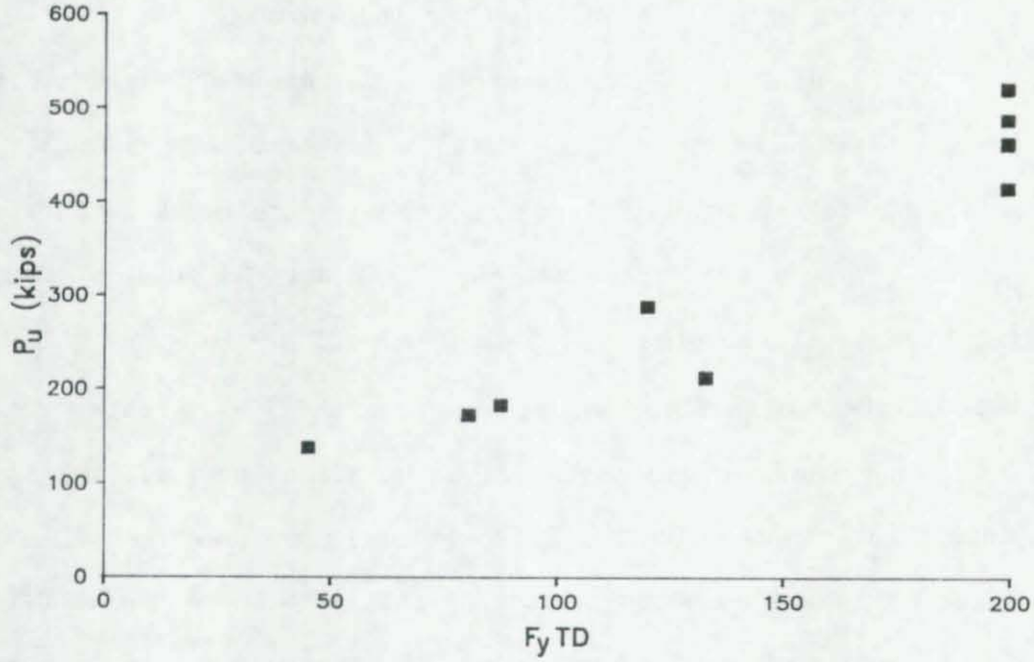

Figure 5.10 P_u versus $F_y TD$ for $\beta = 1.0$ Joints

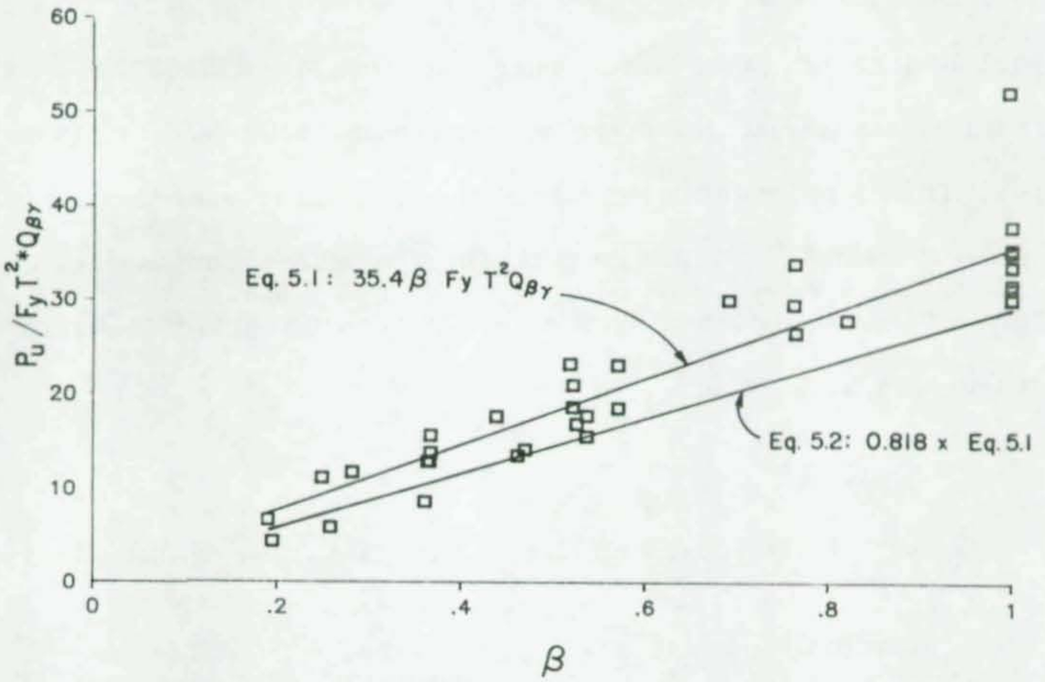

Figure 5.11 Equation 5.1 and 5.2 with Current Ultimate Strength Data Base

of the difficulty in design to know what length to use. Figure 5.11 shows a plot of Eq. 5.1 with the current data base. Table 5.2 gives the results from a statistical analysis of the current mean value equations(see Table 2.1). The analysis is an extension of the presentation in Chapter 2, Table 2.2, but now includes the tests done during this research program. The analysis was done once with only joints with a β less than 0.9 and once with the complete data base. Using the coefficient of variance to compare the equations, Eq. 5.1 compares well with the existing equations when only the joints with β less than 0.9 are included in the analysis. When the complete data base is included the advantage of the beta-thinness factor can really be seen. The coefficient of variance for Eq. 5.1 is almost half of the next best equation. By utilizing the beta-thinness factor, Eq. 5.1 more accurately models DT tension joint behavior especially at $\beta = 1.0$.

Table 5.2 Statistical Analysis of Ultimate Strength Equations

Equation	Average	Standard Deviation	Coefficient of Variance
Data with $\beta \leq 0.9$			
UEG-M (n=26)	0.733	0.168	0.229
Ochi (n=21)	0.785	0.260	0.332
DNV (n=26)	1.023	0.255	0.249
Eq. 5.1 (n=26)	1.003	0.184	0.183
All β Values			
UEG-M (n=36)	0.875	0.336	0.384
Ochi (n=31)	0.931	0.339	0.364
DNV (n=36)	1.183	0.424	0.359
Eq. 5.1 (n=36)	1.000	0.182	0.182
Eq. 5.2 (n=36)	1.222	0.222	0.182

Also shown in Fig. 5.11 is a lower bound equation(Eq. 5.2) that would be more applicable for design purposes. Equation

5.2 was obtained by reducing Eq. 5.1 by the factor (1.0 - standard deviation) which appears to produce a reasonable lower bound. The equation is as follows:

$$P = 0.818 \times \text{Eq. } 5.1 \quad \ldots\ldots\ldots\ldots\ldots\ldots\ldots\ldots(5.2)$$

The UEG approach (95 percentile) was not used because it produces significant reduction in predicted values at large β values. The equation has the same coefficient of variance as Eq. 5.1 and provides a factor of safety for design. Equation 5.2 should be used when designing a DT tubular joint in tension, while Eq. 5.1 is best to determine the actual joint strength.

First Crack Limit

In the current API RP 2A, first crack is used in the design of DT joints in tension. Early in the research program it was unclear what was meant in the literature by first crack -- first surface crack or first full penetration crack. For all of the tests conducted during this program, first full penetration crack occurred at failure. Therefore, it is reasonable to assume that the first crack limit is a first surface crack limit, although depths may vary. Figure 5.12 shows the current API equation(ref. Table 2.1) with the current data base. The X's indicate the tests added by the research program. The $\beta = 0.34$ tests are shown but will not be included in the first crack limit study because of the effect of the stiffeners. The API equation is very conservative for high beta values. The API prediction equation for DT joints in compression applies the following factor(Q_β) to joints with β values greater than 0.6.

$$Q_\beta = 1 \qquad\qquad \beta < 0.6$$

$$Q_\beta = \frac{0.3}{\beta(1-0.833\beta)} \qquad\qquad \beta > 0.6$$

When β = 1.0, the factor increases the predicted value by 80%. If the same correction is applied to the first crack equation

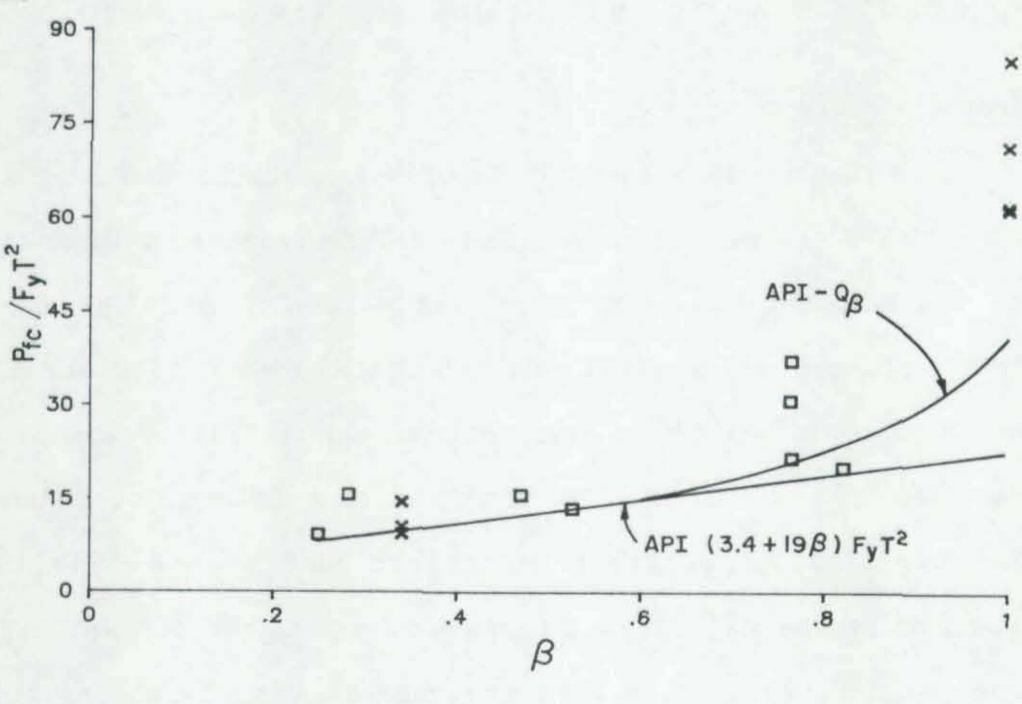

Figure 5.12 API First Crack Equation with First Crack Data Base

(API - Q_β), the equation does a much better job of predicting joint cracking(see Fig. 5.12). The results from a statistical analysis of these two equations is given in Table 5.3. The coefficient of variance for the current API equation is 0.441, while for the modified API equation it drops to 0.236.

Even with the modification to the API equation, there is still a large amount of scatter as β increses. Using the new first crack data and the principles developed for the ultimate strength limit, the following equation(Eq. 5.3) was developed:

$$P = 0.94(6 + 20\beta)\ F_y T^2 Q_{\beta\gamma} \qquad (5.3)$$

$$Q_{\beta\gamma} = 1 \qquad \text{for } \beta < 0.7$$

$$Q_{\beta\gamma} = \frac{0.035\gamma^{.75}}{1-0.86\beta} \qquad \text{for } \beta > 0.7$$

The equation utilizes the same beta-thinness factor used for the ultimate strength limit but the factor is applied at smaller β values. Figure 5.13 shows Eq. 5.3 with the current first crack data base. The equation does a good job of pulling the data together. The results of a statistical analysis of Eq. 5.3 is given in Table 5.3. The coefficient of variance for Eq. 5.3 is 30% of the API equation and 57% of the modified API equation. The beta-thinness factor allows the equation to accurately predict the first crack limit for high β values.

For design the API uses a lower bound equation. Shown below(Eq. 5.4) and plotted in Fig. 5.13 is a lower bound equation that was developed by reducing the mean value equation by the factor (1.0 - the standard deviation) which produces a reasonable lower bound.

$$P = 0.866 \times \text{Eq. } 5.3 \quad \ldots\ldots\ldots\ldots\ldots\ldots\ldots\ldots(5.4)$$

If the design is governed by the first crack limit, Eq. 5.4 would be a very good lower bound prediction to the first crack load.

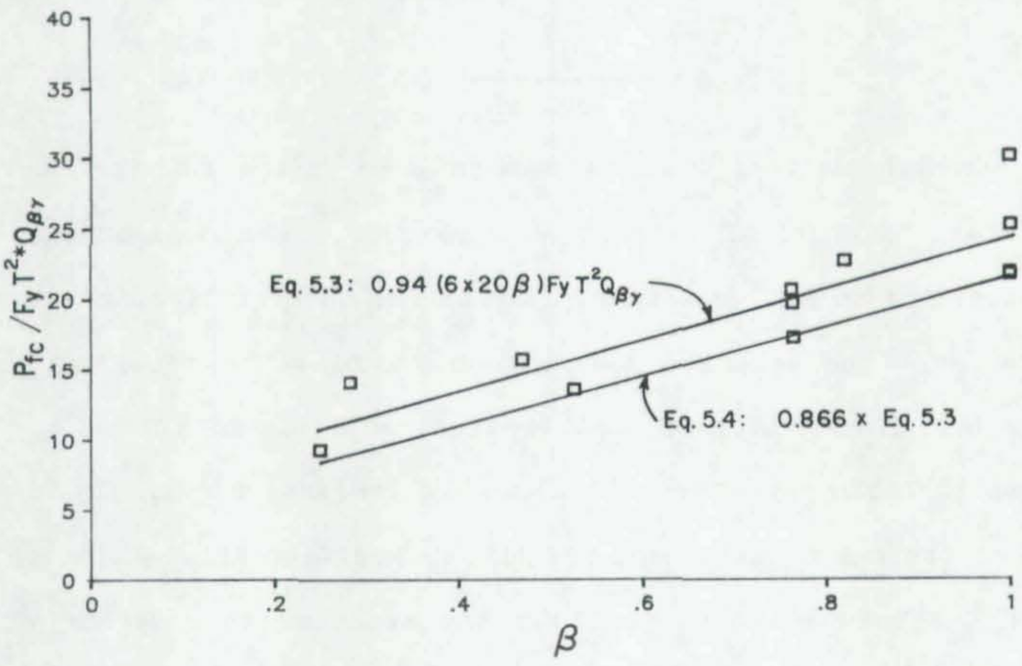

Figure 5.13 Equations 5.3 and 5.4 with First Crack Data Base

Table 5.3 Statistical Analysis of First Crack Equation

Equation	Average	Standard Deviation	Coefficient of Variance
API (n=13)	2.025	0.892	0.441
API-Q_β (n=13)	1.466	0.346	0.236
Eq. 5.3 (n=13)	1.000	0.134	0.134
Eq. 5.4 (n=13)	1.147	0.154	0.134

CHAPTER 6

SUMMARY AND CONCLUSIONS FOR DT JOINTS IN TENSION

1. The amount of branch reserve capacity (P/P_y) has no affect on the amount of post-crack strength. Hence, API should consider the elimination of the first crack concept for tension capacity.

2. The chord member contributes greatly to the strength of small β joints. Tests done on $\beta = 0.34$ specimens showed significant reduction in strength when the length of the chord from the branch was 15.5 in. or approximately D. Additional research is needed to determine if the current API joint strengthening requirements, 12-in. or D/4, are adequate.

3. The chord length beyond D/4 has no effect on the joint capcity of $\beta = 1.0$ joints. Therefore, current API requirements for strengthening are conservative for $\beta = 1.0$ joints.

4. Compression chord load has no effect on the ultimate tension capacity for $\beta = 1.0$ joints. Therefore, no reduction in strength is required for $\beta = 1.0$ joints. Additional chord load tests are required for DT joints with smaller β ratios to determine the effects on the capacity.

5. The following mean equation was developed to better model ultimate tension joint behavior:

$$P = 35.4\ \beta\ F_y T^2 Q_{\beta\gamma} \ldots\ldots\ldots\ldots\ldots \quad (5.1)$$

$$Q_{\beta\gamma} = 1 \qquad \text{for } \beta < 0.9$$

$$Q_{\beta\gamma} = \frac{0.035\gamma^{.75}}{1-0.86\beta} \qquad \text{for } \beta > 0.9$$

The equation utilizes the beta-thinness factor to modify the equation above β greater than 0.9. The equation has a coefficient of variance (0.182) that is almost half of the next best equation, DnV (0.359).

6. The current first crack equation in API is very conservative for $\beta = 1.0$ joints. The following mean equation was developed to improve first crack predictions:

$$P = 0.94(6 + 20\beta)\ F_y T^2 Q_{\beta\gamma} \ldots\ldots\ldots \quad (5.3)$$

$$Q_{\beta\gamma} = 1 \qquad \text{for } \beta < 0.7$$

$$Q_{\beta\gamma} = \frac{0.035\gamma^{.75}}{1-0.86\beta} \qquad \text{for } \beta > 0.7$$

This equation has a coefficient of variance (0.134) that is one-third the value (0.441) determined from the API formula. As a minimum, the current API first crack formula should be multiplied by the Q_β factor used for DT compression joints.

$$P = (3.4 + 19\beta)\ F_y T^2 Q_\beta \ldots\ldots\ldots \quad (5.4)$$

$$Q_\beta = 1 \qquad \beta < 0.6$$

$$Q_\beta = \frac{0.3}{\beta(1-0.833\beta)} \qquad \beta > 0.6$$

This modified API formula gives a coefficient of variance (0.236) that is one-half the value of the current API formula.

A P P E N D I X

Table A.1 Screened Current Data Base, DT Joints in Tension

REFERENCE	D (in)	T (in)	d (in)	t (in)	L (in)	F_y (ksi)	F_u (ksi)	γ	β	P_y (kips)	Pfc (kips)	P_u (kips)	(Maximum)
Akiyama (1)	6.504	.185	1.681	.130	32.520	68.310	-- --	17.58	.258	16.096	-- --	13.67	(34.395)
	6.504	.181	3.004	.114	32.520	68.310	-- --	17.96	.462	27.336	-- --	30.23	(48.496)
	6.504	.181	4.500	.150	32.520	68.310	-- --	17.96	.692	24.481	-- --	67.24	(68.891)
	6.504	.181	6.504	.181	32.520	68.310	-- --	17.96	1.000	85.986	---- --	172.18	
	12.539	.173	2.382	.118	62.717	68.959	-- --	36.24	.190	16.748	-- --	13.69	(32.192)
	12.539	.173	5.504	.173	62.717	68.959	-- --	36.24	.439	26.459	-- --	36.44	(40.352)
	12.529	.173	6.504	.177	62.717	61.204	-- --	36.24	.519	16.523	-- --	42.56	
	12.539	.173	12.539	.173	62.717	61.204	-- --	36.24	1.000	68.116	-- --	211.63	
	18.000	.193	3.508	.118	90.000	58.303	-- --	46.63	.195	16.523	-- --	9.44	(35.721)
	18.000	.193	6.504	.177	90.000	58.303	-- --	46.63	.361	23.582	-- --	18.67	(44.308)
Gibstein (6)	7.626	.263	1.902	- ----	-- --	48.296	-- --	14.52	.249	-- --	30.90	37.25	
	7.626	.259	4.012	- ----	-- --	48.296	-- --	14.70	.526	-- --	43.90	54.67	
	7.626	.262	6.260	- ----	-- --	48.296	-- --	14.57	.821	-- --	66.64	92.60	
Kaiho (7)	6.504	.305	6.504	.307	38.189	44.090	70.490	10.66	1.000	119.270	-- --	182.55	
	6.504	.432	6.504	.433	34.921	42.640	62.510	7.53	1.000	198.870	-- --	287.05	
Makino (9)	5.512	.352	2.004	.366	33.071	45.830	70.340	7.82	.364	45.950	-- --	73.29	
	6.508	.217	2.390	.224	38.976	73.387	84.410	15.00	.367	25.880	-- --	47.73	
	6.504	.217	2.386	.224	38.976	119.797	127.480	15.02	.367	47.390	-- --	88.29	
	6.504	.217	2.382	.220	38.976	119.797	127.480	15.02	.366	48.078	-- --	72.75	
Makino (10)	8.508	.0866	6.504	.177	52.362	31.182	50.036	49.12	.764	3.687	8.70	7.94	
	8.524	.119	6.504	.177	52.362	41.624	50.036	35.97	.763	10.228	18.14	17.42	
	8.496	.150	6.500	.177	52.362	50.906	69.181	28.25	.765	17.624	24.71	30.42	
	8.476	.148	2.390	.126	52.362	50.036	69.036	28.56	.282	9.824	15.43	12.85	(18.79)
	8.528	.151	4.008	.091	52.362	49.311	68.775	28.21	.470	10.476	17.64	15.91	(22.12)
Makino (11)	6.500	.167	6.480	.177	55.118	41.480	57.720	19.47	.997	36.260	-- --	137.79	
Rodriquez (14)	16.142	.374	8.661	.307	31.496	46.580	-- --	21.58	.537	-- --	-- --	101.39	
	16.142	.374	8.661	.307	78.402	51.468	-- --	21.58	.537	-- --	-- --	127.69	
Sammet (15)	6.260	.197	3.268	----	-- --	49.311	-- --	15.90	.522	-- --	-- --	35.72	
	6.260	.197	3.268	----	-- --	49.311	-- --	15.90	.522	-- --	-- --	40.13	
Takizowa (17)	55.008	1.417	31.496	.472	118.11	36.838	67.440	19.45	.571	379.750	-- --	1710.88	
	55.118	1.417	31.496	.472	118.11	48.371	75.997	19.45	.571	465.090	-- --	1816.70	

Table A.2 Test Data

LOAD STAGE	1	2	3	4	5	6	7	8	9	10	11	12	13	14	15	16	17	18	19	20
Test T1																				
P (kips)	0.1	50.5	99.7	148.7	173.1	198.5	223.0	247.0	270.2	275.1	298.3	318.4	344.6	368.0	393.1	413.2				
Δ (in)	0.0	.017	.037	.059	.072	.089	.109	.131	.157	.160	.187	.219	.262	.308	.367	—				
Test T2																				
P (kips)	0.0	49.9	99.4	147.8	172.3	196.6	221.4	245.5	269.1	294.9	319.5	343.5	367.1	390.1	406.2	430.8	448.4	466.3	485.9	491.5
Δ (in)	0.0	.015	.034	.061	.079	.100	.123	.150	.183	.216	.260	.303	.352	.413	.460	.536	.603	.673	.748	—
Test T3																				
P (kips)	0.0	49.3	101.7	151.3	175.5	200.7	221.5	247.8	273.1	294.1	319.7	342.5	366.6	389.4	413.6	436.6	459.7	483.6	506.8	519.4
Δ (in)	0.0	.020	.044	.075	.095	.119	.145	.176	.207	.234	.270	.305	.348	.398	.460	.528	.605	.690	.780	—
Test TP4																				
P (kips)	0.0	51.0	99.3	147.7	172.9	197.8	221.8	243.8	271.1	292.2	316.4	340.4	362.8	386.9	408.2	433.4	455.0	461.3		
Δ (in)	0.0	.019	.039	.064	.081	.100	.123	.145	.179	.210	.251	.305	.371	.449	.541	.653	.753	.828		
Test T4																				
P (kips	0.0	53.5	99.1	151.0	175.2	200.0	220.7	246.7	271.2	295.2	318.1	342.1	363.6	389.3	412.7	435.7	460.2	475.2		
Δ (in)	0.0	.019	.034	.057	.072	.087	.106	.133	.162	.195	.232	.279	.332	.407	.494	.599	.712	—		
Test T6																				
P (kips)	0.0	5.6	15.1	24.3	33.0	41.6	46.5	49.3	49.8											
Δ (in)	0.0	.090	.294	.593	.897	1.475	2.101	2.679	3.483											
Test T7																				
P (kips)	0.0	5.5	10.5	20.0	28.5	38.7	48.1	43.4	57.5	67.1	74.8									
Δ (in)	0.0	.027	.052	.096	.154	.217	.282	.397	.503	.662	.976									
Test T8																				
P (kips)	0.0	6.2	10.4	20.1	29.3	39.6	48.5	58.2	62.9	67.6	72.6	77.4	82.3	86.5	91.5	95.7				
Δ (in)	0.0	.018	.028	.060	.090	.131	.170	.220	.245	.272	.304	.341	.381	.430	.496	.577				
Test T9																				
P (kips)	0.0	5.7	10.9	20.6	29.3	39.1	48.5	57.5	67.3	77.5	81.5	85.5								
Δ (in)	0.0	.027	.047	.090	.120	.164	.214	.271	.343	.434	.503	.609								
Test T10																				
P (kips)	0.0	7.2	10.4	19.4	29.8	39.2	47.8	57.9	68.5	72.6	77.4	80.7	82.6	84.9						
Δ (in)	0.0	.022	.031	.061	.098	.134	.166	.208	.255	.277	.311	.344	.369	.520						
Test T11																				
P (kips)	0.0	7.5	13.6	20.0	29.5	38.4	47.1	52.3	57.2	62.1	66.5	71.4	76.3	80.7	83.8					
Δ (in)	0.0	.027	.050	.072	.103	.127	.131	.137	.153	.179	.206	.249	.301	.382	.485					
Test T12																				
P (kips)	0.0	5.1	10.5	19.5	29.8	39.3	43.6	49.1	53.3	58.0	67.4	76.4	82.7							
Δ (in)	0.0	.017	.036	.090	.152	.215	.243	[illegible]	.314	[illegible]	[illegible]	[illegible]	.779							

REFERENCES

1. Akiyama, N. et al., "Experimental Study on Strength of Joints in Steel Tubular Structurs,"(in Japanese) Journal of Society of Steel Construction, Tokyo, Vol. 10, No. 102, June 1974, pp. 37-68.

2. American Petroleum Institute, Recommended Practice for Planning, Designing, and Constructing Fixed Offshore Platforms, RP 2A, Fifteenth Edition, October 22, 1984.

3. American Society of Testing Materials, Standard Metnods and Definitions for Mechanical Testing of Steel Products, ASTM A370-77.

4. Boone, T.J., Yura, J.A. and Hoadley, P.W., "Chord Stress Effects on the Ultimate Strength of Tubular Connections," Phil M. Ferguson Structural Engineering Laboratory, The University of Texas at Austin, Report No. 82-1, December 1982.

5. DNV, Rules for the Design, Construction, and Inspection of Fixed Offshore Structures, Det Norske Veritas, 1977.

6. Gibstein, M.B., "Static Strength of Tubular Joints," Det Norske Veritas Report No. 73-86-C, May 1973.

7. Kaiho, Y. et al., "Study on Structure of Intersection of Spherical Tank Pipe Bracings," (in Japanese with English Summary) Technical Reports, Kawasaki Technical Review, No. 64, Kawasaki Heavy Industries Ltd. Aug. 1977, pp 72-75.

8. Kurobane, Y., Makino, Y., and Ochi, K., "Ultimate Strength Formulae for Simple Tubular Joints," International Institute of Welding, Doc XV-385-76, May 1976.

9. Makino, Y. et al., " Experimental Study on Ultimate Strength of Tubular Joints with High Strength Steel and Heavy Walled Chord," (in Japanese) Research Report, Chugoku-Kyushu Branch of Architectual Institute of Japan, No. 4, Feb. 1978, pp. 225-258.

10. Makino, Y., Kurobane, Y., and Minoda, Y., "Design of CHS X and T-Joints Under Tensile Brace Loading," International Institute of Welding, Doc XV-487-81, May 1981.

11. Makino, Y., Kurobane, Y., and Ochi, K., "Reliability-Based Design Criteria for Tubular X-Joints under Tension," Summary Papers, Annual Conference of Architectural Institute of Japan, Sendai, Japan, 1982, pp. 1781-1782.

12. Marshall, P.W. and Toprac, A.A. "Basis for Tubular Joint Design Code", Welding Journal, May 1974, p. 192-S.

13. Ochi, K., Makino, Y., and Kurobane, K., "Basis for Design of Unstiffened Tubular Joints Under Axial Brace Loading," International Institute of Welding, Doc XV-561-84, May 1984.

14. Pan, R., Plummer, F., and Kuang, J., "Ultimate Strength of Tubular Joints", OTC Paper No. 2644, 1977; Offshore Technology Conference, Proceedings, Houston, Texas, May 3-6, 1976.

15. Rodriguez, M., "Ultimate Capacity of Circular Tubular X-Joint Under Static Axial Brace Loading," National University of Mexico, Mexico, 1985.

16. Sammet, H., "Die Festigkeit Knotenblechloser Rohrverbindungen im Stahlbau," Schweisstechnik, Vol. 13, No. 11, Berlin, Now. 1963.

17. Swensson, K.D., Hoadley, P.W., Yura, J.A. and Sanders, D.H. "Stress Concentration Factors in Double-Tee Tubular Joints," Phil M. Ferguson Structural Engineering Laboratory, The University of Texas at Austin, January, 1986.

18. Takizawa, S. et al., "Full Scale Experiments of Tee and Cross Type Tubular Joints under Static and Cyclic Loading," Technical Reports, Kawasaki Steel Technical Review, Vol. 11, No. 2, Kawasaki Steel Corporation, 1979, pp. 115-125.

19. Togo, T., "Experimental Study on Mechanical Behavior of Tubular Joints," (in Japanese) Osaka University, January 1967.

20. UEG, Design of Tubular Joints for Offshore Structures, UEG Publication UR33, 1985.

21. Wardenier, J., Hollow Section Joints, Delft University Press, The Netherlands, 1982.

22. Washio, K., Togo, T., and Mitsui, N., "Cross Joints of Tubular Memebers," (in Japanese) Report Kinki Branch of AIJ, May 1966.

23. Weinstein, R. and Yura, J.A., "The Effect of Chord Stresses on the Static Strength of DT Tubular Connections", Phil M. Ferguson Structural Engineering Laboratory Report No. 85-1, The Univerisity of Texas at Austin, January 1985.

24. Yura, J.A., "Connections with Round Tubes", Proceedings, Symposium on Hollow Structural Sections in Building Construction, ASCE Structural Engineering Congress'85, Chicago, Sept. 17, 1985.

25. Yura, J.A., Zettlemoyer, N. and Edwards, I.F., "Ultimate Capacity Equations for Tubular Joints, OTC Paper No. 3690, Offshore Technology Conference, Proceedings, Houston, Texas, 1980.